

# UC Davis

## UC Davis Previously Published Works

### Title

Gut dysbiosis was inevitable, but tolerance was not: temporal responses of the murine microbiota that maintain its capacity for butyrate production correlate with sustained antinociception to chronic morphine.

### Permalink

<https://escholarship.org/uc/item/1579575s>

### Journal

Gut Microbes, 17(1)

### Authors

Sall, Izabella  
Foxall, Randi  
Felth, Lindsey  
et al.

### Publication Date

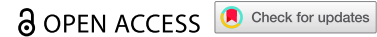
2025-12-01

### DOI

10.1080/19490976.2024.2446423

Peer reviewed

RESEARCH PAPER



# Gut dysbiosis was inevitable, but tolerance was not: temporal responses of the murine microbiota that maintain its capacity for butyrate production correlate with sustained antinociception to chronic morphine

Izabella Sall<sup>a,b,\*</sup>, Randi Foxall<sup>a,\*</sup>, Lindsey Felth<sup>c</sup>, Soren Maret<sup>a</sup>, Zachary Rosa<sup>c</sup>, Anirudh Gaur<sup>c</sup>, Jennifer Calawa<sup>a,d</sup>, Nadia Pavlik<sup>a</sup>, Jennifer L. Whistler<sup>c,e</sup>, and Cheryl A. Whistler<sup>id a</sup>

<sup>a</sup>Department of Molecular, Cellular, & Biomedical Sciences, University of New Hampshire, Durham, NH, USA; <sup>b</sup>Graduate program in Molecular and Evolutionary Systems Biology, University of New Hampshire, Durham, NH, USA; <sup>c</sup>Center for Neuroscience, University of California–Davis, Davis, CA, USA; <sup>d</sup>Microbiology Graduate Program, University of New Hampshire, Durham, NH, USA; <sup>e</sup>Department of Physiology and Membrane Biology, UC Davis School of Medicine, Davis, CA, USA

## ABSTRACT

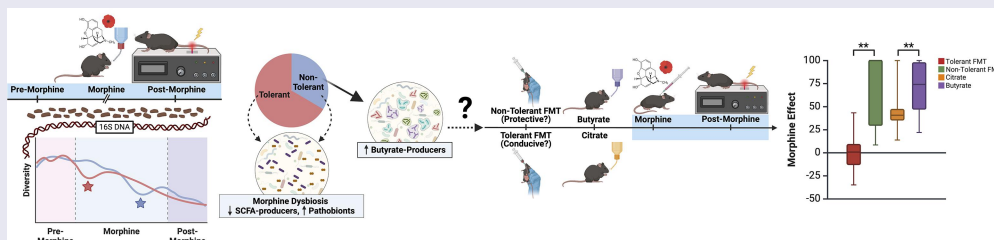
The therapeutic benefits of opioids are compromised by the development of analgesic tolerance, which necessitates higher dosing for pain management thereby increasing the liability for drug dependence and addiction. Rodent models indicate opposing roles of the gut microbiota in tolerance: morphine-induced gut dysbiosis exacerbates tolerance, whereas probiotics ameliorate tolerance. Not all individuals develop tolerance, which could be influenced by differences in microbiota, and yet no study design has capitalized upon this natural variation. We leveraged natural behavioral variation in a murine model of voluntary oral morphine self-administration to elucidate the mechanisms by which microbiota influences tolerance. Although all mice shared similar morphine-driven microbiota changes that largely masked informative associations with variability in tolerance, our high-resolution temporal analyses revealed a divergence in the progression of dysbiosis that best explained sustained antinociception. Mice that did not develop tolerance maintained a higher capacity for production of the short-chain fatty acid (SCFA) butyrate known to bolster intestinal barriers and promote neuronal homeostasis. Both fecal microbial transplantation (FMT) from donor mice that did not develop tolerance and dietary butyrate supplementation significantly reduced the development of tolerance independently of suppression of systemic inflammation. These findings could inform immediate therapies to extend the analgesic efficacy of opioids.

## ARTICLE HISTORY

Received 16 April 2024  
Revised 24 November 2024  
Accepted 18 December 2024

## KEYWORDS





Microbiota; opioid; analgesic tolerance; butyrate; short-chain fatty acid; inflammation; dysbiosis; opioid use disorder; morphine




## Introduction

A surge in research has demonstrated the importance of the gut microbiota to neurological function, leading to the recognition of a gut-microbiota-brain (GMB) axis.<sup>1–5</sup> Whereas the brain influences the gut microbiota by control of gut motility and thereby transit, the microbiota signals the brain via

production or modification of neurotransmitters, hormones, microbial byproducts, and neuroactive metabolites.<sup>4,6,7</sup> The gut microbiota is often referred to nondescriptly as commensals, but many are mutualistic symbionts that support host health. Some others are pathobionts, which are correlated with, or capable of causing, disease in

**CONTACT** Cheryl A. Whistler  [cheryl.whistler@unh.edu](mailto:cheryl.whistler@unh.edu)  Department of Molecular, Cellular, & Biomedical Sciences, University of New Hampshire, 46 College Rd., Durham, NH 03824, USA; Jennifer L. Whistler  [jlwhistler@ucdavis.edu](mailto:jlwhistler@ucdavis.edu)  Center for Neuroscience, University of California–Davis, 1544 Newton Ct., Davis, CA 95618, USA

\*Contributed equally to this work.

 Supplemental data for this article can be accessed online at <https://doi.org/10.1080/19490976.2024.2446423>

© 2025 The Author(s). Published with license by Taylor & Francis Group, LLC.

This is an Open Access article distributed under the terms of the Creative Commons Attribution License (<http://creativecommons.org/licenses/by/4.0/>), which permits unrestricted use, distribution, and reproduction in any medium, provided the original work is properly cited. The terms on which this article has been published allow the posting of the Accepted Manuscript in a repository by the author(s) or with their consent.

a context-specific manner. The high load of pro-inflammatory microbial antigens at the microbiota-intestinal mucosa interface, produced even by mutualists, requires that the host immune responses be trained by the microbiota to be tolerogenic and not over-react but to still appropriately clear commensals that breach the gut barrier.<sup>8</sup> Paramount among neuroactive signals in the GMB-axis produced by the gut microbiota that maintain homeostasis – balance of gut and host – are various short-chain fatty acids (SCFAs) generated during fermentation of dietary fiber. SCFAs can exert direct local effects by inhibiting host histone deacetylases, thereby epigenetically modifying mucosal immunity to attenuate inflammation while enhancing gut barriers.<sup>9–13</sup> In addition, as ligands of host G protein-coupled receptors (GPCRs), SCFAs regulate key functions of the gut, including transit and mucus secretion.<sup>6,9–13</sup> Upon entering the circulatory system, SCFAs can also signal the brain and other organ axes.<sup>6,9,13,14</sup> SCFAs that reach the central nervous system cross and bolster the integrity of the blood–brain barrier and promote neurogenesis and neuroplasticity.<sup>9</sup> Disruption of GMB signaling cascades contributes to cardio-metabolic and gastric system diseases linked to inflammation and a plethora of neurobiological dysfunctions, including opioid use disorder (OUD).<sup>15–22</sup>

The utility of opioids for treating chronic pain is compromised by the development of tolerance to its analgesic effects, which necessitates dose escalation that can produce physical dependence and place an individual at heightened risk for the development of an OUD. Opioids mediate their effects through activation of G<sub>i</sub>-coupled GPCRs, including the primary target of opioid analgesic drugs, the mu opioid receptor (MOR), which is expressed in the central and peripheral nervous systems, including the enteric nervous system.<sup>23</sup> MORs are also expressed by immune cells, some of which reside in the lamina propria of intestinal mucosa.<sup>24</sup> Many mechanisms have been hypothesized to contribute to analgesic tolerance. Broadly, these fall into two classes: loss of receptor function (receptor desensitization) and homeostatic cellular adaptations that recalibrate baseline signal transduction, thereby masking signaling from functional MORs.<sup>25</sup> The processes by which distinct types of MOR-

expressing cells adapt to counteract repeated MOR stimulation by chronic opioid likely differ by cell type.<sup>25,26</sup> Crucially, in MOR-expressing cells such as neurons that transmit sensation, known as nociceptors, the adaptations to chronic opioid drug cause a loss of morphine analgesia or antinociceptive tolerance to drug.<sup>27</sup> Removal of drug can produce rebound withdrawal effects that include a heightened sensation of pain known as hyperalgesia,<sup>28</sup> and severe gastric pain.<sup>29</sup> These rebound effects indicate that, in at least some tolerant states, MORs are present and functioning and that removal of drug unmasks the homeostatic cellular adaptations that produced the tolerance.<sup>30</sup> In humans and even in genetically inbred mice exposed to the same dose of opioid, the degree of antinociceptive tolerance varies, indicating factors beyond genetics or degree of drug exposure contribute to loss of opioid potency.<sup>31–33</sup> Understanding what underlies this variability in response to chronic opioid could produce new mechanistic insight. Preventing or delaying analgesic tolerance would reduce the need for dose escalation, thereby mitigating the risk of overdose and OUD development, and improving the utility of opioids.<sup>34</sup> Through their activation of MORs in the gastrointestinal tract, opioids impair motility and electrolyte secretion leading to constipation<sup>35,36</sup> and alter the gut microbiota.<sup>10,37–42</sup> Gut microbiota dysbiosis is implicated in opioid-induced changes in drug reward,<sup>42,43</sup> dependence,<sup>39,44,45</sup> hyperalgesia,<sup>42,46</sup> and analgesic tolerance.<sup>17,37,40</sup> Several studies document that morphine-induced gut microbiota dysbiosis and subsequent translocation of pathobionts across a morphine-compromised gut barrier trigger systemic inflammation that exacerbates the development of tolerance.<sup>26,34,40,47</sup> In agreement with this model, eliminating gut commensals prevents tolerance, and introduction of a common probiotic harboring *Lactobacillus* and *Bifidobacteria* or replenishment of gut commensals via fecal microbial transplantation (FMT) from opioid-naïve donors counters dysbiosis and antinociceptive tolerance.<sup>37,40,47,48</sup> Importantly, whereas opioid-driven dysbiosis contributes to tolerance, it is not sufficient, as FMT from opioid-induced tolerant donors does not compromise morphine antinociception<sup>40,48</sup> though it can

accelerate opioid-driven tolerance.<sup>40</sup> Indeed, opioid stimulation of MOR is necessary for tolerance as demonstrated by the ability of a peripherally restricted MOR antagonist to counter tolerance even in the presence of inflammation resulting from impaired barrier function.<sup>46,47</sup> Whether microbiota dysbiosis has a synergistic causative effect or tangentially influences tolerance, or if inflammation is its primary mediator, is yet unknown and awaits more mechanistic studies.

Importantly, the foundational studies above all minimized and collapsed natural variation in animal and microbiome responses to opioid by using high doses of opioid and aggregating data. Here, we designed a study to leverage both natural variability in the degree of antinociceptive tolerance to morphine and microbiota composition with the goal of identifying informative native microbiota signatures that could explain individual differences in the development of tolerance. We analyzed temporal changes in microbiota abundance, presence, variability, stability and interrogated the potential role of community interactions and metabolic functions<sup>49–52</sup> to expand our understanding of how opioid-induced gut dysbiosis contributes to liability of tolerance. We demonstrated that morphine-induced dysbiosis is inevitable, but tolerance is not. Furthermore, since morphine-induced progressive dysbiosis occurred in all mice, this largely obscured temporal signatures differentiating tolerant from non-tolerant mice that were only discernable by comparative approaches that control for common morphine-induced changes. While tolerant mice shared few distinguishing patterns other than the expected higher abundance of pathobionts, mice that did not develop tolerance displayed more shared and predictive features, pointing to a protective role of the microbial neuroactive metabolite butyrate, for preventing the development of tolerance.

## Materials and methods

### Animal use and care

Male wildtype C57/BL6J mice, *Mus musculus* (Jackson Laboratory) age matched, were used for both the oral morphine paradigm ( $n = 16$ , 8-week-old upon entering lever training with 0.2%

saccharine reward, and 11-week old at first morphine exposure)<sup>53</sup> and subcutaneous (s.c.) morphine paradigm ( $n = 52$ , 8-week-old at start of dietetic pre-treatment and 10–11-weeks at morphine exposure). An additional cohort of 8 ( $n = 4$  female and  $n = 4$  male, 11-week at first morphine exposure) wild-type C57/BL6J mice bred in-house at UC Davis were also subjected to the oral morphine paradigm and used as a test dataset for assessing the specificity and accuracy of microbiota associations in prediction models of morphine exposure. All mice had food *ad libitum* and were provided running wheels for enrichment. Mice in the oral morphine paradigm had two bottles, one with water and one with morphine, and they were individually housed allowing for the measurement of morphine consumption. Mice in the s.c. paradigm were communally housed (3–4 mice per cage) to minimize discomfort since all mice received the same morphine dosing. Mice used for the assessment of dietetic supplementation on tolerance had access only to water supplemented with either sodium butyrate (Sigma-Aldrich) or pH-matched (9.30–9.50) monosodium citrate (EMD) as a control at 100 mM, a concentration informed by a survey of prior studies evaluating benefits of butyrate.<sup>54,55</sup> Bottles containing freshly prepared and filter-sterilized butyrate and citrate were changed every 3 d for 3-weeks prior to morphine exposure and for the duration of the experiment.<sup>48,54,56</sup> All procedures involving animals were reviewed and approved by the Institutional Animal Care and Use Committees of the University of California, Davis (IACUC protocol number: 22085) or University of New Hampshire (IACUC protocol number: 230101).

### Morphine and naloxone administration

For the 18-week oral self-administration paradigm ( $n = 24$ <sup>53</sup>), mice had access *ad libitum* 5 d per week to both water and water supplemented with morphine sulfate (Mallinckrodt Pharmaceuticals, St. Louis, MO) sweetened with 0.2% saccharin to improve palatability, where the concentration of morphine sulfate was gradually escalated from 0.3 mg/mL, to 0.5 mg/mL, to a final concentration of 0.75 mg/mL during the first 3 weeks. Each week, mice had 2

d where only water was available. Voluntary morphine consumption was determined from bottle weight. Morphine treatment mice in the non-contingent subcutaneous (s.c.) morphine paradigm received 8 mg/kg morphine (Cayman Chemical, Ann Arbor, Michigan) in sterile 0.9% saline (Patterson Veterinary Supply, Greeley, CO) once each day for either 4 d ( $n = 14$ ) or 9 days ( $n = 27$ ) or received 10 mg/kg of s.c. morphine once each day for 9 d ( $n = 36$ ). Immediately following some assays for nociception using the ED<sub>90</sub> dose of morphine (5 + 2 mg/kg) on day 10 of the s.c. paradigm, mice were treated with 5 mg/kg s.c. naloxone, an antagonist of MOR, to displace morphine allowing observation of reversal of morphine-impaired constipation, where the number of fecal pellets produced in 20 min was recorded for each mouse and a greater number of pellets represents morphine-driven decreased transit.

#### **Determination of nociception and morphine antinociception**

The radiant heat tail-flick assay (Tail-flick Meter, Columbus Instruments) was used to assess baseline nociception and morphine antinociception. Light intensity was set to produce a baseline tail-flick latency of ~2.0 s with a maximum cutoff of 6 s (for oral paradigm) or 5 s (for s.c. paradigm) to minimize tissue damage. Latency was measured without morphine, and then 30 min after morphine injection. For the oral paradigm, mice received 6 mg/kg morphine (ED<sub>80</sub>)<sup>59</sup> before the study's start and again at the study's completion (Figure 2a). For the s.c. paradigm with FMT or butyrate/citrate feeding, antinociception was determined on days 1, 7 and 10 at 30 min after a 5 mg/kg dose of morphine (ED<sub>60</sub>), followed by a second dose of +2 mg/kg morphine (combined ED<sub>90</sub>) and a second latency was measured 30 min later. Saline control mice ( $n = 31$ ) only received morphine for the antinociception tests on day 10. The percent maximum possible effect (%MPE) was calculated with the following formula:  $100 * [(drug\ response\ time - population\ baseline\ latency) / (cutoff\ time - population\ baseline\ latency)]$ . All tail-flick tests were blinded to prevent bias. Dose responses were evaluated with 12-week-old male mice to optimize

doses for maximum statistical power and effect size using power analysis. These and the cumulative-dose responses for evaluating tolerance were fit using GraphPad Prism. The ED<sub>50</sub> values of morphine and their 95% confidence intervals were calculated, and a shift in ED<sub>50</sub> from day 1 to day 10 was calculated. Statistical support for a change in morphine potency was determined by a two-tailed Ptest, testing the null hypothesis that the dose response slope on day 10 did not differ from the slope on day 1. Mice with the same %MPE at both doses (either at ceiling at 5 mg/kg or at floor at 5 + 2 mg/kg) were not used to calculate change in slope. Mice with sustained antinociception at the end of either the oral or s.c. paradigm (100% MPE) were classified as “non-tolerant”, whereas mice with reduced morphine antinociception from day 1 values (<100% MPE) were classified as “tolerant”.

#### **Fecal microbiota transplantation**

To generate feces for fecal microbial transplantation (FMT), a small cohort of male wildtype C57BL/6J mice ( $n = 14$ ) received 8 mg/kg s.c. morphine for 4 d were assessed for tolerance on day 5 with 6 mg/kg s.c. morphine using the radiant heat tail-flick assay. A total of 2.7 g of feces pooled from multiple individuals of two populations, one that did not become tolerant (maintained 100% MPE) and one that did become tolerant (displayed < 100% MPE), were collected and immediately cryopreserved at -80°C both for use in FMT and for microbiota analysis. These feces were sufficient for the inoculation of each treatment group ( $n = 14$  for each FMT treatment group;  $n = 9$  receiving s.c. morphine and  $n = 5$  receiving s.c. saline carrier). The feces from tolerant and non-tolerant mice were subsequently defrosted on ice and suspended in a total of 32.4 mL of cold (4°C) phosphate-buffered saline (PBS) containing 10% glycerol.<sup>48</sup> The suspension was homogenized and then centrifuged at 800 g for 3 min,<sup>48</sup> and the supernatant of each was aliquoted in 2.8 mL volumes in separate tubes and cryopreserved at -80°C. Additionally, 100 µL aliquots of each homogenized suspension from pooled tolerant and pooled non-tolerant mice were reserved for microbiota (16S) analysis. Upon entering the FMT study, recipient mice were administered 100 µL of the fecal supernatant twice

daily<sup>48</sup> for 9 d via intragastric gavage. Feces were collected from all mice on day 0 (pre-treatment) and 10 and stored at  $-80^{\circ}\text{C}$ . Analyses of the microbiota of tolerant and non-tolerant pooled donor feces were limited due to lack of statistical power (of only two samples), but comparison of compositional differences was illustrated using the `ps_venn` function in the `MicEco` R package (v0.9.15)<sup>60</sup> to determine the overall number of unique and shared amplicon sequence variants (ASVs).

### **Statistical analysis of animal data**

Linear regression analyses using Pearson's correlation coefficient<sup>61</sup> determined whether morphine antinociception significantly correlated with total morphine consumption using the R package `ggpubr` (v0.6.0).<sup>62</sup> Normality of data was assessed using a Shapiro–Wilk test, and homogeneity of variance was assessed using Levene's test. Data with a p-value greater than 0.05 were considered normal. One-way ANOVA followed by post-hoc analysis using Tukey's Test for multiple comparisons was used to compare differences between groups where assumptions for normality and homogeneity of variance were met. The Kruskal–Wallis test followed by the pairwise Wilcoxon test with corrections for multiple comparisons was used when assumptions of normality and homogeneity of variance were not met. All statistics were conducted using the R package `stats` (v4.3.0).<sup>63</sup> Visuals were generated using R 4.2.0 software, GraphPad Prism, BioRender, and some composite figures were modified with Adobe Illustrator.

### **16S rDNA library preparation and sequencing**

Individual mice were placed in clean cages with no bedding for an hour to defecate normally. Fresh feces were collected and immediately cryopreserved at  $-80^{\circ}\text{C}$ . Samples were randomized across 96-well plates using the R package `wpm` (v1.14.0) to minimize the introduction of batch effects from multiple DNA extractions and sequencing runs.<sup>64</sup> Feces were lysed using the Qiagen TissueLyser II (Qiagen, Germantown, MD) for 5 min at 30 hz. Microbial genomic DNA was extracted from frozen feces (~100 mg, or five pellets) with the ZymoBIOMICS 96 MagBead DNA Kit with lysis

tubes (Zymo Research, Irvine, CA), according to manufacturer's protocol. DNA was quantified using the iT dsDNA Broad-Range kit (Invitrogen, Life Technologies, Grand Island, NY) using a Tecan M200 plate reader (excitation 480 nm/emission 530 nm) (Tecan, Männedorf, Switzerland) in a Costar black, clear bottom plate (Corning, Corning, NY). Genomic DNA samples were standardized (11 ng/ $\mu\text{L}$ ) and freshly diluted up to 1.1 ng/ $\mu\text{L}$  prior to two successive polymerase chain reaction (PCR) amplifications. The V4–V5 16S variable regions were first amplified in 10  $\mu\text{L}$  reactions in triplicate using the NEB Q5 hot Start HiFi 2X master mix (New England BioLabs, Ipswich, MA) and 515F and 926R primers as described<sup>65,66</sup> and modified to include the forward and reverse primer pad and linker at the 5' end of each primer. The cycling parameters were as follows:  $98^{\circ}\text{C}$  for 2 min, followed by 22 cycles of  $98^{\circ}\text{C}$  for 10 s,  $53^{\circ}\text{C}$  for 15 s, and  $72^{\circ}\text{C}$  for 15 s, and completing with  $72^{\circ}\text{C}$  for 2 min. Following estimation of size, quality, and quantity of amplicons by gel electrophoresis, pooled amplicons were enzymatically cleaned with ExoSap-IT (Applied Biosystems, Thermo Fisher Scientific, Waltham, MA) and diluted 1:5 in nuclease-free water prior to indexing. In the second step, amplicons were indexed using xGen UDI Primer Pairs (10 mm) in 12  $\mu\text{L}$  reactions using the NEB Q5 Hot Start HiFi 2X master mix (New England BioLabs, Ipswich, MA) with the following parameters:  $98^{\circ}\text{C}$  for 30 s, followed by 10 cycles of  $98^{\circ}\text{C}$  for 10 s,  $65^{\circ}\text{C}$  for 15 s, and  $72^{\circ}\text{C}$  for 20 s, and a final step of  $72^{\circ}\text{C}$  for 2 min. Amplicon band size, quality, and quantity were verified using 2% agarose by gel electrophoresis. Indexed amplicons were pooled in a final library and purified with the Mag-Bind Total Pure NGS kit (Omega Bio-Tek, Norcross, GA). The pooled library was quantified using the Qubit dsDNA High Sensitivity kit (Invitrogen, Life Technologies, Grand Island, NY) and the Qubit 2.0 fluorometer (Invitrogen, Life Technologies, Grand Island, NY). Final amplicon libraries were sequenced and demultiplexed on the Illumina NovaSeq 6000 platform (2  $\times$  250 bp paired end) at the Hubbard Center for Genome Studies at the University of New Hampshire (Durham, NH). Computations were performed on Premise, a central, shared HPC cluster at the University of

New Hampshire (Durham, NH) supported by the Research Computing Center and PIs who have contributed compute nodes.

### **Processing of 16S rDNA sequencing reads**

All components needed to generate microbial community profiles (e.g., taxonomic assignments, sequence counts, sample metadata, phylogenetic tree) and to conduct downstream analyses were stored in an experiment-level object using the R package phyloseq (v1.40.0).<sup>67</sup> For a summary of 16S processing and analysis, see Supplemental Figure S1.

Amplicon sequencing primers were removed from demultiplexed sequencing reads using the cutadapt plugin<sup>68</sup> in the QIIME 2 2020.2 pipeline<sup>69</sup> before being processed using the R package DADA2 (v1.18) quality control pipeline<sup>70</sup> and custom scripts for post-processing artifact removal. Taxonomy was assigned using the GreenGenes reference database (v13.8).<sup>71</sup> Species, where applicable, were identified using rRNA/ITS databases with the nucleotide basic local alignment search tool (blastn).<sup>72</sup> A taxonomic filter was applied to remove unclassified phyla, chloroplasts, and mitochondria, along with an additional abundance filter to remove singletons and doubletons from the dataset (phyloseq v1.40.0).<sup>67</sup> Maximum likelihood phylogenetic trees with bootstraps were estimated from MAFFT (v7.305b)<sup>73,74</sup> alignments using RAxML (v8.2.10),<sup>75</sup> followed by tip-agglomeration ( $h = 0.05$ ) to combine similar amplicon sequence variants (ASVs) into one representative taxon sequence or taxa agglomeration to the genus level using phyloseq (v1.40.0).<sup>67</sup> Sequencing counts were transformed to relative abundances (phyloseq v1.40.0)<sup>67</sup> or normalized to center-log ratios (R package microbiome v1.18.0).<sup>76</sup>

The presence of batch effects that may introduce bias was assessed by comparing sequenced controls using the R package MMUPHin (v1.10.0)<sup>77</sup> and principal coordinate analyses (PCoA). The controls used to assess bias included 1) a ZymoBIOMICS Microbial Community Standard II (Log Distribution) to detect bias introduced during DNA extraction, 2) a ZymoBIOMICS Microbial Community DNA Standard II (Log Distribution)

to detect bias introduced during amplification, 3) a randomized representative mouse fecal sample to detect bias introduced from multiple sequencing runs, and 4) a no-template mock DNA extraction to capture potential contaminants.

### **Analysis of microbiota diversity**

Overall gut microbiota diversity and temporal changes assessed by weighted UniFrac,<sup>78</sup> unweighted UniFrac<sup>79</sup> (membership), and Bray-Curtis dissimilarity (relative abundance) were analyzed using PCoA. Permutation Multivariate Analysis of Variance (PERMANOVA) tests<sup>80</sup> determined any statistical differences between experiences and the development of antinociceptive tolerance throughout the paradigm using the permanova pairwise function in the R package ecole (v0.9–2021).<sup>81</sup> Prior to using PERMANOVA, pairwise permutation tests<sup>82,83</sup> for homogeneity of multivariate dispersion<sup>84–86</sup> determined any statistical differences in group variances of experiences and the development of antinociceptive tolerance throughout the paradigm using the betadisper and permutest functions in the R package vegan (v2.6–4).<sup>87</sup>

Alpha-diversity of non-tolerant and tolerant gut microbiota were analyzed using the estimate\_richness function for Shannon diversity in the R package phyloseq (v1.40.0).<sup>67</sup> Average alpha-diversity and standard errors were plotted sequentially and abrupt variations over time that may represent key transitions were detected using a Bayesian analysis of change point in the R package bcp (v4.0.3),<sup>88</sup> which implements the Barry and Hartigan product partition model for the standard change point problem using Markov Chain Monte Carlo.<sup>89</sup> Timepoints with a posterior probability of change in the mean abundance greater than 0.70 of community members in tolerant or non-tolerant mice were marked on time-series plots.

### **Differential abundance and biomarker analyses**

Community members, grouped at the genus level, that were different in abundance between tolerant and non-tolerant mice, and between pre-, during, and post- morphine exposure

phases of the paradigm were determined using the differential test within the R package `corn-cob` (v0.3.1).<sup>90</sup> Non-normalized counts were used with the Wald (abundance) or LRT (variability) setting within the differential test to distinguish community members associated with the covariate of interest controlling only for sequencing run and phase of morphine. The count abundance for each genus was fit to a beta-binomial model using the logit link functions for both the mean and overdispersion simultaneously. The null and non-null overdispersion models were specified with the same confounding variables (paradigm experience and sequencing plate) to identify only genera having differential abundances associated with the covariate of interest. The list of differentially abundant and/or variable community members produced was further analyzed using linear discrimination analyses of effect size (LEfSe Galaxy v1.0)<sup>91</sup> to identify any community members that most likely explain differences between a covariate of interest. These community members were visualized using the `amp_heatmap` function in the R package `ampvis2` (v 2.8.9) on a log<sub>2</sub> color scale and the minimum abundance set to null.

### **Indicator species and prediction models**

We used an indicator species analysis to determine community members unique to experiences and to provide evidence for the impacts of experience on the gut microbiota.<sup>58</sup> Furthermore, we tested whether there were combinations of up to 3 indicator species that could predict whether a sample was from a morphine exposed gut microbiota. Abundance data for the cohort was transformed into presence absence data and indicator value analysis with experience as the grouping (pre-morphine, morphine, post-morphine) was performed using the `multipatt()` function with 999 permutations in the R package `indicspecies`.<sup>58</sup> To determine which combinations of community members could best predict whether a sample was from morphine exposure, we reduced the dataset to samples that were from pre-morphine or mid-late morphine and used the `indicators()` function with up to 3 combinations of community members, and

subsequently the `pruneindicators()` function to assess which combinations were best predictors. Next, we tested whether the combinations which were only found in mid-late morphine samples (Probability  $A = 1$ ) could accurately predict which samples were most likely from morphine-exposed microbiota from a separate cohort of eight animals ( $n = 4$  female,  $n = 4$  male) that consisted of 40 pre-morphine, 102 morphine samples, and 15 post-morphine samples.

### **Longitudinal change point analysis**

Abrupt variations over time that may represent key transitions in community members that were differentially abundant between tolerant and non-tolerant mice were detected using a Bayesian analysis of change point in the R package `bcp` (v4.0.3),<sup>88</sup> which implements the Barry and Hartigan product partition model for the standard change point problem using Markov Chain Monte Carlo.<sup>89</sup> Timepoints with a posterior probability of change in the mean abundance greater than 0.790 of community members in tolerant or non-tolerant mice were marked on time-series plots.

### **Analysis of temporal stability**

The temporal stability of populations (All ASVs, grouped at the genus level) exposed to morphine was evaluated and visualized within the context of Taylor's power law, which describes the ubiquitous macroecological relationships between the mean and variance of an individual taxon.<sup>92</sup> Two extensions of this law were used to examine whether the microbiota of tolerant and non-tolerant mice differ in variability or stability. The Type I power law extension was used to detect differences in temporal variability of tolerant and non-tolerant microbiota across all phases of morphine experience and the Type IV power law extension was used to examine differences in microbiota stability relative to starting composition at each phase of morphine experience.<sup>93</sup> When applying the Type IV extension, Taylor's power law which is described by the formula  $V = aM^b$ , where  $V$  is the variance,  $a$  is a scalar parameter,  $M$  is the mean, and  $b$  is an exponential parameter, the formula was



log-transformed,  $\ln(V) = b\ln(M) + \ln(a)$ , where  $b$  is the slope parameter.<sup>93,94</sup> The exponential/slope parameter  $b$  of the Type IV power law extension was standardized by subtracting the mean  $b$  of all individuals pre-morphine from each individual mouse's value for  $b$  at each morphine experience to produce the change in slope. Positive values of the slope parameter  $b$  represent instability, whereas 0 or negative values of the slope parameter  $b$  represent stability relative to pre-morphine.

### Microbiome association networks

Microbial association networks were inferred from the gut microbiomes of mice before entering the self-administration of oral morphine phase in the paradigm compared to the gut microbiomes after 18-weeks of morphine administration to 1 week post-administration. Community members were grouped at the genus level using the `tax_glom` function from `phyloseq` (v1.40.0).<sup>67</sup> Seventy out of 165 taxa grouped at the genus level were at the highest frequency. SPRING associations were measured in the gut microbiota split by whether they were taken before or after morphine exposure and another iteration where microbiota were split based on the development of antinociceptive tolerance. Microbial association networks for each group were inferred using the signed distance, `nlambda`, and `rep.num` (100) functions in the R package `NetCoMi` (v1.1.0).<sup>57</sup> For reproducibility, microbial association network analyses used the random seed "12345". Differential networks were inferred from SPRING association networks using fisher test adjusting for false discovery rate.

### Analysis of predicted functional profiles

Functional profiles of gut microbiota from tolerant and non-tolerant mice were predicted from representative ASVs of 16S rDNA sequences using phylogenetic investigation of communities by reconstruction of unobserved states (PICRUSt 2.0) pipeline.<sup>95</sup> Gene content, represented by Enzyme Classification (EC) numbers (i.e., gene family copy numbers of ASVs and abundances per sample) per ASV,

was predicted<sup>96</sup> by aligning ASVs to reference sequences and placement into a reference phylogenetic tree.<sup>97-99</sup> MetaCyc functional pathways and associated abundance were inferred from EC number abundances.<sup>100</sup> Differential abundance testing of functional pathways between tolerant and non-tolerant mice was analyzed<sup>101</sup> across three models, including ALDEx2,<sup>102</sup> DESeq2,<sup>103</sup> and edgeR<sup>104</sup> using the R package `ggpicrust2` (v1.7.3).<sup>101</sup>

### Assessment of butyrate biosynthetic capacity

To assess the ability of intestinal microbiota to synthesize butyrate, we quantified two genes that encode proteins in the butyrate production pathways, including butyryl-CoA transferase (BCoAT; *bcoat* or *but*) and butyrate kinase (*buk*) using the primers *bcoat*-F 5'-GCIGAICATTTTCACITG GAAYWSITGGCAYATG-3' and *bcoat*-R 5'-CCTGCCTTTGCAATRTCIACRAANGC-3',<sup>105</sup> along with Buk-5F1 5'-CCATGCATTAATA TCAAAAAGC-3', Buk-5F2 5'-CCATGCGTT AAACCAAAAAGC-3', Buk-6R1 5'-AGTA CCTCCACCCATGTG-3', Buk-6R2 5'-AATACC TCCGCCCATATG-3' and Buk-6R3 5'-AATACCGCCRCCCATATG-3'.<sup>106</sup> by quantitative real-time PCR (qPCR). Copy numbers were normalized to the bacterial 16S rRNA gene copy number amplified by the universal primer set 16S rRNA-F 5'-AGAGTTTGATYMTGGCTCAG-3' and 16S rRNA-R 5'ACGGCTACCTT GTTACGACTT-3'.<sup>105</sup> The qPCR was performed in duplicate in a final volume of 20  $\mu$ l using PerfeCTa SYBR Green FastMix Low ROX (Quantabio, Beverly, MA) with fecal DNA (30 ng for BCoAT, 10 ng for *buk*, and 1 ng for 16S rRNA) and 100 nM of each primer for *bcoat* and 16S rRNA, and for *buk* 800 nM forward primers, and 1400 nM reverse primers (400 nM buk-6R1, 200 nM buk-6R2 and 800 nM buk-6R3). Cycling conditions for both BCoAT and 16S rRNA were as follows: 95°C for 3 min followed by 40 cycles at 95°C for 30 s, 56°C for 30 s, 72°C for 40 s for BCoAT and 2 min for 16S rRNA and a final extension at 72°C for 5 min.<sup>105</sup> The cycling parameters for *buk* were an initial denaturation at 95°C for 5 min followed by 40 cycles at 95°C for 30 s, 52°C

for 30 s, and 71°C for 30 s.<sup>107</sup> Student's T-test determined significant differences between groups.

### **Blood serum biomarkers of inflammation and bacterial translocation**

Serum was separated from clotted blood collected via terminal bleed by cardiac puncture using an 18-gauge needle and assayed for various indicators of systemic inflammation and bacterial translocation. Briefly, collected blood was allowed to clot for 30 min before a 10-min centrifugation at  $2,000 \times g$  and 4°C. Each serum sample was aliquoted into replicate tubes and stored at -80°C, each of which was only thawed once for subsequent assays. Serum cytokines (IL-1 $\beta$ , IL-6, and TNF- $\alpha$ ) were quantified using reagents and manufacturer's protocols for the BioPlex Pro mouse cytokine Th17 Panel A kit from BioRad (Hercules, CA, USA) at the IDDRC Biological Analysis Core laboratory (UC Davis, CA, USA).

To assess the extent of bacterial translocation from the intestines, serum was assayed for bacterial lipopolysaccharide (LPS) and for LPS binding protein (LBP) as a surrogate for liver response to bacterial translocation. Serum was diluted 1:100 in endotoxin-free tris buffer pH 8.0 and LPS quantified in duplicate using the Pierce LAL Chromogenic Endotoxin Quantification Kit (Thermo Scientific, Waltham, MA, USA) with the low range standards and following manufacturer's protocol. The resulting chromogenic substrate was quantified at OD<sub>405</sub> nm using an Infinite M200 plate reader (Tecan, Morrisville, NC, USA). LBP was quantified from serum diluted 1:100 in dilution buffer using the Mouse LBP Elisa kit (Invitrogen, Waltham, MA, USA) following the manufacturer's protocol. The resulting chromogenic substrate was quantified at OD<sub>450</sub> nm using a Tecan Infinite M200 plate reader (Morrisville, NC, USA).

## **Results**

### **Not all mice developed antinociceptive tolerance to chronic voluntary oral morphine**

To examine the variables that contribute to differences in OUD liability, particularly antinociceptive tolerance to morphine, individually

housed wild-type mice underwent an 18-week longitudinal paradigm of voluntary oral morphine self-administration, where they had *ad libitum* access to both morphine and water.<sup>53</sup> To determine the development of tolerance, we used reflexive tail-flick to radiant heat to measure nociception – the ability to sense – and antinociception – the ability of morphine to block sensation – with a non-contingent morphine dose (6 mg/kg, s.c.) at the start and end of the self-administration phase of the paradigm (Figure 1a). Mice in this paradigm displayed variability in day 0 baseline morphine antinociception and in tolerance to antinociception after 18-weeks of morphine self-administration (Figure 1b). More than a third of mice (6/16) maintained 100% of the maximum possible effect (MPE) to morphine antinociception (i.e. non-tolerant) after 18-weeks of self-administration. As a population, after 18-weeks of morphine, mice in our paradigm did not display a significant decrease in the baseline nociceptive threshold in the absence of morphine (i.e. hyperalgesia), despite consuming, on average, 25 mg/kg of morphine daily (range of 5–120 mg/kg daily; Figure 1c & Supplemental Figure S2). Tolerance to morphine (e.g. decreased % MPE from individual day 0 measurements) did not correlate with a change in baseline nociceptive threshold in the absence of morphine, indicating that tolerance was not driven solely by hyperalgesia (Supplemental Figure S2B). Importantly, individual variation in morphine tolerance also did not correlate with the amount of morphine each mouse consumed (Figure 1c), indicating that variables beyond the degree of drug intake influenced the development of tolerance. Individual pre-morphine microbiota, as determined from 16S rRNA libraries generated from feces, were highly variable (Figure 1d,  $p_{\text{PERMANOVA}} = 0.0001$ , Supplemental Table S1) even though the mice were of the same age, sex, inbred genotype, and from the same commercial source. This led us to hypothesize that holobiont genetic variation in the form of the hosts' starting microbiome and/or its response to morphine might explain differences in the development of antinociceptive tolerance.

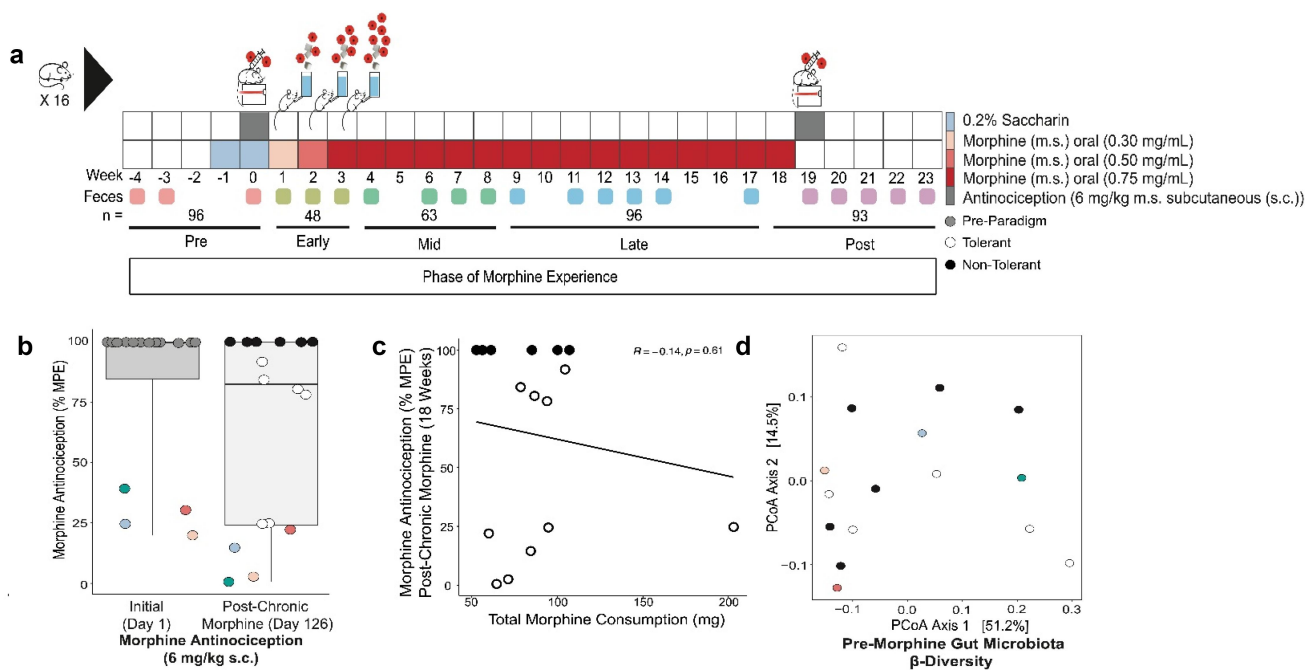


**Figure 1.** Natural variability in antinociceptive tolerance to chronic morphine does not correlate with the amount of morphine mice voluntarily consumed. a) Mouse ( $n = 16$ ) chronic morphine oral self-administration paradigm where voluntary morphine consumption was monitored.<sup>53</sup> Feces were collected and used to generate 16S (V4-V5 region, see methods) for microbiota analysis. b) Morphine antinociception (6 mg/kg s.c.,  $ED_{80}$ ) was determined pre- and post- chronic morphine (week 19) using a radiant heat tail flick assay to determine tolerance to morphine. Data is reported as maximum possible effect (% MPE). Colored individuals exhibited low starting antinociception which decreased further after chronic morphine consumption consistent with tolerance c). Linear regression of total morphine consumption with degree of tolerance ( $y = 78 - 0.16x$ ;  $R^2 = -0.14$ ; Pearson's correlation  $p$ -value = .61). d) Pre-morphine gut microbiota  $\beta$ -diversity (Bray-Curtis dissimilarity) was visualized by principal coordinates analysis (PCoA). See supplemental table S1 for details.

### **Morphine induced progressive dysbiosis in all mice regardless of whether they did or did not develop tolerance**

We capitalized upon our unique experimental design of intensive sampling to map the temporal impact of morphine on gut microbiota, thereby capturing snapshots of mouse guts at different phases of morphine experience. We then evaluated whether differences in microbiota were associated with variability in tolerance (Figure 2 and Supplemental Figure S3; details provided in Supplemental Tables S1 & S2). Preliminary exploration of microbiota using Bray-Curtis dissimilarity of all amplicon sequence variants (ASVs) demonstrated how morphine caused progressive shifts in bacterial community assemblages ( $p_{\text{PERMANOVA}} \leq 0.01$  for all pair-wise comparisons, Supplemental Table S1), even in mice that did not develop antinociceptive tolerance to morphine (Figure 2a, Supplemental Table S1). The microbiomes of tolerant and non-tolerant mice did not

form separate clusters at any phase of the paradigm, and because of this, it is apparent that the experience of morphine was the primary driver of microbial communities (Figure 2a and Supplemental Figure S3). We also investigated whether morphine increased variability as a dimension of dysbiosis (Supplemental Figure S4). Early morphine exposure increased the number of variable genera relative to pre-morphine, and as morphine exposure continued, the number of variable genera increased again later in the paradigm and remained variable even post-morphine.

To further visualize dysbiosis, we examined how global network properties and differential networks of microbiota were impacted by morphine, as context for identifying differences between tolerant and non-tolerant mice.<sup>57</sup> Comparisons of high-level relationships revealed that the connections among the most central nodes that represent keystone species (community members that connect the most community members) were significantly weaker and at times

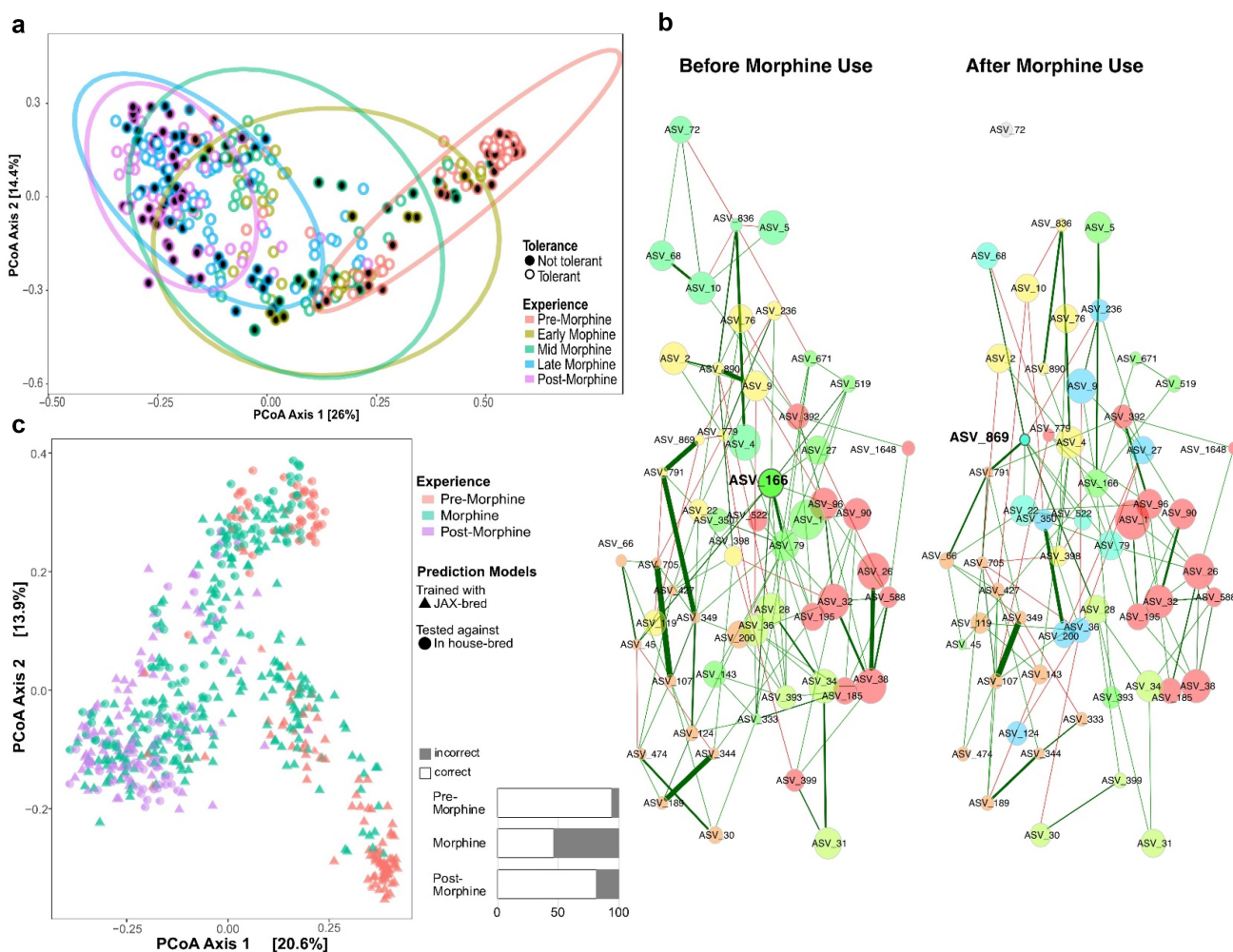


**Figure 2.** Chronic morphine-induced predictive dysbiosis in all mice. a) Temporal changes in gut microbiota  $\beta$ -diversity (all ASVs, Bray-Curtis dissimilarity) as visualized by principal coordinates analysis (PCoA). See supplemental table S1 for details. b) Comparison of bacterial association networks before (left) and after 18 weeks (right) of oral morphine using the SPRING method in NetCoMi.<sup>57</sup> edges are colored by sign (positive: green, negative: red), representing estimated associations between community members. *Adlercreutzia* (ASV\_166) and *Streptococcus* (ASV\_869) are the only two community members identified as hubs (bolded text and borders). Eigenvector centrality was used for scaling node sizes and colors representing clusters of genera (determined using greedy modularity optimization). Clusters have the same color in both networks if they share at least two taxa. Nodes that are not connected in both groups were excluded. Corresponding taxa names detailed in supplemental table S3. c) Predictive modeling of morphine-exposed microbiota (using R program indicpecies).<sup>58</sup>  $\beta$ -diversity (all ASVs, Bray-Curtis dissimilarity) as visualized by principal coordinates analysis (PCoA). The starting composition of microbiota of mice that trained the models (jax-bred, orange triangles), which group in the lower right corner, and of mice that tested the models (in-house-bred, orange circles;  $n = 8$  mice), which group in the upper right corner, differ but converge upon exposure to morphine. The right bar graphs show % accuracy of the models to predict whether microbiota from in-house-bred mice resulted from morphine exposure (as % correct/incorrect). See supplemental tables S4 and S5 for details.

eliminated by chronic morphine, but these changes were not driven by individual genera within each central node (Figure 2b, detailed in Supplemental Table S3). Subsequent examination of pair-wise community member associations from these networks further reflected how morphine weakened or caused a loss of many associations (Supplemental Table S3). One positive association between two potential

pathobionts, *Desulfovibrionaceae* and *Bacteroidales*, became stronger and one association between related Gram-positive taxa, an unclassified member of family *Erysipelotrichaceae* and genus *Coprobacillus*, was gained.

Since morphine experience in the paradigm appears to be a strong driver of microbiome assemblages, we evaluated whether morphine-

driven disturbances were predictive of morphine use, thereby strengthening inferences from microbiota associations. We did this by determining how well combinations of associated taxa identified from our experimental cohort could distinguish between pre-morphine versus morphine-treated microbiota from a different cohort of mice that experienced the same self-administration paradigm (Figure 1a). To evaluate this, we trained models on 30,295 different combinations of up to three community members associated with mid- to late morphine with our experimental cohort of mice (bred at Jackson Laboratory, JAX). We then tested these models on microbiota from a second cohort of mice bred in-house ( $n = 4$  female,  $n = 4$  male) (Figure 2c, data and statistics summarized in Supplemental Table S4 & S5). Even though the starting composition of the two experimental cohorts differed substantially, likely reflecting breeding facility, predictive models using the top eight ranking community profiles accurately identified most pre-morphine microbiota (Figure 2c). Furthermore, the models also had similar predictive power on all morphine-exposed microbiota of the in-house-bred mice compared to JAX-bred mice (46% as opposed to 57%). The robustness of the models across independent experiments throughout the paradigm suggests that nuances in starting microbiota composition did not strongly impact global morphine-induced compositional changes, even those that were sustained after morphine was removed and that morphine induced common, predictive changes in the microbiota. This also exemplifies how co-occurrence indicator analyses could prove useful for identifying morphine use.

**Morphine concurrently depleted mutualistic community members that support gut homeostasis and increased relative abundance of pathobionts**

Using taxonomic assignments, we identified the genera that were altered by morphine and best explained differences between pre-morphine and morphine-exposed microbiota, representing biomarkers of morphine exposure.<sup>90</sup> We then visualized temporal changes in their abundance during the different phases of morphine experience (see

Figure 1a) compared to pre-morphine to glean insight into the dynamics of morphine dysbiosis (Figure 3a, Supplemental Table S2). Among 33 taxa identified as biomarkers, most were depleted by morphine and only emerged as biomarkers after prolonged morphine exposure. Fewer taxa increased in abundance with morphine exposure (Figure 3a, Supplemental Table S2). All biomarker taxa were also differentially variable in response to morphine (e.g. Supplemental Figure S4). Congruent with the expectation of morphine-driven dysbiosis, some potential pathobionts, including *Allobaculum*, *Prevotella*, *Erysipelotrichaceae*, and *Streptococcus*,<sup>108–113</sup> increased in abundance with morphine treatment, whereas some potential mutualistic taxa, including *Akkermansia*, *Bacteroides*, *Clostridium*, and *Rosburia*,<sup>26,114,115</sup> decreased in abundance (Figure 3b, Supplemental Table S2). Notably, many of the microbiota depleted by morphine are associated with gut barrier integrity and/or are predicted SCFA-producing taxa<sup>26,116–120</sup> (Figure 3b, Supplemental Tables S6 & S7). Though these potentially beneficial genera trended toward a gradual depletion, some increased in abundance at times, including *Clostridium*, *Parabacteroides*, *Lactobacillus* and *Blautia*<sup>116,121,122</sup> (Figure 3a, Supplemental Table S6 & S7).

Collectively, these analyses highlight the significant, progressing, and enduring effects of prolonged morphine use, where the microbiota did not return to its pre-morphine exposure state, at least not within the several weeks after morphine was removed (see Figure 1a for paradigm details). These changes also align well with evidence that morphine-driven dysbiosis precipitates tolerance via pathobiont overgrowth which has the potential to trigger uncontrolled inflammation due to loss of commensals that help to attenuate this inflammatory response.<sup>10,37–42</sup> However, morphine produced significant, progressing dysbiosis in all mice, even those that did not develop tolerance and, as such, tolerance cannot be explained simply by these global changes. We posited that if nuanced differences in the responses of the microbiota contributed to differences in the development of tolerance, they would likely be overshadowed unless the analyses accounted for the common morphine experience through time.

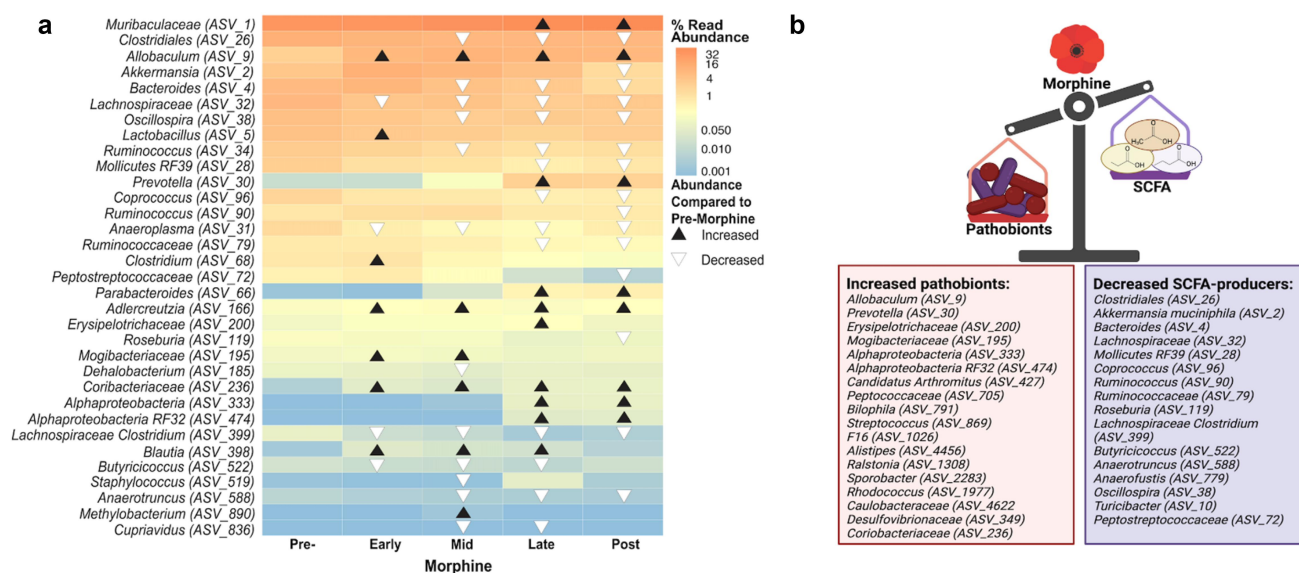


**Figure 3.** Morphine led to concurrent increase in pathobionts and decrease in mutualists that produce short chain fatty acids (SCFAs). a) Biomarkers of morphine consumption were identified from among the community members whose abundance was significantly altered by morphine (37 species, ~21% of taxa) using corn-cob binomial regression models,<sup>90</sup> followed by a linear discrimination analysis (LDA) of effect size (LEfSe).<sup>91</sup> Triangles indicate where in the paradigm the community member was a biomarker and whether its abundance increased (black) or decreased (white) compared to pre-morphine. Community members are labeled at the lowest taxonomic classification available. See supplemental table S2 for details. b) Functions of the microbiota that were differentially abundant during and after morphine exposure relative to their starting abundances were inferred from published studies (see supplemental table S7). Figure created with BioRender.com.

### Tolerant mice exhibited earlier microbiota instability and depletion of beneficial taxa

Even with the dominating morphine-induced dysbiosis in all mice, there were clues that morphine disturbed the microbiota differently in tolerant and non-tolerant mice. We explored this potential using a Bayesian methodology to examine change-points in  $\alpha$ -diversity. This analysis revealed a significant decrease in count and balance of ASVs, and this occurred earlier, by week five of morphine exposure in tolerant mice as opposed to week 9 in non-tolerant mice (Figure 4a). Analysis of  $\beta$ -diversity also revealed that the microbiota of tolerant and non-tolerant mice differed in membership and abundance during morphine consumption ( $p_{\text{PERMANOVA}} = 0.0022$ , weighted UniFrac), though diversity did not differ either before or after morphine (Supplemental Table S1). These results suggest a link between the progression of microbiome dysbiosis and the difference in tolerance. The dramatic drop in diversity identified in microbiota from tolerant mice was detected during the mid-morphine phase of exposure but may have resulted from an earlier loss of

stabilizing community members, as evidenced by divergences in diversity during the early morphine phase of exposure (Figure 4a).

We next identified differentially abundant genera associated with the development of tolerance/protection from tolerance using a beta-binomial regression model to control for the phase of morphine experience.<sup>90</sup> From among these genera, we identified biomarkers – genera that are significantly correlated with and most explained the difference between tolerant and non-tolerant mice.<sup>91</sup> These analyses revealed relatively few biomarkers, eight for tolerant mice and 11 for non-tolerant mice (Figure 4b, see Supplemental Table S8 for details and statistics). Three genera, all recognized as “probiotic,” were biomarkers before morphine exposure. Specifically, tolerant mice initially harbored higher abundances of *Lactobacillus* and *Bifidobacterium*, whereas non-tolerant mice exhibited higher abundances of *Akkermansia muciniphila* (Figure 4b). Although *A. muciniphila* increased after morphine exposure in tolerant and non-tolerant mice alike, a higher level was maintained longer in non-tolerant mice (Figure 4b, Supplemental Figure S5). Earlier change-points, or

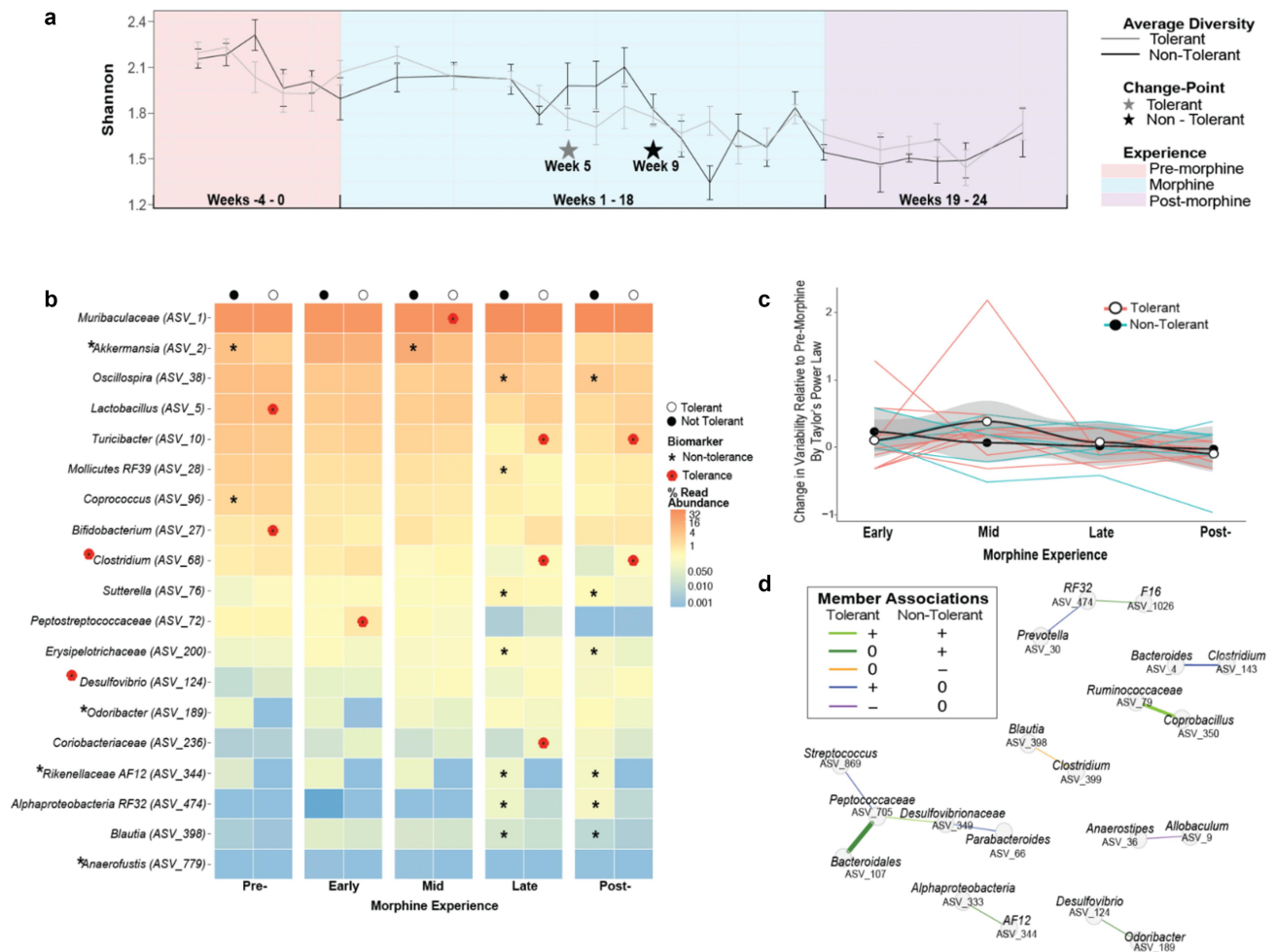


**Figure 4.** Analysis of differential responses of the microbiota to morphine disturbance reveal microbiota associations with variability of tolerance. a) Change in average microbiota  $\alpha$ -alpha diversity at the genus level is plotted sequentially by sample number for tolerant (gray line) and non-tolerant (black line) mice, assessed using number and evenness of species (Shannon). Bayesian change-points in diversity of tolerant (gray star) and non-tolerant (black star) mice are shown. Error bars represent SEM. b) Biomarkers of antinociceptive tolerance to morphine were identified from among the community members whose abundance was explained by tolerance (as identified using corncob regression models),<sup>90</sup> followed by a linear discrimination analysis (LDA) of effect size (LEfSe)<sup>91</sup> representing genera that most likely explain differences between the microbiota of tolerant (poppy symbol) or non-tolerant (asterisk) mice. Community members are labeled at the genus level or at the lowest taxonomic classification available. *Desulfovibrio*, *Odoribacter*, and *Anaerofustis* were only identified as biomarkers when microbiota from all experiences were combined. See supplemental table S8 for details. c) Temporal stability of the gut microbiota of individual mice at each phase of morphine experience was assessed by analysis of type IV Taylor's power law parameters.<sup>92,93</sup> the average slope parameter for each mouse at each phase of morphine exposure was normalized by subtracting the average pre-morphine slope parameter. Positively increasing average change in slope (black line with gray confidence intervals) represents microbiota instability. See methods for details and supplemental figure S7 for type I analysis representing normal stochasticity. d) Differences in network associations between non-tolerant and tolerant mice. Associations of genera that were different between tolerant and non-tolerant mice, extracted from supplemental figure S8 are represented by a connecting line where colors indicate positive or negative associations and thickness indicates relative difference in strength of connection between non-tolerant and tolerant mice. See supplemental table S10 for statistics.

periods of instability, led to some divergent patterns of abundance in tolerant versus non-tolerant mice, including higher abundance of pathobiotic genera *Desulfovibrio* and *Coriobacteraceae* and lower abundance of potentially beneficial taxa *Rikenellaceae* AF12 and *Odoribacter* in tolerant mice (Figure 4b, Supplemental Figure S5).

Most biomarkers were only apparent after morphine had substantially altered microbiota composition, with notable exceptions (e.g. *A. muciniphila*), but this does not preclude that individual microbiota differences earlier in the paradigm, or even prior to morphine exposure, impacted antinociception and/or the trajectory of

morphine tolerance. For example, four mice exhibited low morphine antinociception prior to chronic morphine consumption and antinociception in these mice was further compromised by chronic morphine reflecting tolerance (Figure 1b, colored mice). The most noteworthy difference between the pre-morphine microbiota of mice with high and low starting antinociception was the near absence of *Odoribacter*<sup>123</sup> in mice with low starting antinociception (Supplemental Figure S6; detailed statistics in Supplemental Table S9).

We also evaluated the stability of the gut microbiota of individual mice as a measure of dysbiosis and assessed whether the two populations – tolerant and non-tolerant mice – met the expectations of Taylor's power law.<sup>92,124,125</sup> Taylor's power law describes the scalable relationship between the variance in abundance of a taxon to its population mean and it can be used to explore ecologically meaningful differences in population dynamics that result from external drivers and interactions among different taxa.<sup>93,126</sup> Application of the Type I power law extension<sup>93</sup> showed an expected correlation of variance of individual genera with their population means regardless of phase of morphine experience and development of tolerance as demonstrated by significant aggregation and linear clustering of data (Supplemental Figure S7). However, application of the Type IV power law extension, which examines individual communities over time,<sup>93</sup> detected differences in temporal stability between microbiota from tolerant and non-tolerant mice (Figure 4c, see methods for details). Specifically, the slope parameter of microbiota from tolerant mice increased (positive value) during mid-morphine indicating greater variance relative to starting variance, a result that was not driven by any one individual mouse. In contrast, the slope parameter of microbiota from non-tolerant mice did not increase (0 or negative value). The increase in population variance in tolerant mice indicates temporal instability among these populations (Figure 4c). Importantly, this trend coincides with the change in  $\alpha$ -diversity observed in tolerant mice at week 5 of the paradigm (Figure 4a).

Since morphine significantly altered relationships of the most central community members in all mice (Figure 2b), we wondered whether

the relationships of microbiota of mice that did or did not develop tolerance differed.<sup>57</sup> Overall microbiota connectivity did not differ between tolerant and non-tolerant mice, further reinforcing that all mice experienced dysbiosis (Supplemental Figure S8). However, network differences between tolerant and non-tolerant mice were revealed by an assessment of whether the abundance of paired community members correlated with each other and were different in the two populations (Figure 4d, Supplemental Table S10). This analysis identified six stronger positive associations and two unique negative (inverse) correlations in mice that did not develop tolerance and four positive associations and one negative correlation that were unique to tolerant mice.

We also interrogated whether patterns in unique membership or indicator genera were linked to tolerance.<sup>58</sup> Only three taxa altered by morphine were differentially present in tolerant mice, and these were identified late and post-morphine or when all phases of morphine experience were combined (Table 1). In contrast, nine indicator taxa were identified from non-tolerant mice, some from every phase of morphine experience (Table 1). With the exceptions of *Odoribacter*, *Rickenellaceae AF12*, and *Flexispira*, which are indicators of non-tolerance, and *Rhodococcus*, an indicator of tolerance, all indicator taxa were significantly impacted by morphine in terms of abundance (Figure 3a, Supplemental Table S2), as indicator species (Supplemental Table S4), or changes in network centrality (Figure 2c, Supplemental Table S3). *Bilophilia* was an indicator of both tolerance and morphine. *Streptococcus* was both an indicator of tolerance and displayed a unique network association in tolerant mice (Table 1, Supplemental Table S3, Supplemental Table S4).

#### **Genera differentially associated with and predictive of non-tolerant mice were more stably maintained during morphine disturbance than genera associated with tolerant mice**

To further examine the strength and patterns of microbiota associations with differences in the development of tolerance, we applied predictive



**Table 1.** Indicator taxa of microbiota from morphine tolerant and non-tolerant mice .

Phase	Tolerant	Community Member	Specificity <sup>a</sup> Probability	Sensitivity <sup>b</sup> Probability	Indicator Value <sup>c</sup>	p-value
Pre	No	<i>Rikenellaceae AF12</i> (ASV_344) <sup>d</sup>	0.7955	0.1944	0.393	0.038
Early	No	<i>Burkholderia</i> (ASV_1302) <sup>e</sup>	0.8929	0.2778	0.498	0.024
	No	<i>Xanthomonas</i> (ASV_2124) <sup>e</sup>	1	0.1667	0.408	0.045
Mid	No	<i>Parabacteroides</i> (ASV_66) <sup>e</sup>	0.7852	0.375	0.543	0.012
	Late	No	<i>RF32</i> (ASV_474) <sup>e</sup>	0.7353	0.5556	0.639
Post	No	<i>AF12</i> (ASV_344) <sup>d</sup>	0.8475	0.2778	0.485	0.004
	No	<i>F16</i> (ASV_1026) <sup>e</sup>	0.7534	0.3056	0.48	0.018
	Yes	<i>Rhodococcus</i> (ASV_1977) <sup>e</sup>	1	0.15	0.387	0.021
	No	<i>Anaerofustis</i> (ASV_779) <sup>e</sup>	0.7143	0.7143	0.714	0.001
	No	<i>Odoribacter</i> (ASV_189) <sup>d</sup>	0.6829	0.5714	0.625	0.008
	No	<i>RF32</i> (ASV_474) <sup>e</sup>	0.7538	0.5	0.614	0.005
	No	<i>F16</i> (ASV_1026) <sup>e</sup>	0.7333	0.3929	0.537	0.015
	No	<i>Stenotrophomonas</i> <sup>e</sup> (ASV_7876)	1	0.1071	0.327	0.047
	Yes	<i>Streptococcus</i> (ASV_869) <sup>e</sup>	1	0.2245	0.474	0.02
	All	No	<i>RF32</i> (ASV_474) <sup>e</sup>	0.70664	0.31081	0.469
No	<i>AF12</i> (ASV_344) <sup>d</sup>	0.73464	0.25676	0.434	0.001	
No	<i>F16</i> (ASV_1026) <sup>e</sup>	0.71212	0.20946	0.386	0.002	
No	<i>Flexispira</i> (ASV_704) <sup>d</sup>	1	0.02027	0.142	0.038	
Yes	<i>Bilophila</i> (ASV_791) <sup>e, f</sup>	0.7886	0.1008	0.282	0.016	

<sup>a</sup>Specificity is the estimate of the probability that the ASV belongs to the experience given the fact that the ASV was found. This conditional probability is called the *specificity* or *positive predictive value* of the species as indicator of the site group.

<sup>b</sup>Sensitivity is sample estimate of the probability of finding the ASV in samples belonging to the experience. This second conditional probability is called the *fidelity* or *sensitivity* of the ASV as indicator of the target site group.

<sup>c</sup>Indicator value index (accounts for unequal group sizes) given probabilities A and B.

<sup>d</sup>Identified as a biomarker of non-tolerance but not influenced by morphine use (See Figure 4).

<sup>e</sup>Identified as biomarker, indicator species, or by centrality measures and linked to morphine use (See Figure 3a and Supplemental Table S3).

<sup>f</sup>Identified in higher abundance in mice with poor starting antinociception (see Supplemental Figure S5).

models of abundance and presence of up to 3 community members identified at each phase of morphine experience in association with either tolerant or non-tolerant mice<sup>58</sup> (Summarized in Figure 5 and Supplemental Table S11, see Supplemental Table S12 for a full description models and statistics). Starting composition was not predictive of either outcome, in agreement with the individual variability of pre-morphine microbiota (Figure 1d, Supplemental Figure S3), similar alpha and beta diversity (e.g. Figure 4a), and the limited number of biomarkers identified pre-morphine (Figure 4b). The models built from morphine as well as post-morphine associations were more specific to non-tolerant microbiota and assigned these with an average of 86% accuracy, as opposed to only 45% accuracy for tolerant mice, indicating distinguishing differences had developed in the microbiota of non-tolerant mice even during early morphine. By the post-morphine phase, models assigned microbiota from individual fecal samples to the tolerant and non-tolerant groups with 97% accuracy, reflecting that the microbiota were divergent.

A visual exploration of the temporal distribution of the genera that informed these

predictive models reveals that many genera predictive of non-tolerant microbiota spanned multiple phases of morphine experience, reflecting their stable association (Figure 5). In keeping with this, the statistically supported ( $p < .05$ ) non-tolerant microbiota models, built at discrete phases of morphine exposure, had more cross predictability of samples from other phases of the paradigm (68% of non-tolerant samples correctly identified versus 57% tolerant samples). Collectively, these data support that microbiota from tolerant mice were more temporally unstable and more divergent from each other than the microbiota of non-tolerant mice. This is perhaps not surprising considering non-tolerant mice did not vary in antinociception, whereas tolerant mice varied more from one another (Figure 1b). However, the cross-predictability between the microbiota of just six non-tolerant mice suggests a convergence in mechanisms of sustained antinociception as well as resistance to some morphine-driven changes (Figure 4).

Considering that tolerant mice appear less alike each other and non-tolerant mice appear more convergent in shared and predictive genera, we reevaluated similarity among microbiota

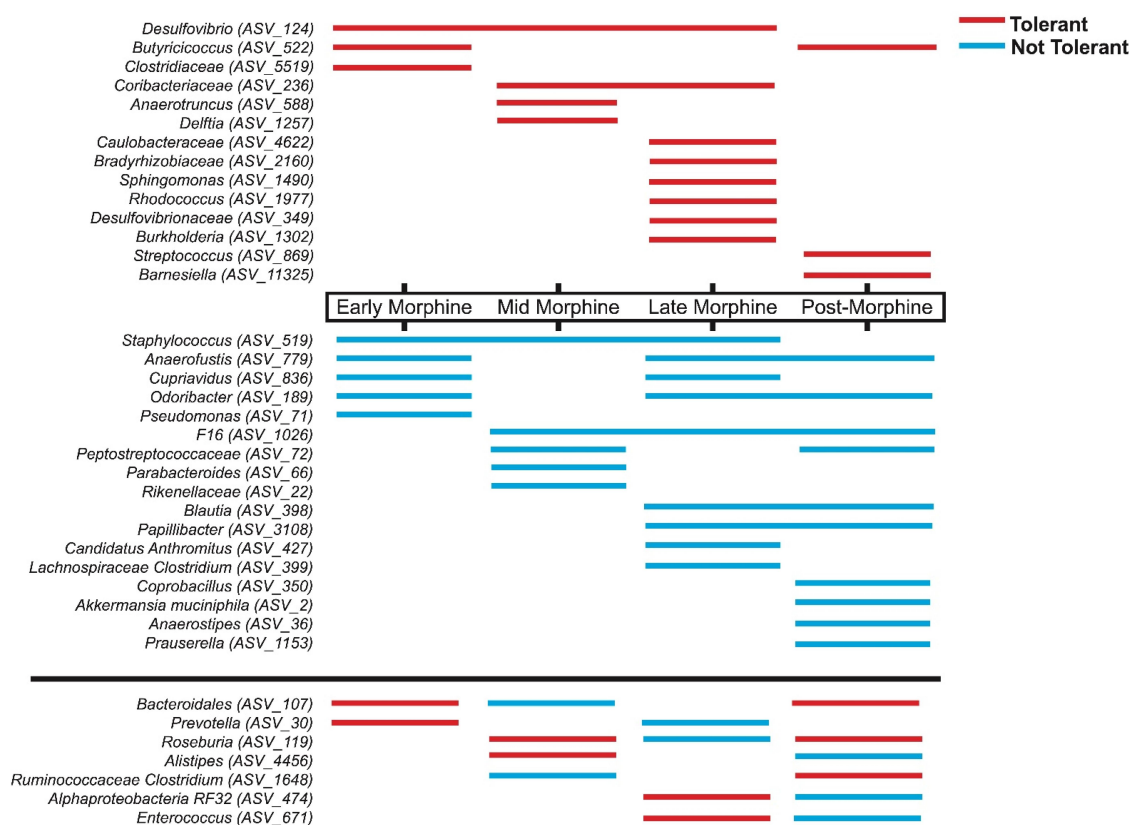


**Figure 5.** Summary of genera informing predictive models exemplifying more stable associations and shared predictive genera among non-tolerant than tolerant mice. Summary of taxa used in combinations to predict whether a microbiota sample was from a tolerant mouse (red) or a non-tolerant mouse (blue) in different phases of morphine experience. No models were predictive during pre-morphine. Three genera that were inconsistently identified in biomarker, indicator, or network analyses (showing the opposite associations in prior analyses at the same phase of morphine experience compared to these models) were excluded from this visual summary. See supplemental table S11 and S12 for details.

that were from tolerant or non-tolerant mice and differences between these two populations using only biomarker genera and a phylogenetically informed metric of  $\beta$ -diversity (weighted UniFrac; Supplemental Figure S9). This analysis indicated that phase of morphine experience was still the major driver of assemblages, even when considering a restricted dataset (19 ASVs at the genus level). In addition, this analysis revealed more variability among the microbiota of tolerant mice than non-tolerant mice during mid-morphine (Supplemental Figure S9). This agrees with the timing in which we predicted community instability in tolerant mice (Figure 4c) following their notable earlier changepoint in  $\alpha$ -diversity (Figure 4a). In contrast, microbiota of non-tolerant mice clustered more tightly mid-morphine, suggesting more similarity and perhaps shared functions (Supplemental Figure S9).

### **Greater relative microbiota capacity for butyrate production during morphine exposure correlated with prolonged morphine antinociception**

The finding that mice that did not develop tolerance to morphine share more predictive genera and that associations were still quite different from each other in terms of community structure even when only considering biomarker genera (Figure 5, Supplemental Figure S9, Supplemental Table S8, and Supplemental Table S12), led us to consider whether functions among shared taxa could elucidate what these mice have in common. Assessment of previously described attributes of biomarker and indicator genera (Table 2) revealed a striking pattern among genera associated with non-tolerant mice: a higher abundance and association of butyrate producers that was corroborated by a bioinformatic analysis that predicts the functional capacity of taxa (Supplemental Figure S10).

**Table 2.** Butyrate producers were associated with non-tolerant mice.<sup>1</sup>

Taxa	Association <sup>b</sup>	Experience	Notable Feature(s)
<i>Akkermansia muciniphila</i> (ASV_2) <sup>c</sup>	B A M	Pre, Mid Early, Late Post	Mucin degrading, acetate producer; syntrophic support of <b>butyrate</b> producers <sup>117,127</sup> Modulates immune responses and gut homeostasis <sup>128–132</sup>
<i>Oscillospira</i> ( <i>Oscillibacter ruminantium</i> ) (ASV_38) <sup>c</sup>	B A	Late, Post Early-Late/Post	<b>Butyrate</b> <sup>133</sup> Chronic constipation correlated with CD post-operative remission <sup>133,134</sup>
<i>Rikenellaceae</i> ( <i>Alistipes onderdonkii</i> ) (ASV_22)	M	Mid	Potential acetate and propionate producer based on taxa <sup>135</sup> May affect tryptophan bioavailability in MDD <sup>136</sup>
<i>Mollicutes</i> RF39 ( <i>Breznakia pachnodae</i> )(ASV_28) <sup>c</sup>	B	Late	Acetate producer; inversely correlated with inflammation, and BMI <sup>137,138</sup>
<i>Coprococcus</i> ( <i>Eubacterium xylanophilum</i> ) (ASV_96) <sup>c</sup>	B	Pre-	<b>Butyrate</b> and acetate based on taxa; inversely correlates with IBD, depression and PD <sup>116,139,140</sup>
<i>Sutterella</i> ( <i>Parasutterella excrementihominis</i> ) (ASV_76)	B	Late, Post	Bile acid maintenance <sup>141</sup> ; Morphine dysbiosis, inflammation <sup>142</sup> ; Loperamide reduces butyrate production and <i>Sutterella</i> <sup>143</sup>
<i>Peptostreptococcaceae</i> ( <i>Romboutsia timonensis</i> ) (ASV_72)	M	Mid, Post	Mucin degrading, tryptophan metabolism and indole acrylic acid production promotes barrier function; controversially (positively/negatively) correlated with anxiety and depressive disorders <sup>144–147</sup>
<i>Parabacteroides</i> ( <i>Parabacteroides chongii</i> ) (ASV_66)	I M	Early-Mid Mid, All	<b>Butyrate</b> , anti-inflammatory <sup>121</sup>
<i>Odoribacter</i> ( <i>Odoribacter splanchnicus</i> ) (ASV_189)	B A I	Combined Pre-Late/Post Early, Late, Post	<b>Butyrate</b> , inversely correlated with gut inflammation, associated with exercise and weight control <sup>120,123,148–150</sup>
<i>Erysipelotrichaceae</i> ( <i>Clostridium; Longibaculum muris</i> ) (ASV_143) <sup>c</sup>	B	Late, Post	Glucose absorption/glycemic control; Linked to intestinal inflammation <sup>111</sup> Potential butyrate producer based on taxa <sup>116</sup>
<i>Rikenellaceae</i> AF12 ( <i>Millionella massiliensis</i> ) (ASV_344)	B A I	Late, Post Pre-Late/Post Pre, Early-Mid	<b>Butyrate</b> producer associated with exercise <sup>123</sup>
<i>Alphaproteobacteria</i> RF32 ( <i>Kiloniella laminariae</i> ) (ASV_474) <sup>c</sup>	B I M <sup>d</sup>	Late, Post Early-Mid, Post Post	Colonic damage, <sup>151</sup> inverse with 5-HT <sup>152</sup>
<i>Lachnospiraceae</i> ( <i>Clostridium colinum</i> ) (ASV_399)	M	Late, All	Potential <b>Butyrate</b> , and Indoleacrylic acid producer based on taxa <sup>116,144,153</sup>
<i>Coprobacillus</i> ( <i>Longibaculum muris</i> ) (ASV_350)	M	Late	Positively correlated with leptin (anti-obesity) <sup>154</sup>
<i>Blautia</i> ( <i>Murimonas intestini</i> ) (ASV_398) <sup>c</sup>	B A I A	Late, Post Early-Post Post Late	Acetate producer (Potential co-metabolism feeding for <b>Butyrate</b> producers), inversely correlated with PD <sup>122</sup> Linked to gut homeostasis <sup>140,155</sup> Grooming <sup>156</sup>
<i>Staphylococcus</i> ( <i>Staphylococcus saprophyticus</i> ) (ASV_519)	M	Late, Post	Potential <b>Butyrate</b> producer based on taxa <sup>115,116</sup> Linked to inflammation <sup>157</sup> Controversial taxonomic assignment <sup>158,159</sup>
<i>Candidatus Anthromitus</i> ( <i>Clostridium oryzae</i> ) (ASV_427)	B I M	Combined Post Early, Late, Post, All	Acetate and <b>Butyrate</b> <sup>160</sup>
<i>Anaerofustis</i> ( <i>Anaerofustis stercorihominis</i> ) (ASV_779)	I	Early-Mid, Post	Associated with gut dysbiosis and inflammation <sup>161,162</sup>
TM7 F16 ( <i>Geomonas terrae</i> ) (ASV_1026) <sup>c</sup>	M	Early, Late	Environmental contaminant <sup>163</sup>
<i>Cupriavidus</i> ( <i>Cupriavidus metallidurans</i> ) (ASV_836)	M	Early	Becomes more virulent in the presence of morphine <sup>164</sup>
<i>Pseudomonas</i> ( <i>Pseudomonas aeruginosa</i> ) (ASV_71)	M	Late, Post	Potential <b>Butyrate</b> producer based on taxa <sup>115,116</sup>
<i>Papillibacter</i> ( <i>Clostridium viride</i> ) (ASV_3108)	I	Early	Potential pathogen <sup>165,166</sup>
<i>Xanthomonas</i> ( <i>Xanthomonas albilineans</i> ) (ASV_2124) <sup>c</sup>	I	Early-Mid	Participate in bile acid metabolism <sup>167,168</sup>
<i>Stenotrophomonas</i> ( <i>Xanthomonas floridensis</i> )*(ASV_7876) <sup>c</sup>	I	Post	Associated with gut inflammation <sup>169,170</sup>

<sup>a</sup>Ordered by decreasing abundance. Species (in parentheses) were identified using rRNA/ITS databases with the nucleotide basic local alignment search tool (blastn).<sup>72</sup>

<sup>b</sup>B: Biomarker of non-tolerance; A: High starting antinociception; I: Indicator taxa of non-tolerance; M: Predictive modeling.

<sup>c</sup>Altered by morphine exposure.

<sup>d</sup>Identified in predictive models for both tolerance and non-tolerant mice but in combination with different taxa.

Congruent with this observation, butyrate bolsters gut barrier function and curtails inflammatory responses while stimulating macrophage differentiation and production of antimicrobial peptides to

remove invading pathobionts, thereby promoting gut homeostasis.<sup>48,171,172</sup> It is notable that many of the butyrate producing genera associated with non-tolerant mice were also lower in mice with poor

starting antinociception prior to morphine exposure and some were subsequently depleted even more by morphine, in parallel with the further decline of morphine antinociception in these mice (Figure 1b, Supplemental Figure S6). This suggests that morphine-driven differential loss of some butyrate-producing organisms might exacerbate tolerance and, by extension, that butyrate could protect against tolerance.

To further investigate associations of the microbiota and its capacity to produce butyrate with sustained antinociception to morphine, we optimized a shorter paradigm for hypothesis testing that uses moderate but consistent non-contingent morphine exposure to produce tolerance (Figure 6a). This shorter paradigm more closely resembles a post-operative regime and eliminates the potentially confounding variable of different amounts of voluntary oral morphine on microbiome composition. While it accelerates the timeline for the development of tolerance, it preserves variations in both microbiota composition and the development of tolerance (Figure 6a,b). Five days of morphine produced antinociceptive tolerance in most mice, with ~30% of mice maintaining 100% MPE morphine antinociception (Figures 1b, 6b). The microbiota derived from feces pooled from non-tolerant and pooled from tolerant mice from this paradigm differed from each other post-morphine, suggesting microbiota differences could relate to variability in antinociceptive tolerance (Figure 6b).

To more directly examine the connection between the microbiota and variability in morphine tolerance, we used tolerant and non-tolerant mice (Figure 6b) as fecal microbial transplantation (FMT) donors to investigate whether the microbiota of tolerant mice predisposed or accelerated the development of tolerance in recipients<sup>40,48</sup> and/or whether the microbiota of mice that did not develop tolerance could delay or prevent the development of tolerance in recipients. For these FMT experiments, mice received s.c. morphine (10 mg/kg) for 9 d to reliably produce tolerance in controls (receiving oral carrier, Figure 6c). After 9 d of morphine, the resulting microbiota of control mice receiving carrier (Figure 6d, dark blue circles) clustered tightly and generally among microbiota from the mid-morphine phase of the original oral

paradigm. Furthermore, the predictive models built from microbiota associations with morphine exposure in the oral paradigm and that were able to detect fecal microbiota exposed to morphine from a separate cohort of mice treated with the same oral paradigm (Figure 2c, Supplemental Table S5) also correctly assigned eight out of nine feces from these morphine treated carrier-gavaged mice, reinforcing that 9 d of s.c. morphine produces similar dysbiosis (Figure 6d, Supplemental Table S13). The short paradigm also caused similar changes among many of the same community members (Figure 3a) (e.g. *Muribaculaceae*, *Clostridiales*, *Lachnospiraceae*, *Akkermansia*, *Anaeroplasma*, and *Butyricoccus*) and a depletion of beneficial community members characteristic of morphine dysbiosis, notably some of which are butyrate producers (e.g. *Butyricoccus*, Figure 6e, detailed statistics in Supplemental Table S14). Oral carrier-gavaged mice readily developed tolerance by day 7 of daily morphine treatment as evidenced by their reduced latency to tail flick (Figure 6f) and decreased morphine antinociception at 5 + 2 mg/kg which was the ED<sub>90</sub> dose in morphine-naïve mice (Supplemental Figure S11a,b). Mice that received 2× daily tolerant mouse FMT similarly developed tolerance by day 7 and displayed further profound loss of morphine antinociception at day 10 (Figure 6f,g, Supplemental Figure S11B). Remarkably, mice receiving 2× daily non-tolerant donor FMT during morphine treatment did not develop tolerance by day 7 and as a population their morphine antinociception did not differ on day 10 compared to day 1, where five of the nine mice retained 100% MPE (Supplemental Figure S11B). Compared to control carrier mice that exhibited a significant decrease in morphine potency from day 1 (ED<sub>50</sub> 5.66 mg/kg) to day 10 (ED<sub>50</sub> 9.47 mg/kg,  $p = 0.012$ ), non-tolerant FMT mice exhibited no significant change in morphine potency from day 1 (ED<sub>50</sub> 5.37 mg/kg) to day 10 (ED<sub>50</sub> 5.63 mg/kg,  $p = 0.34$ ) (Figure 6g). Morphine-treatment mice had no increase in baseline nociception in any gavage group indicating they did not develop hyperalgesia (Figure 6h). Furthermore, 9 d of any FMT treatment without chronic morphine did not significantly alter baseline nociception or morphine antinociception (Supplemental Figure S11C, D).

Since the above data reinforce the link between differential morphine-induced changes

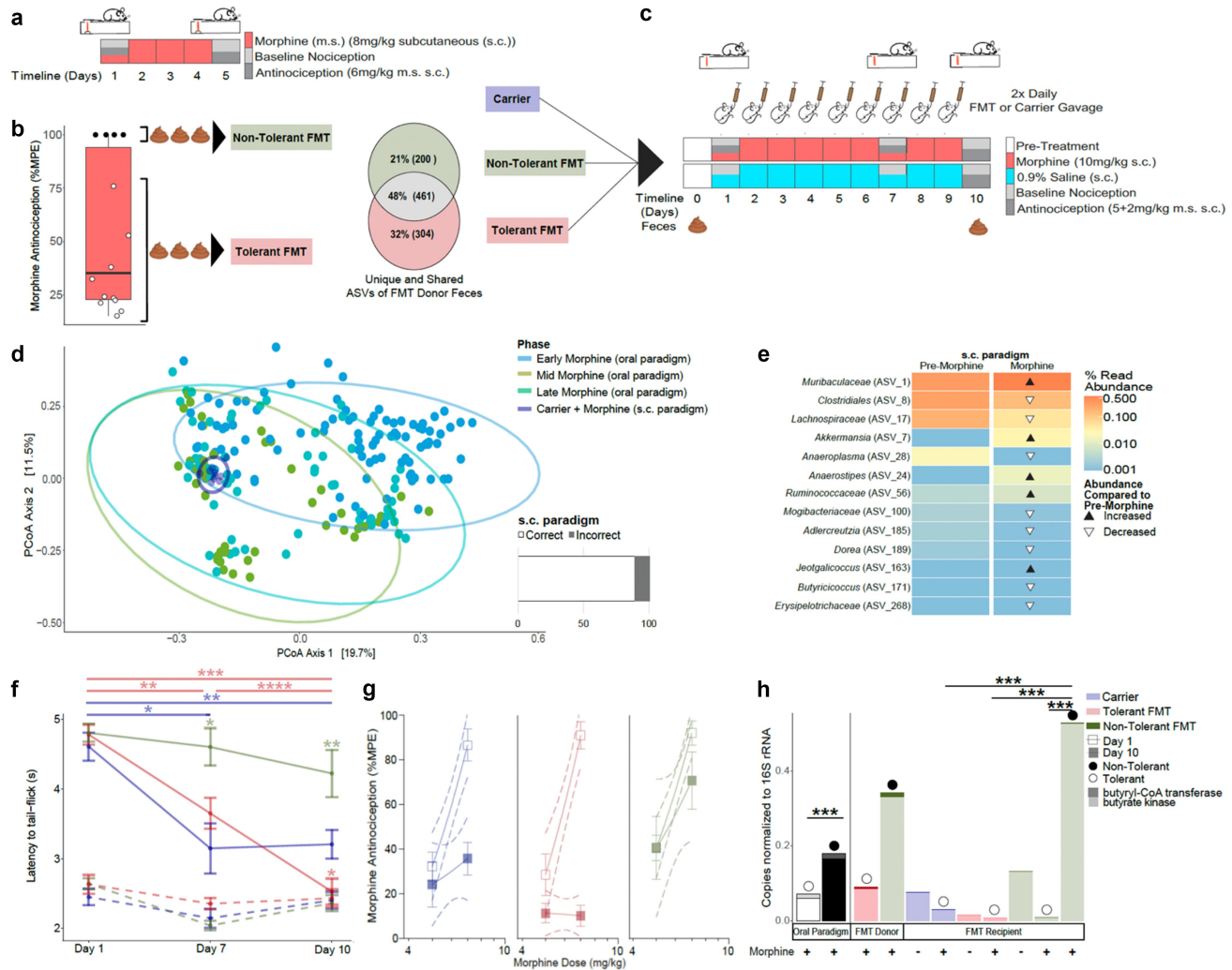


**Figure 6.** Microbiota enriched for butyrate biosynthetic capacity protected fecal microbiota transplantation (FMT) recipients from developing antinociceptive tolerance to morphine. **a**) Schematic of sub-cutaneous (s.c.) morphine (m.s.) (8 mg/kg m.s. s.c., 1x daily) paradigm. **b**) Baseline nociception and antinociception (6 mg/kg m.s.) was assessed on days 1 and 5 using a radiant heat tail-flick assay to identify tolerant (<100% maximum possible effect [MPE], light red) and non-tolerant mice (= 100% MPE, light green). Day-5 feces were pooled from each category for FMT, and for analysis of microbiota (16S) where compositional comparisons were illustrated using the ps\_venn function in the MicEco R package (v0.9.15).<sup>60</sup> **c**) Schematic of FMT paradigm where mice were orally gavaged 2x daily with saline carrier (dark blue), or cleared fecal slurries (see Figure 6b) in conjunction with daily s.c. m.s. administration ( $n = 9$  ea treatment) or saline ( $n = 5$  ea treatment). **d**) Gut microbiota  $\beta$ -diversity (all ASVs, Bray-Curtis dissimilarity) of saline gavaged mice post-m.s. In comparison with microbiota from the oral paradigm as visualized by principal coordinates analysis (PCoA). The bar graph to the right shows accuracy by which the predictive models built from microbiota associations with m.s. exposure in the oral paradigm (Figure 2c) could predict microbiota from the s.c. paradigm were derived from m.s. treatment (presented as % correct/incorrect). See supplemental tables S5 and S13 for details. **e**) Biomarkers of s.c. m. s. exposure were identified from among the community members whose abundance was significantly altered by m.s. (as identified using corncob regression models),<sup>90</sup> followed by a linear discrimination analysis (LDA) of effect size (LEfSe)<sup>91</sup> of day 0 and day 10 microbiota. Triangles indicate whether the community members' abundance increased (black) or decreased (white) day 10 relative to day 0. Community members are labeled at the lowest taxonomic classification available. See supplemental table S14 for details. **f**) The trajectory of tolerance was visualized as a decrease in latency to tail-flick in seconds following 5 + 2 mg/kg s.c. m.s. (cumulative ED<sub>90</sub>) and reported as mean; error bars are SEM. Kruskal-Wallis test followed by pairwise Wilcoxon test for multiple comparisons were used to determine whether carrier and FMT groups (solid lines) changed over time (horizontal bars) and differed from each other (asterisks above data points) (\* $p < 0.05$ ; \*\* $p < 0.01$ ; \*\*\* $p < 0.001$ ; \*\*\*\* $p < .0001$ ). Baseline latencies to tail-flick for carrier and FMT groups (dashed lines) were used to assess hyperalgesia post-chronic m.s. **g**) Change in morphine potency was assessed by comparison of linear regressions of dose responses (ED<sub>60</sub> and ED<sub>90</sub> doses) reported as % MPE on day 1 (open squares) and day 10 (closed squares). Outer dashed lines represent 95% confidence intervals of the linear regressions and error bars represent SEM. Shift in ED<sub>50</sub> from day 1 to day 10 extrapolated from these regressions is reported in text. **h**) Butyrate biosynthesis capacity determined by quantitative real-time polymerase chain reaction (qPCR) via gene copy number quantification of butyryl-CoA transferase (bcoat; upper stacked bar) and butyrate kinase (buk; lower stacked bar) normalized to total 16S rDNA copy number. Relative butyrate production capacity of tolerant (white bar) and non-tolerant (black bar) mice in the oral paradigm is presented in the first bar graph, followed by capacity in FMT donor slurries and recipients at day 10 for control carrier (blue), tolerant FMT (light red), and non-tolerant FMT (light green). Circles above the bars designate whether the mice that were tolerant (white) or non-tolerant (black) representing data from Figure 1b and supplemental figure S11B. Student's T-test determined significant differences of butyrate capacity, (ns  $p > .05$ ; \* $p < .05$ ; \*\* $p < .01$ , \*\*\* $p < .001$ ).

in the microbiome with variability in the development of antinociceptive tolerance and implicated butyrate producers, we used this paradigm to assess whether sustained antinociception was associated with butyrate production capacity. To this end, we quantified the relative abundance of genes encoding representative enzymes including butyryl-CoA transferase (BCoAT, *bcoat* or *but*) and butyrate kinase (*buk*), necessary for each of the two known pathways for butyrate biosynthesis,<sup>105,106</sup> as a proxy of butyrate production capacity in the microbiota of tolerant and non-tolerant mice. We performed this analysis of microbiota of the individual mice from the voluntary oral paradigm (Figure 1a,b), of feces pooled from tolerant and pooled from non-tolerant mice used as FMT donors (Figure 6a,b), and from the individual FMT/saline carrier recipients at day 10 (Figure 6f–g). This revealed that the microbiota of mice that did not develop morphine antinociceptive tolerance consistently had significantly higher capacity for butyrate production (Figure 6h). The ending microbiota (18 weeks) of non-tolerant mice from the oral paradigm had ~26% higher butyrate production capacity than tolerant mice (Figure 6h, oral paradigm). Pooled feces from non-tolerant mice from the s.c. paradigm used as FMT donors also had substantially higher butyrate production capacity than the pooled feces of tolerant counterpart mice (3.7-fold greater, Figure 6h, “donor”). The non-tolerant FMT recipients that maintained 100% MPE antinociception had significantly higher butyrate production capacity than those that did become tolerant, including those that received non-tolerant FMT (23-fold greater), those that received a tolerant FMT gavage (60-fold greater), or a saline gavage (17.4-fold greater, Figure 6h, “recipient”).

**Dietetic butyrate supplementation prevented the development of tolerance which arose without systemic inflammation or hyperalgesia**

Since the short paradigm recapitulated the original microbiome associations and reinforces the hypothesis that butyrate is protective, we used

this paradigm to evaluate the impact of dietetic butyrate supplementation on tolerance. Mice were supplied with sodium butyrate, or as a control sodium/pH-matched sodium citrate *ad libitum* in their drinking water for 3 weeks prior to morphine exposure, where we estimate mice consumed ~3 g/kg butyrate daily. Day one latencies to tail flick without and with morphine did not differ between butyrate and citrate supplemented mice (Supplemental Figure S12A). However, only one butyrate mouse (~6%) was below 100% MPE at the 5 + 2 cumulative morphine dose as opposed to four citrate mice (~22%). This implies that butyrate pretreatment may modestly bolster morphine antinociception.

Mice were then treated with non-contingent morphine (10 mg/kg s.c. 1× day for 9 d) or saline while continuing to receive supplementation (Figure 7a). On day 10, the baseline nociception of neither supplementation group treated with morphine differed from their respective saline control groups, and few individuals exhibited an increase in nociception which also did not correlate with decreased antinociception, indicating that these mice did not develop hyperalgesia (Supplemental Figure S12B,C). As expected, morphine modestly reduced gut transit, as assessed by an increase in production of fecal pellets by reversal with the MOR antagonist naloxone, in all morphine-treated mice, indicating that butyrate did not appear to counter morphine-driven constipation (i.e. reduced gut motility) (Supplemental Figure S12D) as previously shown.<sup>48</sup>

Morphine-mediated antinociception declined precipitously in citrate-supplemented mice, and as a population only citrate-supplemented mice were tolerant by day 7 (Figure 7b). Furthermore, on day 10, butyrate-supplemented mice maintained significantly higher morphine antinociception than citrate-supplemented mice (Figure 7c). More specifically, only citrate-supplemented mice exhibited a significant decline in morphine potency from ED<sub>50</sub> of 5.9 mg/kg to 8.1 mg/kg ( $p = 0.0001$ ), whereas the butyrate-supplemented mice exhibited a significantly smaller decrease in morphine potency (from ED<sub>50</sub> 5.46 mg/kg to 5.88 mg/kg,  $p = 0.0028$ ) from day 1 to day- (Figure 7d). Furthermore, both citrate and butyrate similarly altered the microbiome composition of mice

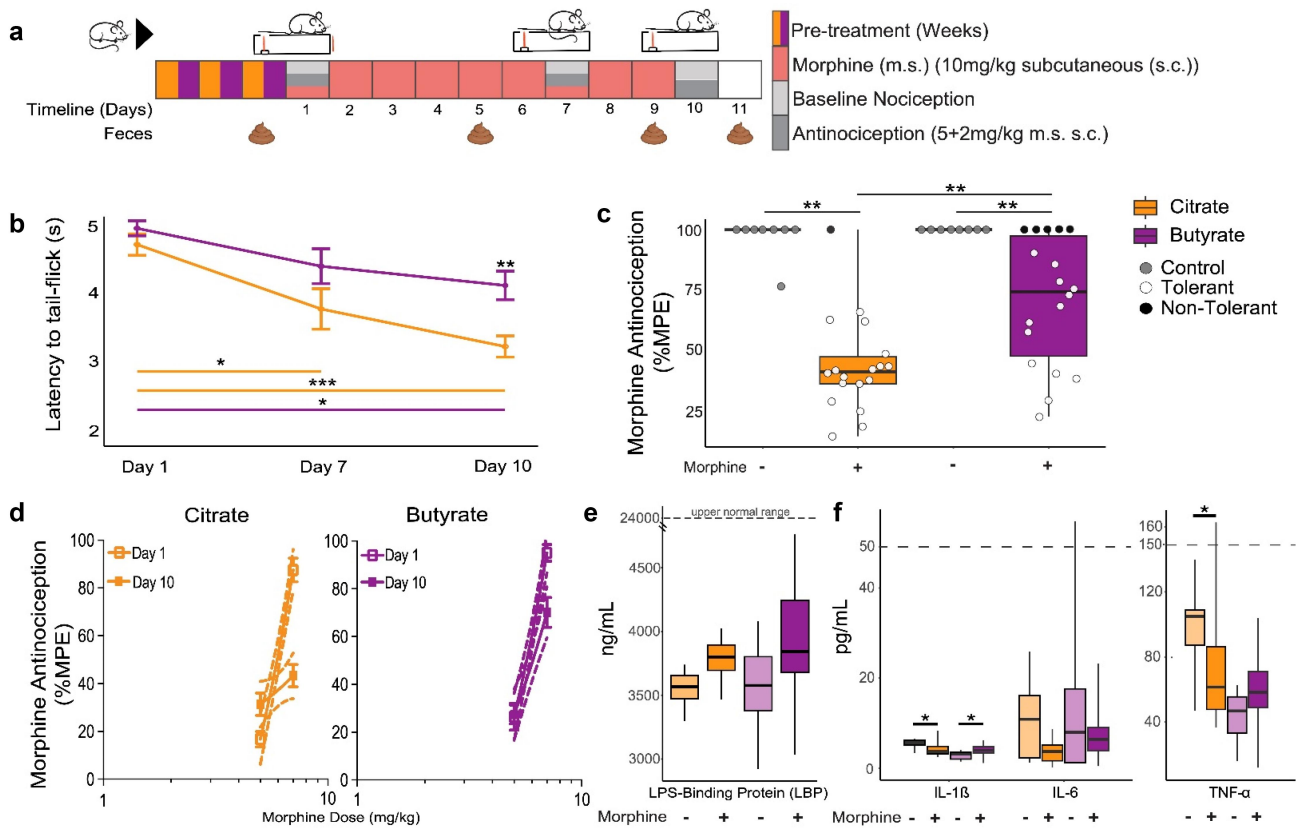


**Figure 7.** Butyrate supplementation prolongs morphine antinociception independently of curtailment of inflammation. a) Schematic of mouse paradigm where mice were fed 100 mm sodium butyrate or sodium citrate, followed either by 9-d morphine (m.s.) (10 mg/kg s.c.) ( $n = 18$  ea), or daily saline (0.9% s.c.) ( $n = 8$  ea). Mice treated daily with m.s. were assessed for baseline nociception and antinociception on days 1, 7, and 10 at 5 mg/kg and 30 minutes later at 5 + 2 mg/kg m.s. s.c. ( $ED_{60}$  and  $ED_{90}$  respectively, see supplemental figure S11a). Feces were collected on days 1, 5, 9, and 11 of the paradigm to generate 16S (V4-V5 regions, see methods). b) The trajectory of tolerance was visualized as a decrease in latency to tail-flick (s) (5 + 2 mg/kg s.c. m.s.) and reported as mean; error bars are SEM. Kruskal–Wallis test followed by pairwise Wilcoxon test for multiple comparisons were used to determine whether citrate and butyrate groups changed over time (horizontal bars) and differed from each other (asterisks above data points) ( $*p < .05$ ;  $**p < .01$ ;  $***p < .001$ ). c) Antinociception (5 + 2 mg/kg s.c. m.s.) as determined on day 10 using the radiant heat tail flick assay. Data is reported as maximum possible effect (% MPE). Kruskal–Wallis test followed by pairwise Wilcoxon test for multiple comparisons determined significant differences between m.s. treated citrate and butyrate supplementation groups and between m.s. treatments and saline controls ( $**p < .01$ ;  $***p < .001$ ). d) Change in morphine potency was assessed by comparison of linear regressions of dose responses ( $ED_{60}$  and  $ED_{90}$  doses) reported as %MPE on day 1 (open squares) and day 10 (closed squares). Outer dashed lines represent 95% confidence intervals of the linear regressions and error bars represent SEM. Shift in  $ED_{50}$  from day 1 to day 10 extrapolated from these regressions is reported in text. e) Day 10 serum levels of LPS binding protein (LBP) of mice supplemented with citrate (orange) or butyrate (purple) and their saline controls. LBP upper normal range (dashed line), as indicated by manufacturer, is marked for reference (Invitrogen, Waltham, MA). f) Day 10 serum levels of pro-inflammatory cytokines (IL-1 $\beta$ , IL-6, and  $tnf-\alpha$ ) of mice supplemented with citrate (orange) or butyrate (purple) and their saline controls. Dashed lines represent normal ranges of serum cytokine levels (50 pg/mL: IL-1 $\beta$ , IL-6; 150 pg/mL: TNF- $\alpha$ ).<sup>175</sup> Kruskal–Wallis test followed by pairwise Wilcoxon test for multiple comparisons determined significant differences between m.S. treated citrate and butyrate supplementation groups and between m.S. treatments and saline controls ( $*p < .05$ ).

(Supplemental Figure S12E), and as expected,<sup>48</sup> s.c. morphine-induced dramatic microbiota changes even with butyrate supplementation (Supplemental Figure S12F, statistics detailed in Supplemental Table S15). Even so, morphine drove less dramatic changes in microbiota diversity and caused less instability in the microbiota of

butyrate than in citrate-supplemented mice (Supplemental Figure S12G, H).

Finally, we evaluated whether butyrate supplementation during morphine exposure improved barrier function by assessing serum LPS and LPS-binding protein (LBP) produced by the liver in response to bacterial translocation as surrogates

of a “leaky gut.” We also assessed whether butyrate supplementation during morphine exposure curtailed systemic inflammation through quantification of blood serum inflammatory cytokines. In the short s.c. tolerance paradigm, the modest morphine dosing did not drive detectable increases in serum LPS, which were at or below the detection threshold (data not shown) indicating the mice were not septic.<sup>173</sup> Morphine also did not significantly elevate LBP levels, which were well below those expected if bacterial translocation had increased<sup>174</sup> and these levels did not differ between supplementation groups (Figure 7e). In keeping with the low observed bacterial translocation, neither citrate nor butyrate-supplemented mice displayed a notable increase in pro-inflammatory cytokines (IL-1 $\beta$ , IL-6, TNF- $\alpha$ ) in serum post-morphine, and levels were all within the expected normal range (Figure 7f, dashed line). Indeed, the level of these were at times lower post-morphine compared to control mice that did not receive morphine perhaps because of the anti-inflammatory properties of morphine. These data indicate that in this paradigm, systemic inflammation was not required for the development of tolerance. It also suggests that paradigms that use super-physiological morphine doses may create phenomena that are less relevant to the clinical phenomenon.

## Discussion

Prior studies examining contributions of the microbiome to OUD have intentionally reduced behavioral variations inherent to mouse models by using high non-contingent morphine doses. These prior studies have thereby gleaned insight from common microbiome responses, not all of which are likely to explain tolerance.<sup>17,37,40</sup> In contrast, through our experimental design, we preserved and leveraged natural variation in both tolerance and the microbiota with the specific goal to identify microbiota signatures associated with degree of tolerance (Figures 1 and 6). We demonstrate that chronic voluntary morphine self-administration induced similar, even predictive, dysbiosis in all mice, regardless of whether they develop antinociceptive tolerance (Figure 3a, Table 1), and these global temporal changes largely

masked informative microbiome associations that tracked with differences in morphine tolerance. To uncover latent patterns associated with tolerance, we used complimentary high resolution temporal analyses and cross-referenced results to identify repetitive trends. These analyses revealed a divergence in the timing of progression of dysbiosis between tolerant and non-tolerant mice (Figure 4). More importantly, there were noteworthy differences in the response of microbiota to morphine disturbance that best distinguished between mice that did and did not develop tolerance (Figures 4, 5, Table 2). Key among these findings was that non-tolerant mice maintained a higher capacity for the production of butyrate (Table 2, Figure 6h).<sup>8,175</sup> We then showed that both FMT from morphine-treated non-tolerant donor mice is relatively enriched for butyrate production capacity and diet supplementation with butyrate is protected against the development of tolerance to morphine (Figures 6f–h, and 7). Although butyrate is known to bolster barrier function and suppress inflammation, our data indicate that our moderate morphine tolerance paradigm does not produce systemic inflammation nor compromise barrier function (Figure 7e,f). This uncoupling of tolerance from systemic inflammation and the ability of butyrate, either produced from the microbiota or as a dietary supplement, to reduce tolerance suggests a role of butyrate as a ligand of communication in the GMB axis independent from these palliative effects (Figures 6 and 7).

As researchers increasingly recognize the importance of the gut microbiota and its signaling through the GMB-axis to host health and disease,<sup>1–4</sup> there has been a shift in thinking about how hosts and their associated microbial communities, known as the holobiont, interact to influence individual phenotypes.<sup>176–178</sup> Prior studies suggest that the gut microbiota enhances morphine tolerance through its translocation across a morphine-compromised gut barrier, as tolerance can be reduced by elimination of the gut microbiota via antibiotics, or in germ-free mice.<sup>37,40,109</sup> The implication that the microbiota is the problem paints an incomplete picture, especially considering that depletion of gut mutualists, and their supportive functions, is arguably the most apparent feature of morphine-induced dysbiosis (Figure 3).<sup>142</sup>



Furthermore, a diverse gut microbiota is crucial for both immune and neurological functions.<sup>3,179–181</sup> Indeed, supplementation with a probiotic mix of *Lactobacillus* and *Bifidobacteria*, gram-positive genera shown to be depleted by morphine,<sup>38,39,41</sup> improves barrier integrity and attenuates morphine tolerance.<sup>40</sup> Oddly enough, higher populations of these same genera were biomarkers of tolerance in our study here (Figure 4b) and *Lactobacillus* modestly increased in response to morphine in tolerant but not in non-tolerant mice (Figure 3a). Depletion of gram-positive bacteria with vancomycin, which targets these probiotic genera also prevents morphine tolerance.<sup>37</sup> We expect this incongruence, whereby these beneficial genera are tied to both tolerance and its attenuation, could reflect that a variety of taxa, not just these two genera, can support homeostasis similarly and support trophic networks of the microbiota to resist or counter morphine's adverse effects (Figure 2d, Table 2). Importantly, these capabilities may not necessarily be defined by or limited to related taxa, or even guaranteed to be expressed equally by every strain within a given species (Supplemental Figure S6 and Table 2).<sup>182,183</sup> Functional redundancy of SCFA production by the microbiota could ensure resiliency to perturbation.<sup>184–187</sup>

Among SCFAs, which include acetate, propionate, and valerate, butyrate is especially important in the intestinal environment as the primary energy source for colonocytes, for promoting barrier function, and for toning the immune system to effectively mitigate translocating bacteria if barriers are breached.<sup>48,171,172,175,188</sup> Notable potential butyrate producers associated with non-tolerance included *Oscillospira*, *Coprococcus*, *Parabacteriodes*, *Anaerofustis*, *Odoribacter*, and *Rickenellaceae AF12*, (Table 2).<sup>116,120,121,123,148,149,153,160,189–193</sup> Many of these genera have been shown to improve gut integrity and inversely correlate with escalatory inflammatory conditions such as inflammatory bowel disease, cardio-metabolic diseases, and neurobiological or neurodegenerative conditions.<sup>120,121,123,129,140,148,149,194–199</sup> Opioid use depletes butyrate-producing genera in humans<sup>200</sup> and drives a decrease in fecal butyrate in mice.<sup>48</sup> Curiously, the morphine agonist loperamide also decreases fecal butyrate even in the

absence of constipation directly implicating MOR-signaling in microbiome dysbiosis.<sup>143</sup> The replication of protection from tolerance by FMT enriched in butyrate biosynthesis capacity and diet supplementation of butyrate alone (Figures 6 and 7) suggests differential loss of such community members contributed to tolerance but did so without causing hyperalgesia and independently of cytokine-directed systemic inflammation that has previously been a suggested cause of microbiome-mediated hyperalgesia and tolerance.<sup>17,37,40</sup> Though the modest morphine regime, we employed did not drive systemic inflammation or hyperalgesia (Supplemental Figure S2A, Figure 7, and Supplemental Figure S12B,C), we did not assess local intestinal inflammation which could still contribute to the pathology of tolerance. It is possible that butyrate concurrently palliatively counters the reduced analgesic benefits of morphine as tolerance develops by attenuating local inflammation, thereby preventing hyperactivation of nociceptor neurons that infiltrate the gut which could underlie hyperalgesia,<sup>40,48,201</sup> and which aligns with a recent study showing butyrate protection from hyperalgesia.<sup>46</sup> Importantly, the modest morphine regimes used herein uncoupled potential confounding side-effects that associate with tolerance when higher than necessary dosing of morphine is used, and these could be confounders resulting from experimental design that are neither required nor the sole basis for microbiome-mediated exacerbation or protection.

As a complementary mechanism to its documented ability to reduce inflammation, butyrate could have modulatory effects on neuronal activity directly that may help explain its protective effects against the development of tolerance that developed in control mice independently of systemic inflammation (Figure 7). The gut is innervated by both enteric and sensory nerves, and both neuronal populations express opioid receptors.<sup>202</sup> When activated, opioid receptors decrease neuronal excitability and reduce neurotransmitter release. Neurons expressing opioid receptors in both the gut and the dorsal root ganglion (DRG) undergo homeostatic adaptations to chronic morphine that increases baseline neuronal activity.<sup>203,204</sup> This neuronal "superactivation" in response to chronic opioid manifests as tolerance in the presence of

drug, and withdrawal signs, including hyperalgesia, upon removal of opioid.<sup>30</sup> Butyrate could change the course/severity of the homeostatic adaptations in neurons thought to underlie tolerance and/or hyperalgesia associated with chronic morphine administration. In support of a direct role of butyrate on neuronal excitability, co-administration of butyrate in morphine-treated mice prevents morphine-induced changes in excitability of opioid receptor expressing neurons in the DRG<sup>46</sup> thought to underlie hyperalgesia. In addition, as a ligand for two of its receptors, including the free-fatty acid receptor 3 (FFAR3) and GPR109A, which, like MOR, are Gi-coupled receptors, butyrate could mask or prevent hyperexcitability by providing Gi signaling. These are not the only possibilities. For example, the microbiota has also been shown to alter brain levels of brain-derived neurotrophic factor (BDNF) independent of the vagus nerve,<sup>205</sup> indicating the existence of microbial-produced signals that can cross the blood-brain barrier beyond the DRG. SCFAs are one of the several such microbial compounds known to be transmitted through the circulatory system that crosses the blood-brain barrier.<sup>6,206,207</sup> Because butyrate was protective for tolerance even in the absence of concurrent effects tied to systemic inflammation, butyrate supplementation could be a useful tool for experimentally identifying and uncoupling parallel mechanisms that contribute to antinociceptive tolerance.<sup>46</sup>

The most abundant biomarker of non-tolerance, *A. muciniphila*, was a particularly intriguing association due to its role in promoting gut homeostasis and barrier function through diverse mechanisms.<sup>10,129,194–197,208,209</sup> It is uniquely adapted to colonize the mucus layer and has a diverse enzyme repertoire to degrade and utilize mucin for growth.<sup>210</sup> It also liberates nutrients from mucin to foster the growth of butyrate producers and its production of acetate enhances butyrate production by syntrophy.<sup>120,127,211–214</sup> In part through its production of acetate, *A. muciniphila*, also stimulates mucin production and does so even better than *Lactobacillus plantarum*, one of the probiotic species previously shown to be protective against morphine dysbiosis and tolerance.<sup>215</sup> Even though pre-morphine microbiota composition was not predictive of non-tolerance, *A. muciniphila* was identified as one of the few biomarkers of non-

tolerance prior to morphine (along with *Coprococcus*) and during mid-morphine (Figure 4b) when tolerant mice displayed microbiota instability, and it was notably depleted in the four mice, with the lowest ending antinociception (Figure 4c, Supplemental Figure S6, Supplemental Figure S7). One could envision that the timing of its higher abundance could prime the mucosa and microbiota to resist some aspects of dysbiosis and did so better than native *Lactobacillus* and *Bifidobacterium*, which were elevated in tolerant mice pre-morphine (Figure 4b). In accordance with this, vancomycin pre-treatment, which substantially enriches for *A. muciniphila*,<sup>216,217</sup> curtails tolerance *in vivo* in mice and *in vitro* in neurons even without decreasing microbiota abundance - an effect suggested to be due to the concurrent general decrease in gram-positive bacteria, many of which are mutualistic and produce butyrate.<sup>37,116,201</sup> Incidentally, vancomycin also improves aspects of autism spectrum disorder, a condition that correlates with low abundance of *A. muciniphila*,<sup>218</sup> and with low SCFA production.<sup>219</sup> Combined, these suggest the possibility that *A. muciniphila* enhances the accumulation of neuroprotective compounds that curtail tolerance, rather than vancomycin simply eliminating gram-positive bacteria and stemming inflammation. Many of the pathobionts identified here and in other studies are gram negative. The abundance of *A. muciniphila* increased in response to morphine as recently shown by others,<sup>48</sup> and even did so modestly in mice that became tolerant, and as such it was not predictive of non-tolerance until post-morphine, where it was substantially depleted in tolerant mice (Figures 4b, 5 and Table 2). As a mucin-degrading bacterium, one could foresee that a higher abundance at the wrong time, or in the absence of butyrate producers that support its immunomodulatory actions, could even compromise barrier functions under morphine stress.<sup>48,220</sup> This may explain why a probiotic bacterium with so many potential benefits also positively correlates with some neurodegenerative disorders, underscoring the need for caution in employing live probiotics therapeutically, while questions persist about modes of action and interaction among the complex microbiota.<sup>153,221–223</sup>

In contrast with the convergence of microbiota and functions among non-tolerant mice, mice that became tolerant had fewer distinguishing microbiota signatures in common other than an increase in some pathobionts that were also predictive of tolerance (Figures 3, 4b). What was apparent was a subtle difference in the timing of shared patterns of earlier disturbance, illustrated by changes in alpha diversity (Figure 4a), and emergence of taxa included in predictive models during early morphine compared to non-tolerant mice. The common microbiota signatures altered by morphine in tolerant mice include recognized pathobionts linked to intestinal inflammation, including gram-negative *Desulfovibrio* and *Bilophila*, and gram-positive *Erysipelotrichaceae* and *Rhodococcus*,<sup>224–234</sup> as well as mucosa-associated taxa, even ones that produce butyrate (e.g. *Anaerotruncus* and *Butyricoccus*).<sup>235</sup> The association of pathobionts with tolerance is compatible with the model that inappropriate pruning of mutualists, combined with a lack of adaptive responses trained on these rarer pathobionts leads to overgrowth and eventual translocation.<sup>38,40,236–239</sup> Notably, mice that did not develop tolerance also had an increase in pathobiotic taxa, and some were even predictive of non-tolerance at some phase of the paradigm (e.g. *Alphaproteobacteria* RF32; Figure 5), underscoring the importance of the temporality of dysbiosis that resulted from a loss of critical stabilizing community members as a contributing to differences in tolerance. The weaker resolution of microbiome associations with tolerance may reflect the fact that tolerant mice exhibited gradients in final antinociception: these mice were less alike than non-tolerant mice (Figure 5 and Supplemental Figure S9). If indeed there are multiple mechanisms of tolerance that contribute to this variability, elucidating microbiome signatures for tolerance would be further constrained by our small cohort size ( $n = 16$  mice) where identification of signatures of non-tolerance benefitted from the higher statistical power of categorical assignment. Differentiation of mice that developed tolerance by different mechanisms would further be aided by assessment of additional morphine-driven behaviors that relate to OUD (e.g. mechanical antinociception, dependence, and impaired neuronal plasticity).<sup>240,241</sup> More comprehensive behavioral data would

support the use of multivariate analyses<sup>242</sup> to extract meaningful signal in the microbiota of tolerant mice.

## Conclusion

Opioids are critical tools in modern medicine and the mainstay for severe and post-operative pain treatment. Unfortunately, opioid use and the ensuing development of tolerance to the analgesic benefits without an accompanying development of tolerance to the respiratory suppressive effects of opioids increases the risk of overdose death as drug dose is necessarily increased to sustain pain management. Only a subset of humans, and as we show here, mice using opioids develop aspects of OUD, yet there has been little mechanistic insight to explain this variability. In this study, we demonstrate that the gut microbiota contributes to variability in the development of antinociceptive tolerance. Importantly, while we show that microbiota dysbiosis is an inevitable outcome of morphine use, tolerance is not, even in genetically inbred mice from the same vivarium. This emphasizes that, as with humans, mice used to model human disease conditions are not monolithic in part due to the flexible genome conferred by the microbiome. By capitalizing upon this variability, we could ascertain meaningful associations of the microbiota with variability in tolerance and uncouple these associations from hyperalgesia and inflammation. We identify microbial biomarkers of protection from tolerance and show how functions provided by these microbes in the community, not individual microbes *per se*, underlie protection. We identified the function of butyrate production, and by proof-of-concept through dietetic supplementation, demonstrated that it can reduce tolerance. Due to the foundational impact of germ theory of disease on the discipline of microbiology, microbes have been historically categorized as the problem, and this pervasive view has impeded progress in understanding the contributions of mutualistic community members to complex health conditions. Our study reinforces the importance of having a more holistic view to understand interactions between the microbiota and host. In the case of

OD, a better understanding of interactions among microbiota and between host and microbiota during morphine use could reveal underlying local or systemic mechanisms of tolerance, an understanding of which could reveal therapeutic targets and produce opportunities for effective pain management while limiting dangerous opioid side effects. Taken together, our studies indicate that the gut microbiota could be leveraged to reduce tolerance to the analgesic benefits of opioids and thereby reduced the risk of OD.

## Acknowledgments

We thank Sarah W. Gooding, Madeline King, Joshua Gipoor, and Benjamin Wasson for assistance with data curation and collection; Maria Emanuel, Stephen Fiering, and Stephen Jones for their immeasurable support. We are grateful for the expertise of the staff at the Hubbard Center for Genome Studies at UNH and especially W. Kelley Thomas for advice, and Anthony Westbrook for bioinformatics assistance. We are grateful for the deep knowledge, helpful guidance, assistance and patience of Linnea Morley and Dean Elder at the Animal Resource Office at UNH.

## Disclosure statement

No potential conflict of interest was reported by the author(s).

## Funding

This work was supported by the National Institutes of Drug Abuse under award numbers [F31DA056222 (LF), R21DA049565 (JLW, CAW), R01DA055708 (JLW), and R15DA058187 (CAW, JLW)]; the National Institute of General Medical Sciences of the NIH through a New Hampshire INBRE Institutional Development Award (IDeA), [P20GM103506] (PI W. Green, award to CAW); the University of New Hampshire through a Collaborative Research Excellence pilot research partnerships project grant (CAW, JLW), a graduate school dissertation year fellowship and summer teaching assistant fellowship (IS), a research apprenticeship grant from the Hamel Center for Undergraduate Research (SM); the state of California as start-up funds (JLW).

## ORCID

Cheryl A. Whistler  <http://orcid.org/0000-0002-2301-2069>

## Data availability statement

The 16S amplicons that support the findings of this study are available in NCBI under the accession number PRJNA1098090. The authors confirm that all processed data supporting the findings of this study are available within the article and/or its supplementary materials.

## References

1. Carabotti M, Scirocco A, Maselli MA, Severi C. The gut-brain axis: interactions between enteric microbiota, central and enteric nervous systems. *Ann Gastroenterol.* 2015;28(2):203–209. PubMed PMID: 25830558; PMCID: PMC4367209.
2. Mayer EA. Gut feelings: the emerging biology of gut-brain communication. *Nat Rev Neurosci.* 2011;12(8):453–466. doi:10.1038/nrn3071. Epub 2011/07/14. PubMed PMID: 21750565; PMCID: PMC3845678.
3. Cryan JF, Dinan TG. Mind-altering microorganisms: the impact of the gut microbiota on brain and behaviour. *Nat Rev Neurosci.* 2012;13(10):701–712. doi:10.1038/nrn3346. Epub 2012/09/13. PubMed PMID: 22968153.
4. Cryan JF, O’Riordan KJ, Cowan CSM, Sandhu KV, Bastiaanssen TFS, Boehme M, Codagnone MG, Cusotto S, Fulling C, Golubeva AV, et al. The microbiota-gut-brain axis. *Physiol Rev.* 2019;99(4):1877–2013. doi:10.1152/physrev.00018.2018. PubMed PMID: 31460832.
5. Griffiths JA, Mazmanian SK. Emerging evidence linking the gut microbiome to neurologic disorders. *Genome Med.* 2018;10(1):98. doi:10.1186/s13073-018-0609-3. Epub 20181221. PubMed PMID: 30577867; PMCID: PMC6302417.
6. O’Riordan KJ, Collins MK, Moloney GM, Knox EG, Aburto MR, Fulling C, Morley SJ, Clarke G, Schellekens H, Cryan JF. Short chain fatty acids: microbial metabolites for gut-brain axis signalling. *Mol Cell Endocrinol.* 2022;546:111572. doi:10.1016/j.mce.2022.111572. Epub 20220120. PubMed PMID: 35066114.
7. Griffiths JA, Yoo BB, Thuy-Boun P, Cantu VJ, Weldon KC, Challis C, Sweredoski MJ, Chan KY, Thron TM, Sharon G, et al. Peripheral neuronal activation shapes the microbiome and alters gut physiology. *Cell Rep.* 2024;43(4):113953. doi:10.1016/j.celrep.2024.113953. Epub 20240321. PubMed PMID: 38517896.
8. Belkaid Y, Hand TW. Role of the microbiota in immunity and inflammation. *Cell.* 2014;157(1):121–141. doi:10.1016/j.cell.2014.03.011. PubMed PMID: 24679531; PMCID: PMC4056765.
9. Silva YP, Bernardi A, Frozza RL. The role of short-chain fatty acids from gut microbiota in gut-brain communication. *Front Endocrinol (Lausanne).* 2020;11:25. doi:10.3389/fendo.2020.00025. Epub

20200131. PubMed PMID: 32082260; PMCID: PMC7005631.
10. Cruz-Lebron A, Johnson R, Mazahery C, Troyer Z, Joussef-Pina S, Quinones-Mateu ME, Strauch CM, Hazen SL, Levine AD. Chronic opioid use modulates human enteric microbiota and intestinal barrier integrity. *Gut Microbes*. 2021;13(1):1946368. doi:10.1080/19490976.2021.1946368. PubMed PMID: 34313547; PMCID: PMC8317955.
  11. Parada Venegas D, De la Fuente MK, Landskron G, González MJ, Quera R, Dijkstra G, Harmsen HJM, Faber KN, Hermoso MA. Short chain fatty acids (SCFAs)-mediated gut epithelial and immune regulation and its relevance for inflammatory bowel diseases. *Front Immunol*. 2019;10:277. doi:10.3389/fimmu.2019.00277. Epub 2019/03/28. PubMed PMID: 30915065; PMCID: PMC6421268.
  12. Priyadarshini M, Kotlo KU, Dudeja PK, Layden BT. Role of short chain fatty acid receptors in intestinal physiology and pathophysiology. *Compr Physiol*. 2018;8(3):1091–1115. doi:10.1002/cphy.c170050. Epub 20180618. PubMed PMID: 29978895; PMCID: PMC6058973.
  13. Koh A, De Vadder F, Kovatcheva-Datchary P, Backhed F. From dietary fiber to host physiology: short-chain fatty acids as key bacterial metabolites. *Cell*. 2016;165(6):1332–1345. doi:10.1016/j.cell.2016.05.041. PubMed PMID: 27259147.
  14. Haghikia A, Jorg S, Duscha A, Berg J, Manzel A, Waschbisch A, Hammer A, Lee DH, May C, Wilck N, et al. Dietary fatty acids directly impact central nervous system autoimmunity via the small intestine. *Immunity*. 2015;43(4):817–829. doi:10.1016/j.immuni.2015.09.007. PubMed PMID: 26488817.
  15. Miller I. The gut–brain axis: historical reflections. *Microb Ecol Health Dis*. 2018;29(2):1542921. doi:10.1080/16512235.2018.1542921. Epub 2018/11/15. PubMed PMID: 30425612; PMCID: PMC6225396.
  16. Rieder R, Wisniewski PJ, Alderman BL, Campbell SC. Microbes and mental health: a review. *Brain Behav Immun*. 2017;66:9–17. doi:10.1016/j.bbi.2017.01.016. Epub 2017/01/31. PubMed PMID: 28131791.
  17. Akbarali HI, Dewey WL. The gut-brain interaction in opioid tolerance. *Curr Opin Pharmacol*. 2017;37:126–130. doi:10.1016/j.coph.2017.10.012. Epub 2017/11/13. PubMed PMID: 29145012; PMCID: PMC5725258.
  18. Kelly JR, Minuto C, Cryan JF, Clarke G, Dinan TG. Cross talk: the microbiota and neurodevelopmental disorders. *Front Neurosci*. 2017;11:490. doi:10.3389/fnins.2017.00490. Epub 2017/10/03. PubMed PMID: 28966571; PMCID: PMC5605633.
  19. Dinan TG, Cryan JF. Gut instincts: microbiota as a key regulator of brain development, ageing and neurodegeneration. *J Physiol*. 2017;595(2):489–503. doi:10.1113/JP273106. Epub 2016/09/20. PubMed PMID: 27641441; PMCID: PMC5233671.
  20. Stefano GB, Pilonis N, Ptacek R, Raboch J, Vnukova M, Kream RM. Gut, microbiome, and brain regulatory axis: relevance to neurodegenerative and psychiatric disorders. *Cell Mol Neurobiol*. 2018;38(6):1197–1206. doi:10.1007/s10571-018-0589-2. Epub 2018/05/29. PubMed PMID: 29802603; PMCID: PMC6061125.
  21. Farzi A, Hassan AM, Zenz G, Holzer P. Diabetes and mood disorders: multiple links through the microbiota-gut-brain axis. *Mol Aspects Med*. 2018;66:80–93. doi:10.1016/j.mam.2018.11.003. Epub 2018/12/05. PubMed PMID: 30513310.
  22. Foster JA, Rinaman L, Cryan JF. Stress & the gut-brain axis: regulation by the microbiome. *Neurobiol Stress*. 2017;7:124–136. doi:10.1016/j.ynstr.2017.03.001. Epub 2017/12/26. PubMed PMID: 29276734; PMCID: PMC5736941.
  23. Galligan JJ, Sternini C. Insights into the role of opioid receptors in the GI tract: experimental evidence and therapeutic relevance. *Handb Exp Pharmacol*. 2017;239:363–378. doi:10.1007/164\_2016\_116. PubMed PMID: 28204957; PMCID: PMC6310692.
  24. Machelska H, Celik M. Opioid receptors in immune and glial cells-implications for pain control. *Front Immunol*. 2020;11:300. doi:10.3389/fimmu.2020.00300. Epub 20200304. PubMed PMID: 32194554; PMCID: PMC7064637.
  25. Gooding SW, Whistler JL. A balancing act: learning from the past to build a future-focused opioid strategy. *Annu Rev Physiol*. 2024;86(1):1–25. doi:10.1146/annurev-physiol-042022-015914. Epub 2023/11/29. PubMed PMID: 38029388; PMCID: PMC10987332.
  26. Muchhala KH, Jacob JC, Kang M, Dewey WL, Akbarali HI. The guts of the opioid crisis. *Physiol (Bethesda)*. 2021;36(5):315–323. doi:10.1152/physiol.00014.2021. PubMed PMID: 34431418; PMCID: PMC8813205.
  27. Varrassi G, Fusco M, Skaper SD, Battelli D, Zis P, Coaccioli S, Pace MC, Paladini A. A pharmacological rationale to reduce the incidence of opioid induced tolerance and hyperalgesia: a review. *Pain Ther*. 2018;7(1):59–75. doi:10.1007/s40122-018-0094-9. Epub 20180328. PubMed PMID: 29594972; PMCID: PMC5993687.
  28. Latremoliere A, Woolf CJ. Central sensitization: a generator of pain hypersensitivity by central neural plasticity. *J Pain*. 2009;10(9):895–926. doi:10.1016/j.jpain.2009.06.012. PubMed PMID: 19712899; PMCID: PMC2750819.
  29. Pergolizzi JV, Raffa RB, Rosenblatt MH. Opioid withdrawal symptoms, a consequence of chronic opioid use and opioid use disorder: current understanding and approaches to management. *J Clin Pharm Ther*. 2020;45(5):892–903. doi:10.1111/jcpt.13114. Epub 20200127. PubMed PMID: 31986228.
  30. Nestler EJ. Reflections on: “A general role for adaptations in G-Proteins and the cyclic AMP system in mediating the chronic actions of morphine and cocaine

- on neuronal function". *Brain Res.* 2016;1645:71–74. doi:10.1016/j.brainres.2015.12.039. Epub 2016/01/08. PubMed PMID: 26740398; PMCID: 4927417.
31. Han B, Compton WM, Blanco C, Crane E, Lee J, Jones CM. Prescription opioid use, misuse, and use disorders in U.S. Adults: 2015 national survey on drug use and health. *Ann Intern Med.* 2017;167(5):293–301. doi:10.7326/M17-0865. Epub 20170801. PubMed PMID: 28761945.
  32. Nadeau SE, Wu JK, Lawhern RA. Opioids and chronic pain: an analytic review of the clinical evidence. *Front Pain Res (Lausanne).* 2021;2:721357. Epub 20210817. PubMed PMID: 35295493; PMCID: PMC8915556. doi:10.3389/fpain.2021.721357.
  33. Volkow N, Benveniste H, McLellan AT. Use and misuse of opioids in chronic pain. *Annu Rev Med.* 2018;69(1):451–465. Epub 20171013. PubMed PMID: 29029586. doi:10.1146/annurev-med-011817-044739.
  34. Zhang L, Roy S. Opioid modulation of the gut–brain axis in opioid-associated comorbidities. *Cold Spring Harb Perspect Med.* 2021;11(9):a040485. doi:10.1101/cshperspect.a040485. Epub 20210901. PubMed PMID: 32816876; PMCID: PMC8415294.
  35. Sobczak M, Salaga M, Storr MA, Fichna J. Physiology, signaling, and pharmacology of opioid receptors and their ligands in the gastrointestinal tract: current concepts and future perspectives. *J Gastroenterol.* 2014;49(1):24–45. doi:10.1007/s00535-013-0753-x. Epub 2013/02/12. PubMed PMID: 23397116; PMCID: PMC3895212.
  36. Sikander A, Rana SV, Prasad KK. Role of serotonin in gastrointestinal motility and irritable bowel syndrome. *Clin Chim Acta.* 2009;403(1–2):47–55. doi:10.1016/j.cca.2009.01.028. Epub 20090204. PubMed PMID: 19361459.
  37. Kang M, Mischel RA, Bhave S, Komla E, Cho A, Huang C, Dewey WL, Akbarali HI. The effect of gut microbiome on tolerance to morphine mediated antinociception in mice. *Sci Rep.* 2017;7(1):42658. Epub 2017/02/18. PubMed PMID: 28211545; PMCID: PMC5314392. doi:10.1038/srep42658.
  38. Banerjee S, Sindberg G, Wang F, Meng J, Sharma U, Zhang L, Dauer P, Chen C, Dalluge J, Johnson T, et al. Opioid-induced gut microbial disruption and bile dysregulation leads to gut barrier compromise and sustained systemic inflammation. *Mucosal Immunol.* 2016;9(6):1418–1428. doi:10.1038/mi.2016.9. Epub 2016/02/26. PubMed PMID: 26906406; PMCID: PMC4996771.
  39. Wang F, Meng J, Zhang L, Johnson T, Chen C, Roy S. Morphine induces changes in the gut microbiome and metabolome in a morphine dependence model. *Sci Rep.* 2018;8(1):3596. doi:10.1038/s41598-018-21915-8. Epub 2018/02/28. PubMed PMID: 29483538; PMCID: PMC5827657.
  40. Zhang L, Meng J, Ban Y, Jalodia R, Chupikova I, Fernandez I, Brito N, Sharma U, Abreu MT, Ramakrishnan S, et al. Morphine tolerance is attenuated in germfree mice and reversed by probiotics, implicating the role of gut microbiome. *Proc Natl Acad Sci USA.* 2019;116(27):13523–13532. doi:10.1073/pnas.1901182116. Epub 20190617. PubMed PMID: 31209039; PMCID: PMC6613141.
  41. Wang F, Roy S. Gut homeostasis, microbial dysbiosis, and opioids. *Toxicol Pathol.* 2017;45(1):150–156. doi:10.1177/0192623316679898. Epub 20161128. PubMed PMID: 27895265; PMCID: PMC8607522.
  42. Lee K, Vuong HE, Nusbaum DJ, Hsiao EY, Evans CJ, Taylor AMW. The gut microbiota mediates reward and sensory responses associated with regimen-selective morphine dependence. *Neuropsychopharmacology.* 2018;43(13):2606–2614. doi:10.1038/s41386-018-0211-9. Epub 2018/09/28. PubMed PMID: 30258112; PMCID: PMC6224506.
  43. Hofford RS, Mervosh NL, Euston TJ, Meckel KR, Orr AT, Kiraly DD. Alterations in microbiome composition and metabolic byproducts drive behavioral and transcriptional responses to morphine. *Neuropsychopharmacology.* 2021;46(12):2062–2072. doi:10.1038/s41386-021-01043-0. Epub 2021/06/16. PubMed PMID: 34127799; PMCID: PMC8505488.
  44. Simpson S, Kimbrough A, Boomhower B, McLellan R, Hughes M, Shankar K, de Guglielmo G, George O. Depletion of the microbiome alters the recruitment of neuronal ensembles of oxycodone intoxication and withdrawal. *eNeuro.* 2020;7(3):ENEURO.0312–19.2020. doi:10.1523/ENEURO.0312-19.2020. Epub 20200521. PubMed PMID: 32341122; PMCID: PMC7242819.
  45. Thomaz AC, Iyer V, Woodward TJ, Hohmann AG. Fecal microbiota transplantation and antibiotic treatment attenuate naloxone-precipitated opioid withdrawal in morphine-dependent mice. *Exp Neurol.* 2021;343:113787. doi:10.1016/j.expneurol.2021.113787. Epub 20210618. PubMed PMID: 34153321; PMCID: PMC8477666.
  46. Jessup D, Woods K, Thakker S, Damaj MI, Akbarali HI. Short-chain fatty acid, butyrate prevents morphine- and paclitaxel-induced nociceptive hypersensitivity. *Sci Rep.* 2023;13(1):17805. doi:10.1038/s41598-023-44857-2. Epub 20231018. PubMed PMID: 37853033; PMCID: PMC10584825.
  47. Komla E, Stevens DL, Zheng Y, Zhang Y, Dewey WL, Akbarali HI. Experimental colitis enhances the rate of antinociceptive tolerance to morphine via peripheral opioid receptors. *J Pharmacol Exp Ther.* 2019;370(3):504–513. doi:10.1124/jpet.119.256941. Epub 20190627. PubMed PMID: 31248978; PMCID: PMC6806632.
  48. Muchhala KH, Kallurkar PS, Kang M, Koseli E, Poklis JL, Xu Q, Dewey WL, Fettweis JM, Jimenez NR, Akbarali HI. The role of morphine- and fentanyl-induced impairment of intestinal epithelial antibacterial activity in dysbiosis and its impact on the microbiota-gut-brain axis. *FASEB J.* 2024;38(8):e23603.

- doi:10.1096/fj.202301590RR. PubMed PMID: 38648368; PMCID: PMC11047137.
49. Gilbert JA, Quinn RA, Debelius J, Xu ZZ, Morton J, Garg N, Jansson JK, Dorrestein PC, Knight R. Microbiome-wide association studies link dynamic microbial consortia to disease. *Nature*. 2016;535(7610):94–103. doi:10.1038/nature18850. Epub 2016/07/08. PubMed PMID: 27383984.
  50. Brussow H. Problems with the concept of gut microbiota dysbiosis. *Microb Biotechnol*. 2020;13(2):423–434. doi:10.1111/1751-7915.13479. Epub 20190826. PubMed PMID: 31448542; PMCID: PMC7017827.
  51. Walker AW, Hoyles L. Human microbiome myths and misconceptions. *Nat Microbiol*. 2023;8(8):1392–1396. doi:10.1038/s41564-023-01426-7. Epub 20230731. PubMed PMID: 37524974.
  52. Olesen SW, Alm EJ. Dysbiosis is not an answer. *Nat Microbiol*. 2016;1(12):16228. doi:10.1038/nmicrobiol.2016.228. Epub 20161125. PubMed PMID: 27886190.
  53. Gooding SW, Felth L, Foxall R, Rosa Z, Ireton K, Sall I, Gipoor J, Gaur A, King M, Dirks N, et al. Deletion of arrestin-3 does not reduce drug-seeking behavior in a longitudinal paradigm of oral morphine self-administration. *Front Pharmacol*. 2024;15:1438037. doi:10.3389/fphar.2024.1438037. Epub 20240926. PubMed PMID: 39391692; PMCID: PMC11464476.
  54. Wang H, Zhang M, Li J, Liang J, Yang M, Xia G, Ren Y, Zhou H, Wu Q, He Y, et al. Gut microbiota is causally associated with poststroke cognitive impairment through lipopolysaccharide and butyrate. *J Neuroinflammation*. 2022;19(1):76. doi:10.1186/s12974-022-02435-9. Epub 20220404. PubMed PMID: 35379265; PMCID: PMC8981610.
  55. Lucas S, Omata Y, Hofmann J, Bottcher M, Iljazovic A, Sarter K, Albrecht O, Schulz O, Krishnacoumar B, Kronke G, et al. Short-chain fatty acids regulate systemic bone mass and protect from pathological bone loss. *Nat Commun*. 2018;9(1):55. doi:10.1038/s41467-017-02490-4. Epub 20180104. PubMed PMID: 29302038; PMCID: PMC5754356.
  56. Wang J, Xu W, Wang R, Cheng R, Tang Z, Zhang M. The outer membrane protein Amuc\_1100 of *S* promotes intestinal 5-HT biosynthesis and extracellular availability through TLR2 signalling. *Food Funct*. 2021;12(8):3597–3610. doi:10.1039/d1fo00115a. PubMed PMID: 33900345.
  57. Peschel S, Muller CL, von Mutius E, Boulesteix AL, Depner M. NetCoMi: network construction and comparison for microbiome data in R. *Brief Bioinform*. 2021;22(4). doi:10.1093/bib/bbaa290. PubMed PMID: 33264391; PMCID: PMC8293835.
  58. De Caceres M, Legendre P. Associations between species and groups of sites: indices and statistical inference. *Ecology*. 2009;90(12):3566–3574. doi:10.1890/08-1823.1. PubMed PMID: 20120823.
  59. He L, Gooding SW, Lewis E, Felth LC, Gaur A, Whistler JL. Pharmacological and genetic manipulations at the  $\mu$ -opioid receptor reveal arrestin-3 engagement limits analgesic tolerance and does not exacerbate respiratory depression in mice. *Neuropsychopharmacol*. 2021;46(13):2241–2249. doi:10.1038/s41386-021-01054-x. Epub 2021/07/15. PubMed PMID: 34257415; PMCID: PMC8581001.
  60. Liu C, Cui Y, Li X, Yao M. Microeco: an R package for data mining in microbial community ecology. *FEMS Microbiol Ecol*. 2020;97(2). doi:10.1093/femsec/fiaa255.
  61. Freedman D, Pisani R, Purves R. *Statistics (international student edition)*. Pisani RP, editor. (NY): WW Norton & Company; 2007.
  62. Kassambara A. Ggpubr: ‘ggplot2’ based publication ready plots. R package version 0.6.0 2023. <https://rpkgs.datanovia.com/ggpubr/>.
  63. Team RC. R: a language and environment for statistical computing. Vienna: R Foundation for Statistical Computing; 2013. <http://www.R-project.org/>.
  64. Borges H, Hesse AM, Kraut A, Coute Y, Brun V, Burger T, Kelso J. Well plate maker: a user-friendly randomized block design application to limit batch effects in large-scale biomedical studies. *Bioinformatics*. 2021;37(17):2770–2771. doi:10.1093/bioinformatics/btab065. PubMed PMID: 33538793.
  65. Parada AE, Needham DM, Fuhrman JA. Every base matters: assessing small subunit rRNA primers for marine microbiomes with mock communities, time series and global field samples. *Environ Microbiol*. 2016;18(5):1403–1414. doi:10.1111/1462-2920.13023. Epub 20151014. PubMed PMID: 26271760.
  66. Quince C, Lanzen A, Davenport RJ, Turnbaugh PJ. Removing noise from pyrosequenced amplicons. *BMC Bioinf*. 2011;12(1):38. doi:10.1186/1471-2105-12-38. Epub 20110128. PubMed PMID: 21276213; PMCID: PMC3045300.
  67. McMurdie PJ, Holmes S, Watson M. Phyloseq: an R package for reproducible interactive analysis and graphics of microbiome census data. *PLOS ONE*. 2013;8(4):e61217. doi:10.1371/journal.pone.0061217. Epub 20130422. PubMed PMID: 23630581; PMCID: PMC3632530.
  68. Martin M. Cutadapt removes adapter sequences from high-throughput sequencing reads. *EMBnet J*. 2011;17(1):3. doi:10.14806/ej.17.1.200. Epub 2011-08-02.
  69. Bolyen E, Rideout JR, Dillon MR, Bokulich NA, Abnet CC, Al-Ghalith GA, Alexander H, Alm EJ, Arumugam M, Asnicar F, et al. Reproducible, interactive, scalable and extensible microbiome data science using QIIME 2. *Nat Biotechnol*. 2019;37(8):852–857. doi:10.1038/s41587-019-0209-9. PubMed PMID: 31341288; PMCID: PMC7015180.
  70. Callahan BJ, Sankaran K, Fukuyama JA, McMurdie PJ, Holmes SP. Bioconductor workflow for microbiome data analysis: from raw reads to community analyses.

- F1000Res. 2016;5:1492. doi:10.12688/f1000research.8986.1. Epub 20160624. PubMed PMID: 27508062; PMCID: PMC4955027.
71. McDonald D, Price MN, Goodrich J, Nawrocki EP, DeSantis TZ, Probst A, Andersen GL, Knight R, Hugenholtz P. An improved greengenes taxonomy with explicit ranks for ecological and evolutionary analyses of bacteria and archaea. *Isme J.* 2012;6(3):610–618. doi:10.1038/ismej.2011.139. Epub 2011/12/03. PubMed PMID: 22134646; PMCID: PMC3280142.
  72. Camacho C, Coulouris G, Avagyan V, Ma N, Papadopoulos J, Bealer K, Madden TL. BLAST+: architecture and applications. *BMC Bioinf.* 2009;10(1):421. doi:10.1186/1471-2105-10-421. Epub 20091215. PubMed PMID: 20003500; PMCID: PMC2803857.
  73. Katoh K, Misawa K, Kuma K, Miyata T. MAFFT: a novel method for rapid multiple sequence alignment based on fast Fourier transform. *Nucleic Acids Res.* 2002;30(14):3059–3066. doi:10.1093/nar/gkf436. PubMed PMID: 12136088; PMCID: PMC135756.
  74. Katoh K, Standley DM. MAFFT multiple sequence alignment software version 7: improvements in performance and usability. *Mol Biol Evol.* 2013;30(4):772–780. doi:10.1093/molbev/mst010. Epub 20130116. PubMed PMID: 23329690; PMCID: PMC3603318.
  75. Stamatakis A. RAxML-VI-HPC: maximum likelihood-based phylogenetic analyses with thousands of taxa and mixed models. *Bioinformatics.* 2006;22(21):2688–2690. doi:10.1093/bioinformatics/btl446. Epub 20060823. PubMed PMID: 16928733.
  76. Lahti S, Sea L. Tools for microbiome analysis in R. Version bioconductor. 2017. <http://microbiome.github.com/microbiome>.
  77. Ma S, Shungin D, Mallick H, Schirmer M, Nguyen LH, Kolde R, Franzosa E, Vlamakis H, Xavier R, Huttenhower C. Population structure discovery in meta-analyzed microbial communities and inflammatory bowel disease using MMUPHin. *Genome Biol.* 2022;23(1):208. doi:10.1186/s13059-022-02753-4. Epub 20221003. PubMed PMID: 36192803; PMCID: PMC9531436.
  78. Lozupone CA, Hamady M, Kelley ST, Knight R. Quantitative and qualitative beta diversity measures lead to different insights into factors that structure microbial communities. *Appl Environ Microbiol.* 2007;73(5):1576–1585. doi:10.1128/AEM.01996-06. Epub 20070112. PubMed PMID: 17220268; PMCID: PMC1828774.
  79. Lozupone C, Knight R. UniFrac: a new phylogenetic method for comparing microbial communities. *Appl Environ Microbiol.* 2005;71(12):8228–8235. Epub 2005/12/08. PubMed PMID: 16332807; PMCID: PMC1317376. doi:10.1128/AEM.71.12.8228-8235.2005.
  80. Anderson MJ. Permutational multivariate analysis of variance (PERMANOVA). *Wiley StatsRef: Stat Reference Online.* 2014; 1–15.
  81. Smith RJ. Recole: school of ecology package unpublished R package in development. 2021.
  82. Legendre P., Legendre, Louis. Numerical ecology. 3rd English 24 ed. Amsterdam, Netherlands: Elsevier; 2012 9780444538680.
  83. Legendre P, Oksanen J, Ter Braak CJF, Ter Braak CJF. Testing the significance of canonical axes in redundancy analysis. *Methods Ecol Evol.* 2011;2(3):269–277. doi:10.1111/j.2041-210X.2010.00078.x.
  84. Anderson MJ. Distance-based tests for homogeneity of multivariate dispersions. *Biometrics.* 2006;62(1):245–253. doi:10.1111/j.1541-0420.2005.00440.x.
  85. O'Neill ME, Mathews KL. Levene tests of homogeneity of variance for general block and treatment designs. *Biometrics.* 2002;58(1):216–224. doi:10.1111/j.0006-341x.2002.00216.x. PubMed PMID: 11890318.
  86. Stier AC, Geange SW, Hanson KM, Bolker BM. Predator density and timing of arrival affect reef fish community assembly. *Ecology.* 2013;94(5):1057–1068. doi:10.1890/11-1983.1.
  87. Oksanen SG, Blanchet F, Kindt R, Legendre P, Minchin P, O'Hara SP, Stevens M, Szoecs E, Wagner H, Barbour M, et al. *Vegan: Community Ecol Package\_.* R Package Version 2.6.4. 2022.
  88. Erdman C, Emerson JW. Bcp: an R package for performing a bayesian analysis of change point problems. *J Stat Softw.* 2007;23(3):1–13. doi:10.18637/jss.v023.i03.
  89. Barry D, Hartigan JA. A bayesian analysis for change point problems. *J Am Stat Assoc.* 1993;88(421):309–319. doi:10.1080/01621459.1993.10594323.
  90. Martin BD, Witten D, Willis AD. Modeling microbial abundances and dysbiosis with beta-binomial regression. *Ann Appl Stat.* 2020;14(1):94–115. doi:10.1214/19-aos1283. Epub 20200416. PubMed PMID: 32983313; PMCID: PMC7514055.
  91. Segata N, Izard J, Waldron L, Gevers D, Miropolsky L, Garrett WS, Huttenhower C. Metagenomic biomarker discovery and explanation. *Genome Biol.* 2011;12(6):R60. doi:10.1186/gb-2011-12-6-r60. Epub 2011/06/28. PubMed PMID: 21702898; PMCID: PMC3218848.
  92. Taylor LR, Woiwod IP, Perry JN. The density-dependence of spatial behaviour and the rarity of randomness. *J Anim Ecol.* 1978;47(2):383–406. doi:10.2307/3790.
  93. Ma ZS. Power law analysis of the human microbiome. *Mol Ecol.* 2015;24(21):5428–5445. doi:10.1111/mec.13394. PubMed PMID: 26407082.
  94. Marti JM. Robust analysis of time series in virome metagenomics. *Methods Mol Biol.* 2018;1838:245–260. doi:10.1007/978-1-4939-8682-8\_17. PubMed PMID: 30129001.
  95. Douglas GM, Maffei VJ, Zaneveld JR, Yurgel SN, Brown JR, Taylor CM, Huttenhower C, Langille MGI. PICRUSt2 for prediction of metagenome functions. *Nat Biotechnol.* 2020;38(6):685–688. doi:10.1038/s41587-020-0548-6. PubMed PMID: 32483366; PMCID: PMC7365738.



96. Louca S, Doebeli M. Efficient comparative phylogenetics on large trees. *Bioinformatics*. 2017;34(6):1053–1055. doi:10.1093/bioinformatics/btx701.
97. Barbera P, Kozlov AM, Czech L, Morel B, Darriba D, Flouri T, Stamatakis A, Posada D. Epa-ng: massively parallel evolutionary placement of genetic sequences. *Systematic Biol*. 2018;68(2):365–369. doi:10.1093/sysbio/syy054.
98. Czech L, Barbera P, Stamatakis A, Schwartz R. Genesis and Gappa: processing, analyzing and visualizing phylogenetic (placement) data. *Bioinformatics*. 2020;36(10):3263–3265. doi:10.1093/bioinformatics/btaa070.
99. Mirarab S, Nguyen N, Warnow TS. Saté-enabled phylogenetic placement. *Pac Symp Biocomput*. 2012;247–258. doi:10.1142/9789814366496\_0024. PubMed PMID: 22174280.
100. Ye Y, Doak TG, Ouzounis CA. A parsimony approach to biological pathway reconstruction/inference for genomes and metagenomes. *PLOS Comput Biol*. 2009;5(8):e1000465. doi:10.1371/journal.pcbi.1000465. Epub 20090814. PubMed PMID: 19680427; PMCID: PMC2714467.
101. Yang C, Mai J, Cao X, Burberry A, Cominelli F, Zhang L, Elofsson A. ggpicrust2: an R package for PICRUST2 predicted functional profile analysis and visualization. *Bioinformatics*. 2023;39(8). doi:10.1093/bioinformatics/btad470.
102. Fernandes AD, Macklaim JM, Linn TG, Reid G, Gloor GB, Parkinson J. Anova-like differential expression (ALDEx) analysis for mixed population RNA-Seq. *PLOS ONE*. 2013;8(7):e67019. doi:10.1371/journal.pone.0067019. Epub 20130702. PubMed PMID: 23843979; PMCID: PMC3699591.
103. Love MI, Huber W, Anders S. Moderated estimation of fold change and dispersion for RNA-seq data with DESeq2. *Genome Biol*. 2014;15(12):550. doi:10.1186/s13059-014-0550-8. PubMed PMID: 25516281; PMCID: PMC4302049.
104. Robinson MD, McCarthy DJ, Smyth GK. edgeR: a bioconductor package for differential expression analysis of digital gene expression data. *Bioinformatics*. 2010;26(1):139–140. doi:10.1093/bioinformatics/btp616. Epub 20091111. PubMed PMID: 19910308; PMCID: PMC2796818.
105. Truax AD, Chen L, Tam JW, Cheng N, Guo H, Koblansky AA, Chou W-C, Wilson JE, Brickey WJ, Petrucelli A, et al. The inhibitory innate immune sensor NLRP12 maintains a threshold against obesity by regulating gut microbiota homeostasis. *Cell Host Microbe*. 2018;24(3):364–78.e6. doi:10.1016/j.chom.2018.08.009.
106. Zhu X. Inventor; gas technology institute, Des Plaines, IL, assignee. Rapid Quantif Of Butyric Cid-Producing Bacteria Using Real-Time PCR U States. 2007.
107. Yadav H, Lee J-H, Lloyd J, Walter P, Rane SG. Beneficial metabolic effects of a probiotic via butyrate-induced GLP-1 hormone secretion\*. *J Biol Chem*. 2013;288(35):25088–25097. doi:10.1074/jbc.M113.452516.
108. Rice TA, Bielecka AA, Nguyen MT, Rosen CE, Song D, Sonnert ND, Yang Y, Cao Y, Khetrapal V, Catanzaro JR, et al. Interspecies commensal interactions have nonlinear impacts on host immunity. *Cell Host Microbe*. 2022;30(7):988–1002.e6. doi:10.1016/j.chom.2022.05.004. Epub 20220530. PubMed PMID: 35640610; PMCID: PMC9283318.
109. Meng J, Yu H, Ma J, Wang J, Banerjee S, Charboneau R, Barke RA, Roy S, Buch SJ. Morphine induces bacterial translocation in mice by compromising intestinal barrier function in a tlr-dependent manner. *PLOS ONE*. 2013;8(1):e54040. doi:10.1371/journal.pone.0054040. Epub 20130118. PubMed PMID: 23349783; PMCID: PMC3548814.
110. Larsen JM. The immune response to *Prevotella* bacteria in chronic inflammatory disease. *Immunology*. 2017;151(4):363–374. doi:10.1111/imm.12760. Epub 20170620. PubMed PMID: 28542929; PMCID: PMC5506432.
111. Kaakoush NO. Insights into the role of erysipelotrichaceae in the human host. *Front Cell Infect Microbiol*. 2015;5:84. doi:10.3389/fcimb.2015.00084. Epub 20151120. PubMed PMID: 26636046; PMCID: PMC4653637.
112. Sayols-Baixeras S, Dekkers KF, Baldanzi G, Jonsson D, Hammar U, Lin YT, Ahmad S, Nguyen D, Varotsis G, Pita S, et al. *Streptococcus* species abundance in the gut is linked to subclinical coronary atherosclerosis in 8973 participants from the SCAPIS cohort. *Circulation*. 2023;148(6):459–472. doi:10.1161/CIRCULATIONAHA.123.063914. Epub 20230712. PubMed PMID: 37435755; PMCID: PMC10399955.
113. Tan J, Zhong Z, Tang Y, Qin W. Intestinal dysbiosis featuring abundance of streptococcus associates with Henoch-schonlein purpura nephritis (IgA vasculitis with nephritis) in adult. *BMC Nephrol*. 2022;23(1):10. doi:10.1186/s12882-021-02638-x. Epub 20220103. PubMed PMID: 34979948; PMCID: PMC8722171.
114. Walsh CT, Levine RR. Studies of the enterohepatic circulation of morphine in the rat. *J Pharmacol Exp Ther*. 1975;195(2):303–310. Epub 1975/11/01. PubMed PMID: 1185599.
115. Lopetuso LR, Scaldaferrri F, Petito V, Gasbarrini A. Commensal clostridia: leading players in the maintenance of gut homeostasis. *Gut Pathog*. 2013;5(1):23. doi:10.1186/1757-4749-5-23. Epub 20130813. PubMed PMID: 23941657; PMCID: PMC3751348.
116. Amiri P, Hosseini SA, Ghaffari S, Tutunchi H, Ghaffari S, Mosharkesh E, Asghari S, Roshanravan N. Role of butyrate, a gut microbiota derived metabolite, in cardiovascular diseases: a comprehensive narrative review. *Front Pharmacol*. 2021;12:837509. doi:10.3389/fphar.2021.837509. Epub 20220202. PubMed PMID: 35185553; PMCID: PMC8847574.

117. Riviere A, Selak M, Lantin D, Leroy F, De Vuyst L. Bifidobacteria and butyrate-producing colon bacteria: importance and strategies for their stimulation in the human gut. *Front Microbiol.* 2016;7:979. doi:10.3389/fmicb.2016.00979. Epub 20160628. PubMed PMID: 27446020; PMCID: PMC4923077.
118. Chen W, Zhang S, Wu J, Ye T, Wang S, Wang P, Xing D. Butyrate-producing bacteria and the gut-heart axis in atherosclerosis. *Clin Chim Acta.* 2020;507:236–241. doi:10.1016/j.cca.2020.04.037. Epub 20200504. PubMed PMID: 32376324.
119. Hiippala K, Barreto G, Burrello C, Diaz-Basabe A, Suutarinen M, Kainulainen V, Bowers JR, Lemmer D, Engelthaler DM, Eklund KK, et al. Novel *Odoribacter splanchnicus* strain and its outer membrane vesicles exert immunoregulatory effects in vitro. *Front Microbiol.* 2020;11:575455. doi:10.3389/fmicb.2020.575455. Epub 20201112. PubMed PMID: 33281770; PMCID: PMC7689251.
120. Xia J, Lv L, Liu B, Wang S, Zhang S, Wu Z, Yang L, Bian X, Wang Q, Wang K, et al. *Akkermansia muciniphila* ameliorates acetaminophen-induced liver injury by regulating gut microbial composition and metabolism. *Microbiol Spectr.* 2022;10(1):e0159621. doi:10.1128/spectrum.01596-21. Epub 20220202. PubMed PMID: 35107323; PMCID: PMC8809353.
121. Cui Y, Zhang L, Wang X, Yi Y, Shan Y, Liu B, Zhou Y, Lu X. Roles of intestinal Parabacteroides in human health and diseases. *FEMS Microbiol Lett.* 2022;369(1). doi:10.1093/femsle/fnac072. PubMed PMID: 35945336.
122. Klaring K, Just S, Lagkouvardos I, Hanske L, Haller D, Blaut M, Wenning M, Clavel T. *Murimonas intestini* gen. nov. sp. nov. an acetate-producing bacterium of the family *Lachnospiraceae* isolated from the mouse gut. *Int J Syst Evol Microbiol.* 2015;65(Pt 3):870–878. doi:10.1099/ijs.0.000030. Epub 20141217. PubMed PMID: 25519299.
123. Lai ZL, Tseng CH, Ho HJ, Cheung CKY, Lin JY, Chen YJ, Cheng FC, Hsu YC, Lin JT, El-Omar EM, et al. Fecal microbiota transplantation confers beneficial metabolic effects of diet and exercise on diet-induced obese mice. *Sci Rep.* 2018;8(1):15625. doi:10.1038/s41598-018-33893-y. Epub 2018/10/26. PubMed PMID: 30353027; PMCID: PMC6199268.
124. Taylor LR. Aggregation, variance and the mean. *Nature.* 1961;189s(4766):732–735. doi:10.1038/189732a0.
125. Taylor LR, Woiod IP. Comparative synoptic dynamics. I. Relationships between inter- and intra-specific spatial and temporal variance/mean population parameters. *J Anim Ecol.* 1982;51(3):879–906. doi:10.2307/4012.
126. Kilpatrick AM, Ives AR. Species interactions can explain Taylor's power law for ecological time series. *Nature.* 2003;422(6927):65–68. doi:10.1038/nature01471. PubMed PMID: 12621433.
127. Belzer C, Chia LW, Aalvink S, Chamlagain B, Piironen V, Knol J, de Vos WM, Dubilier N. Microbial metabolic networks at the mucus layer lead to diet-independent butyrate and vitamin B(12) production by intestinal symbionts. *mBio.* 2017;8(5). doi:10.1128/mBio.00770-17. Epub 20170919. PubMed PMID: 28928206; PMCID: PMC5605934.
128. Cani PD, de Vos WM. Next-generation beneficial microbes: the case of *Akkermansia muciniphila*. *Front Microbiol.* 2017;8:1765. doi:10.3389/fmicb.2017.01765. Epub 20170922. PubMed PMID: 29018410; PMCID: PMC5614963.
129. Depommier C, Everard A, Druart C, Plovier H, Van Hul M, Vieira-Silva S, Falony G, Raes J, Maiter D, Delzenne NM, et al. Supplementation with *Akkermansia muciniphila* in overweight and obese human volunteers: a proof-of-concept exploratory study. *Nat Med.* 2019;25(7):1096–1103. doi:10.1038/s41591-019-0495-2. Epub 20190701. PubMed PMID: 31263284; PMCID: PMC6699990.
130. Everard A, Belzer C, Geurts L, Ouwerkerk JP, Druart C, Bindels LB, Guiot Y, Derrien M, Muccioli GG, Delzenne NM, et al. Cross-talk between *Akkermansia muciniphila* and intestinal epithelium controls diet-induced obesity. *Proc Natl Acad Sci USA.* 2013;110(22):9066–9071. doi:10.1073/pnas.1219451110. Epub 20130513. PubMed PMID: 23671105; PMCID: PMC3670398.
131. Si J, Kang H, You HJ, Ko G. Revisiting the role of *Akkermansia muciniphila* as a therapeutic bacterium. *Gut Microbes.* 2022;14(1):2078619. doi:10.1080/19490976.2022.2078619. PubMed PMID: 35613313.
132. Hou X, Zhang P, Du H, Chu W, Sun R, Qin S, Tian Y, Zhang Z, Xu F. *Akkermansia muciniphila* potentiates the antitumor efficacy of FOLFOX in colon cancer. *Front Pharmacol.* 2021;12:725583. doi:10.3389/fphar.2021.725583. Epub 20210917. PubMed PMID: 34603035; PMCID: PMC8484791.
133. Yang J, Li Y, Wen Z, Liu W, Meng L, Huang H. *Oscillospira* - a candidate for the next-generation probiotics. *Gut Microbes.* 2021;13(1):1987783. doi:10.1080/19490976.2021.1987783. PubMed PMID: 34693878; PMCID: PMC8547878.
134. Zhan S, Liu C, Meng J, Mao R, Tu T, Lin J, Chen M, Zeng Z, Zhuang X. Mucosa-associated *Oscillospira* sp. is related to intestinal stricture and post-operative disease course in crohn's disease. *Microorganisms.* 2023;11(3):794. doi:10.3390/microorganisms11030794. Epub 20230320. PubMed PMID: 36985367; PMCID: PMC10055919.
135. Parker BJ, Wearsch PA, Veloo ACM, Rodriguez-Palacios A. The genus *alisticipes*: gut bacteria with emerging implications to inflammation, cancer, and mental health. *Front Immunol.* 2020;11:906. doi:10.3389/fimmu.2020.00906. Epub 20200609. PubMed PMID: 32582143; PMCID: PMC7296073.

136. Caso JR, MacDowell KS, González-Pinto A, García S, de Diego-Adeliño J, Carceller-Sindreu M, Sarramea F, Caballero-Villarraso J, Gracia-García P, De la Cámara C, et al. Gut microbiota, innate immune pathways, and inflammatory control mechanisms in patients with major depressive disorder. *Transl Psychiatry*. 2021;11(1):645. doi:10.1038/s41398-021-01755-3.
137. Shi J, Yang Y, Xu W, Cai H, Wu J, Long J, Cai Q, Zheng W, Flynn CR, Shu XO, et al. Sex-specific associations between gut microbiome and non-alcoholic fatty liver disease among urban Chinese adults. *Microorganisms*. 2021;9(10):2118. doi:10.3390/microorganisms9102118. Epub 20211008. PubMed PMID: 34683439; PMCID: PMC8537656.
138. Yu D, Nguyen SM, Yang Y, Xu W, Cai H, Wu J, Cai Q, Long J, Zheng W, Shu XO. Long-term diet quality is associated with gut microbiome diversity and composition among urban Chinese adults. *Am J Clin Nutr*. 2021;113(3):684–694. doi:10.1093/ajcn/nqaa350. PubMed PMID: 33471054; PMCID: PMC7948864.
139. Yang R, Shan S, Shi J, Li H, An N, Li S, Cui K, Guo H, Li Z. *Coprococcus eutactus*, a potent probiotic, alleviates colitis via acetate-mediated IgA response and microbiota restoration. *J Agric Food Chem*. 2023;71(7):3273–3284. doi:10.1021/acs.jafc.2c06697. Epub 20230214. PubMed PMID: 36786768.
140. Vascellari S, Palmas V, Melis M, Pisanu S, Cusano R, Uva P, Perra D, Madau V, Sarchioto M, Oppo V, et al. Gut microbiota and metabolome alterations associated with Parkinson's disease. *mSystems*. 2020;5(5). doi:10.1128/mSystems.00561-20. Epub 20200915. PubMed PMID: 32934117; PMCID: PMC7498685.
141. Ju T, Kong JY, Stothard P, Willing BP. Defining the role of *Parasutterella*, a previously uncharacterized member of the core gut microbiota. *Isme J*. 2019;13(6):1520–1534. doi:10.1038/s41396-019-0364-5. Epub 20190211. PubMed PMID: 30742017; PMCID: PMC6776049.
142. Kolli U, Jalodia R, Moidunny S, Singh PK, Ban Y, Tao J, Cantu GN, Valdes E, Ramakrishnan S, Roy S. Multiomics analysis revealing the interplay between gut microbiome and the host following opioid use. *Gut Microbes*. 2023;15(2):2246184. doi:10.1080/19490976.2023.2246184. PubMed PMID: 37610102; PMCID: PMC10448978.
143. Hwang N, Eom T, Gupta SK, Jeong SY, Jeong DY, Kim YS, Lee JH, Sadowsky MJ, Unno T. Genes and gut bacteria involved in luminal butyrate reduction caused by diet and loperamide. *Genes (Basel)*. 2017;8(12):350. doi:10.3390/genes8120350. Epub 20171128. PubMed PMID: 29182580; PMCID: PMC5748668.
144. Wlodarska M, Luo C, Kolde R, d'Hennezel E, Annand JW, Heim CE, Krastel P, Schmitt EK, Omar AS, Creasey EA, et al. Indoleacrylic acid produced by commensal peptostreptococcus species suppresses inflammation. *Cell Host Microbe*. 2017;22(1):25–37.e6. doi:10.1016/j.chom.2017.06.007. PubMed PMID: 28704649; PMCID: PMC5672633.
145. Li X, Zhang B, Hu Y, Zhao Y. New insights into gut-bacteria-derived indole and its derivatives in intestinal and liver diseases. *Front Pharmacol*. 2021;12:769501. doi:10.3389/fphar.2021.769501. Epub 20211213. PubMed PMID: 34966278; PMCID: PMC8710772.
146. Knuesel T, Mohajeri MH. The role of the gut microbiota in the development and progression of major depressive and bipolar disorder. *Nutrients*. 2022;14(1):37. doi:10.3390/nu14010037. PubMed PMID.
147. Chung YE, Chen HC, Chou HL, Chen IM, Lee MS, Chuang LC, Liu YW, Lu ML, Chen CH, Wu CS, et al. Exploration of microbiota targets for major depressive disorder and mood related traits. *J Psychiatr Res*. 2019;111:74–82. doi:10.1016/j.jpsychires.2019.01.016. Epub 20190119. PubMed PMID: 30685565.
148. Vital M, Howe AC, Tiedje JM, Moran MA. Revealing the bacterial butyrate synthesis pathways by analyzing (meta)genomic data. *mBio*. 2014;5(2):e00889. doi:10.1128/mBio.00889-14. Epub 20140422. PubMed PMID: 24757212; PMCID: PMC3994512.
149. Hiippala K, Barreto G, Burrello C, Diaz-Basabe A, Suutarinen M, Kainulainen V, Bowers JR, Lemmer D, Engelthaler DM, Eklund KK, et al. Novel odoribacter splanchnicus strain and its outer membrane vesicles exert immunoregulatory effects in vitro. *Front Microbiol*. 2020;11:575455. doi:10.3389/fmicb.2020.575455. Epub 2020/12/08. PubMed PMID: 33281770; PMCID: PMC7689251.
150. Taylor AM, Thompson SV, Edwards CG, Musaad SMA, Khan NA, Holscher HD. Associations among diet, the gastrointestinal microbiota, and negative emotional states in adults. *Nutr Neurosci*. 2020;23(12):983–992. doi:10.1080/1028415X.2019.1582578. Epub 20190222. PubMed PMID: 30794085.
151. Castro-Mejia J, Jaksevic M, Krych L, Nielsen DS, Hansen LH, Sondergaard BC, Kvist PH, Hansen AK, Holm TL. Treatment with a monoclonal anti-IL-12p40 antibody induces substantial gut microbiota changes in an experimental colitis model. *Gastroenterol Res Pract*. 2016;2016:1–12. doi:10.1155/2016/4953120. Epub 20160106. PubMed PMID: 26880890; PMCID: PMC4736578.
152. Zhou Q, Sun T, Wu F, Li F, Liu Y, Li W, Dai N, Tan L, Li T, Song Y. Correlation of gut microbiota and neurotransmitters in a rat model of post-traumatic stress disorder. *J Tradit Chin Med Sci*. 2020;7(4):375–385. doi:10.1016/j.jtcms.2020.10.005.
153. Vacca M, Celano G, Calabrese FM, Portincasa P, Gobbetti M, De Angelis M. The controversial role of human gut lachnospiraceae. *Microorganisms*. 2020;8(4):573. doi:10.3390/microorganisms8040573. Epub 20200415. PubMed PMID: 32326636; PMCID: PMC7232163.

154. Tang D, Wang Y, Kang W, Zhou J, Dong R, Feng Q. Chitosan attenuates obesity by modifying the intestinal microbiota and increasing serum leptin levels in mice. *J Funct Foods*. 2020;64:103659. doi:10.1016/j.jff.2019.103659.
155. Liu X, Mao B, Gu J, Wu J, Cui S, Wang G, Zhao J, Zhang H, Chen W. *Blautia*-a new functional genus with potential probiotic properties? *Gut Microbes*. 2021;13(1):1–21. doi:10.1080/19490976.2021.1875796. PubMed PMID: 33525961; PMCID: PMC7872077.
156. Tavakkol Z, Samuelson D, deLancey Pulcini E, Underwood RA, Usui ML, Costerton JW, James GA, Olerud JE, Fleckman P. Resident bacterial flora in the skin of C57BL/6 mice housed under SPF conditions. *J Am Assoc Lab Anim Sci*. 2010;49(5):588–591. PubMed PMID: 20858360; PMCID: PMC2949428.
157. Yang L, Liu C, Zhao W, He C, Ding J, Dai R, Xu K, Xiao L, Luo L, Liu S, et al. Impaired autophagy in intestinal epithelial cells alters gut microbiota and host immune responses. *Appl Environ Microbiol*. 2018;84(18). doi:10.1128/AEM.00880-18. Epub 20180831. PubMed PMID: 30006408; PMCID: PMC6121970.
158. Thompson CL, Mikaelyan A, Brune A. Immune-modulating gut symbionts are not “candidatus arthromitus”. *Mucosal Immunol*. 2013;6(1):200–201. doi:10.1038/mi.2012.91. Epub 20120926. PubMed PMID: 23013646.
159. Thompson CL, Vier R, Mikaelyan A, Wienemann T, Brune A. ‘Candidatus Arthromitus’ revised: segmented filamentous bacteria in arthropod guts are members of lachnospiraceae. *Environ Microbiol*. 2012;14(6):1454–1465. doi:10.1111/j.1462-2920.2012.02731.x. Epub 20120321. PubMed PMID: 22436008.
160. Finegold SM, Lawson PA, Vaisanen ML, Molitoris DR, Song Y, Liu C, Collins MD. *Anaerofustis stercorihominis* gen. nov. sp. nov. from human feces. *Anaerobe*. 2004;10(1):41–45. doi:10.1016/j.anaerobe.2003.10.002. PubMed PMID: 16701499.
161. Jakobsson HE, Rodriguez-Pineiro AM, Schutte A, Ermund A, Boysen P, Bemark M, Sommer F, Backhed F, Hansson GC, Johansson ME. The composition of the gut microbiota shapes the colon mucus barrier. *EMBO Rep*. 2015;16(2):164–177. doi:10.15252/embr.201439263. Epub 20141218. PubMed PMID: 25525071; PMCID: PMC4328744.
162. Kuehbachner T, Rehman A, Lepage P, Hellmig S, Folsch UR, Schreiber S, Ott SJ. Intestinal TM7 bacterial phylogenies in active inflammatory bowel disease. *J Med Microbiol*. 2008;57(Pt 12):1569–1576. doi:10.1099/jmm.0.47719-0. PubMed PMID: 19018031.
163. Inkster T, Wilson G, Black J, Mallon J, Connor M, Weinbren M. *Cupriavidus* spp. And other waterborne organisms in healthcare water systems across the UK. *J Hosp Infect*. 2022;123:80–86. doi:10.1016/j.jhin.2022.02.003. Epub 20220216. PubMed PMID: 35181399.
164. Babrowski T, Holbrook C, Moss J, Gottlieb L, Valuckaite V, Zaborin A, Poroyko V, Liu DC, Zaborina O, Alverdy JC. *Pseudomonas aeruginosa* virulence expression is directly activated by morphine and is capable of causing lethal gut-derived sepsis in mice during chronic morphine administration. *Ann Surg*. 2012;255(2):386–393. doi:10.1097/SLA.0b013e3182331870. PubMed PMID: 21989372; PMCID: PMC3258463.
165. Lankelma JM, Birnie E, Weehuizen TAF, Scicluna BP, Belzer C, Houtkooper RH, Roelofs J, de Vos AF, van der Poll T, Budding AE, et al. The gut microbiota as a modulator of innate immunity during melioidosis. *PLOS Negl Trop Dis*. 2017;11(4):e0005548. doi:10.1371/journal.pntd.0005548. Epub 20170419. PubMed PMID: 28422970; PMCID: PMC5411098.
166. Eberl L, Vandamme P. Members of the genus *Burkholderia*: good and bad guys. *F1000Res*. 2016;5:1007. doi:10.12688/f1000research.8221.1. Epub 20160526. PubMed PMID: 27303639; PMCID: PMC4882756.
167. Dean M, Cervellati C, Casanova E, Squerzanti M, Lanzara V, Medici A, Polverino De Laureto P, Bergamini CM. Characterization of cholyglycine hydrolase from a bile-adapted strain of *Xanthomonas maltophilia* and its application for quantitative hydrolysis of conjugated bile salts. *Appl Environ Microbiol*. 2002;68(6):3126–3128. doi:10.1128/AEM.68.6.3126-3128.2002. PubMed PMID: 12039776; PMCID: PMC123940.
168. Ndongo S, Beye M, Dubourg G, Nguyen TT, Couderc C, Fabrizio DP, Fournier PE, Raoult D, Angelakis E. Genome analysis and description of *Xanthomonas massiliensis* sp. nov. a new species isolated from human faeces. *New Microbes New Infect*. 2018;26:63–72. doi:10.1016/j.nmni.2018.06.005. Epub 20180621. PubMed PMID: 30258635; PMCID: PMC6154774.
169. He Z, Zhao C, He Y, Liu Z, Fan G, Zhu K, Wang Y, Zhang N, Fu Y, Hu X. Enterogenic *Stenotrophomonas maltophilia* migrates to the mammary gland to induce mastitis by activating the calcium-ROS-AMPK-mTOR-autophagy pathway. *J Anim Sci Biotechnol*. 2023;14(1):157. doi:10.1186/s40104-023-00952-y. Epub 20231220. PubMed PMID: 38124149; PMCID: PMC10731779.
170. Apisarnthanarak A, Fraser VJ, Dunne WM, Little JR, Hoppe-Bauer J, Mayfield JL, Polish LB. *Stenotrophomonas maltophilia* intestinal colonization in hospitalized oncology patients with diarrhea. *Clin Infect Dis*. 2003;37(8):1131–1135. doi:10.1086/378297. Epub 20030918. PubMed PMID: 14523780.
171. Hodgkinson K, El Abbar F, Dobranowski P, Manoojian J, Butcher J, Figeys D, Mack D, Stintzi A. Butyrate’s role in human health and the current progress towards its clinical application to treat gastrointestinal disease. *Clin Nutr*. 2023;42(2):61–75. doi:10.1016/j.clnu.2022.10.024. Epub 20221102. PubMed PMID: 36502573.

172. Chang PV, Hao L, Offermanns S, Medzhitov R. The microbial metabolite butyrate regulates intestinal macrophage function via histone deacetylase inhibition. *Proc Natl Acad Sci USA*. 2014;111(6):2247–2252. doi:10.1073/pnas.1322269111. Epub 20140103 PubMed PMID: 24390544; PMCID: PMC3926023.
173. Sychala MS, Venna VR, Jandzinski M, Doran SJ, Durgan DJ, Ganesh BP, Ajami NJ, Putluri N, Graf J, Bryan RM, et al. Age-related changes in the gut microbiota influence systemic inflammation and stroke outcome. *Ann Neurol*. 2018;84(1):23–36. doi:10.1002/ana.25250. Epub 20180718. PubMed PMID: 29733457; PMCID: PMC6119509.
174. Mishra SP, Jain S, Wang B, Wang S, Miller BC, Lee JY, Borlongan CV, Jiang L, Pollak J, Taraphder S, et al. Abnormalities in microbiota/butyrate/FFAR3 signaling in aging gut impair brain function. *JCI Insight*. 2024;9(3). doi:10.1172/jci.insight.168443. Epub 20240208. PubMed PMID: 38329121; PMCID: PMC10967378.
175. Singh V, Lee G, Son H, Koh H, Kim ES, Unno T, Shin JH. Butyrate producers, “the sentinel of gut”: their intestinal significance with and beyond butyrate, and prospective use as microbial therapeutics. *Front Microbiol*. 2022;13:1103836. doi:10.3389/fmicb.2022.1103836. Epub 20230112. PubMed PMID: 36713166; PMCID: PMC9877435.
176. Simon JC, Marchesi JR, Mougél C, Selosse MA. Host-microbiota interactions: from holobiont theory to analysis. *Microbiome*. 2019;7(1):5. doi:10.1186/s40168-019-0619-4. Epub 20190111. PubMed PMID: 30635058; PMCID: PMC6330386.
177. Nagpal J, Cryan JF. Host genetics, the microbiome & behaviour—a ‘Holobiont’ perspective. *Cell Res*. 2021;31(8):832–833. doi:10.1038/s41422-021-00512-x. PubMed PMID: 33990786; PMCID: PMC8324890.
178. Buffington SA, Dooling SW, Sgritta M, Noecker C, Murillo OD, Felice DF, Turnbaugh PJ, Costa-Mattioli M. Dissecting the contribution of host genetics and the microbiome in complex behaviors. *Cell*. 2021;184(7):1740–56 e16. doi:10.1016/j.cell.2021.02.009. Epub 20210310. PubMed PMID: 33705688; PMCID: PMC8996745.
179. Baganz NL, Blakely RD. A dialogue between the immune system and brain, spoken in the language of serotonin. *ACS Chem Neurosci*. 2013;4(1):48–63. doi:10.1021/cn300186b. Epub 20121207. PubMed PMID: 23336044; PMCID: PMC3547518.
180. Thorburn AN, Macia L, Mackay CR. Diet, metabolites, and “western-lifestyle” inflammatory diseases. *Immunity*. 2014;40(6):833–842. doi:10.1016/j.immuni.2014.05.014. PubMed PMID: 24950203.
181. Erny D, Hrabe de Angelis AL, Jaitin D, Wieghofer P, Staszewski O, David E, Keren-Shaul H, Mahlakoiv T, Jakobshagen K, Buch T, et al. Host microbiota constantly control maturation and function of microglia in the CNS. *Nat Neurosci*. 2015;18(7):965–977. doi:10.1038/nn.4030. Epub 2015/06/02. PubMed PMID: 26030851; PMCID: PMC5528863.
182. Dorrestein PC, Mazmanian SK, Knight R. Finding the missing links among metabolites, microbes, and the host. *Immunity*. 2014;40(6):824–832. doi:10.1016/j.immuni.2014.05.015. PubMed PMID: 24950202; PMCID: PMC4503329.
183. Abu YF, Singh S, Tao J, Chupikova I, Singh P, Meng J, Roy S. Opioid-induced dysbiosis of maternal gut microbiota during gestation alters offspring gut microbiota and pain sensitivity. *Gut Microbes*. 2024;16(1):2292224. doi:10.1080/19490976.2023.2292224. Epub 20231218. PubMed PMID: 38108125; PMCID: PMC10730209.
184. Reichardt N, Vollmer M, Holtrop G, Farquharson FM, Wefers D, Bunzel M, Duncan SH, Drew JE, Williams LM, Milligan G, et al. Specific substrate-driven changes in human faecal microbiota composition contrast with functional redundancy in short-chain fatty acid production. *Isme J*. 2018;12(2):610–622. doi:10.1038/ismej.2017.196. Epub 20171201. PubMed PMID: 29192904; PMCID: PMC5776475.
185. Hubbell SP. Neutral theory in community ecology and the hypothesis of functional equivalence. *Funct Ecol*. 2005;19(1):166–172. doi:10.1111/j.0269-8463.2005.00965.x.
186. Larsen OFA, Claassen E. The mechanistic link between health and gut microbiota diversity. *Sci Rep*. 2018;8(1):2183. doi:10.1038/s41598-018-20141-6. Epub 20180201. PubMed PMID: 29391457; PMCID: PMC5794854.
187. Moya A, Ferrer M. Functional redundancy-induced stability of gut microbiota subjected to disturbance. *Trends Microbiol*. 2016;24(5):402–413. doi:10.1016/j.tim.2016.02.002. Epub 20160317. PubMed PMID: 26996765.
188. Furusawa Y, Obata Y, Fukuda S, Endo TA, Nakato G, Takahashi D, Nakanishi Y, Uetake C, Kato K, Kato T, et al. Commensal microbe-derived butyrate induces the differentiation of colonic regulatory T cells. *Nature*. 2013;504(7480):446–450. doi:10.1038/nature12721. Epub 20131113. PubMed PMID: 24226770.
189. Boesmans L, Valles-Colomer M, Wang J, Eeckhaut V, Falony G, Ducatelle R, Van Immerseel F, Raes J, Verbeke K, Cotter PD. Butyrate producers as potential next-generation probiotics: safety assessment of the administration of butyricococcus pullicaecorum to healthy volunteers. *mSystems*. 2018;3(6). doi:10.1128/mSystems.00094-18. Epub 20181106. PubMed PMID: 30417112; PMCID: PMC6222043.
190. Eeckhaut V, Machiels K, Perrier C, Romero C, Maes S, Flahou B, Steppe M, Haesebrouck F, Sas B, Ducatelle R, et al. Butyricococcus pullicaecorum in inflammatory bowel disease. *Gut*. 2013;62(12):1745–1752. doi:10.1136/gutjnl-2012-303611. Epub 20121222. PubMed PMID: 23263527.

191. Geirnaert A, Calatayud M, Grootaert C, Laukens D, Devriese S, Smaghe G, De Vos M, Boon N, Van de Wiele T. Butyrate-producing bacteria supplemented in vitro to Crohn's disease patient microbiota increased butyrate production and enhanced intestinal epithelial barrier integrity. *Sci Rep.* 2017;7(1):11450. doi:10.1038/s41598-017-11734-8. Epub 20170913. PubMed PMID: 28904372; PMCID: PMC5597586.
192. Yang T, Ahmari N, Schmidt JT, Redler T, Arocha R, Pacholec K, Magee KL, Malphurs W, Owen JL, Krane GA, et al. Shifts in the gut microbiota composition due to depleted bone marrow beta adrenergic signaling are associated with suppressed inflammatory transcriptional networks in the mouse colon. *Front Physiol.* 2017;8:220. doi:10.3389/fphys.2017.00220. Epub 20170412. PubMed PMID: 28446880; PMCID: PMC5388758.
193. Devriese S, Eeckhaut V, Geirnaert A, Van den Bossche L, Hindryckx P, Van de Wiele T, Van Immerseel F, Ducatelle R, De Vos M, Laukens D. Reduced mucosa-associated butyricococcus activity in patients with ulcerative colitis correlates with aberrant claudin-1 expression. *J Crohns Colitis.* 2017;11(2):229–236. doi:10.1093/ecco-jcc/jjw142. Epub 20160801. PubMed PMID: 27484096.
194. Plovier H, Everard A, Druart C, Depommier C, Van Hul M, Geurts L, Chilloux J, Ottman N, Duparc T, Lichtenstein L, et al. A purified membrane protein from *Akkermansia muciniphila* or the pasteurized bacterium improves metabolism in obese and diabetic mice. *Nat Med.* 2017;23(1):107–113. doi:10.1038/nm.4236. Epub 20161128. PubMed PMID: 27892954.
195. Rao Y, Kuang Z, Li C, Guo S, Xu Y, Zhao D, Hu Y, Song B, Jiang Z, Ge Z, et al. Gut *Akkermansia muciniphila* ameliorates metabolic dysfunction-associated fatty liver disease by regulating the metabolism of L-aspartate via gut-liver axis. *Gut Microbes.* 2021;13(1):1–19. doi:10.1080/19490976.2021.1927633. PubMed PMID: 34030573; PMCID: PMC8158032.
196. Yoon HS, Cho CH, Yun MS, Jang SJ, You HJ, Kim JH, Han D, Cha KH, Moon SH, Lee K, et al. *Akkermansia muciniphila* secretes a glucagon-like peptide-1-inducing protein that improves glucose homeostasis and ameliorates metabolic disease in mice. *Nat Microbiol.* 2021;6(5):563–573. doi:10.1038/s41564-021-00880-5. Epub 20210405. PubMed PMID: 33820962.
197. Yan J, Sheng L, Li H. *Akkermansia muciniphila*: is it the holy grail for ameliorating metabolic diseases? *Gut Microbes.* 2021;13(1):1984104. doi:10.1080/19490976.2021.1984104. PubMed PMID: 34674606; PMCID: PMC8726741.
198. Kim CH, Lee YU, Kim KH, Kang S, Kang GH, Chu H, Lee S. Comparison of metabolites and gut microbes between patients with ulcerative colitis and healthy individuals for an integrative medicine approach to ulcerative colitis—a pilot observational clinical study (STROBE compliant). *Diagn (Basel).* 2022;12(8):1969. doi:10.3390/diagnostics12081969. Epub 20220815. PubMed PMID: 36010319; PMCID: PMC9407185.
199. Bonnechere B, Amin N, van Duijn C. What are the key gut microbiota involved in neurological diseases? A systematic review. *Int J Mol Sci.* 2022;23(22):13665. doi:10.3390/ijms232213665. Epub 20221108. PubMed PMID: 36430144; PMCID: PMC9696257.
200. Gicquelais RE, Bohnert ASB, Thomas L, Foxman B. Opioid agonist and antagonist use and the gut microbiota: associations among people in addiction treatment. *Sci Rep.* 2020;10(1):19471. doi:10.1038/s41598-020-76570-9. Epub 20201110. PubMed PMID: 33173098; PMCID: PMC7655955.
201. Mischel RA, Muchhala KH, Dewey WL, Akbarali HI. The “culture” of pain control: a review of opioid-induced dysbiosis (OID) in antinociceptive tolerance. *J Pain.* 2020;21(7–8):751–762. doi:10.1016/j.jpain.2019.11.015. Epub 20191211. PubMed PMID: 31841668; PMCID: PMC7286790.
202. Stein C. Opioid receptors. *Annu Rev Med.* 2016;67(1):433–451. doi:10.1146/annurev-med-062613-093100. Epub 20150826. PubMed PMID: 26332001.
203. Ossipov MH, Lai J, King T, Vanderah TW, Porreca F. Underlying mechanisms of pronociceptive consequences of prolonged morphine exposure. *Biopolymers.* 2005;80(2–3):319–324. doi:10.1002/bip.20254. PubMed PMID: 15795927.
204. Akbarali HI, Inkisar A, Dewey WL. Site and mechanism of morphine tolerance in the gastrointestinal tract. *Neurogastroenterol Motil.* 2014;26(10):1361–1367. doi:10.1111/nmo.12443. PubMed PMID: 25257923; PMCID: PMC4423201.
205. Bercik P, Denou E, Collins J, Jackson W, Lu J, Jury J, Deng Y, Blennerhassett P, Macri J, McCoy KD, et al. The intestinal microbiota affect central levels of brain-derived neurotrophic factor and behavior in mice. *Gastroenterology.* 2011;141(2):599–609.e3. doi:10.1053/j.gastro.2011.04.052. Epub 20110430. PubMed PMID: 21683077.
206. Hoyles L, Pontifex MG, Rodriguez-Ramiro I, Anis-Alavi MA, Jelane KS, Snelling T, Solito E, Fonseca S, Carvalho AL, Carding SR, et al. Regulation of blood-brain barrier integrity by microbiome-associated methylamines and cognition by trimethylamine N-oxide. *Microbiome.* 2021;9(1):235. doi:10.1186/s40168-021-01181-z. Epub 20211127. PubMed PMID: 34836554; PMCID: PMC8626999.
207. Margolis KG, Cryan JF, Mayer EA. The microbiota-gut-brain axis: from motility to mood. *Gastroenterology.* 2021;160(5):1486–1501. doi:10.1053/j.gastro.2020.10.066. Epub 20210122. PubMed PMID: 33493503; PMCID: PMC8634751.
208. Reunanen J, Kainulainen V, Huuskonen L, Ottman N, Belzer C, Huhtinen H, de Vos WM, Satokari R. *Akkermansia muciniphila* adheres to enterocytes and

- strengthens the integrity of the epithelial cell layer. *Appl Environ Microbiol.* 2015;81(11):3655–3662. doi:10.1128/AEM.04050-14. Epub 20150320. PubMed PMID: 25795669; PMCID: PMC4421065.
209. Chelakkot C, Choi Y, Kim DK, Park HT, Ghim J, Kwon Y, Jeon J, Kim MS, Jee YK, Gho YS, et al. Akkermansia muciniphila-derived extracellular vesicles influence gut permeability through the regulation of tight junctions. *Exp Mol Med.* 2018;50(2):e450. doi:10.1038/emm.2017.282. Epub 20180223. PubMed PMID: 29472701; PMCID: PMC5903829.
210. Derrien M, Vaughan EE, Plugge CM, de Vos WM. Akkermansia muciniphila gen. nov. sp. nov. a human intestinal mucin-degrading bacterium. *Int J Syst Evol Microbiol.* 2004;54(Pt 5):1469–1476 doi:10.1099/ijls.0.02873-0. PubMed PMID: 15388697.
211. van Passel MW, Kant R, Zoetendal EG, Plugge CM, Derrien M, Malfatti SA, Chain PS, Woyke T, Palva A, de Vos WM, et al. The genome of Akkermansia muciniphila, a dedicated intestinal mucin degrader, and its use in exploring intestinal metagenomes. *PLOS ONE.* 2011;6(3):e16876. doi:10.1371/journal.pone.0016876. Epub 2011/03/11. PubMed PMID: 21390229; PMCID: PMC3048395.
212. Liu L, Huh JR, Shah K. Microbiota and the gut-brain-axis: implications for new therapeutic design in the CNS. *EBioMedicine.* 2022;77:103908. doi:10.1016/j.ebiom.2022.103908. Epub 20220304. PubMed PMID: 35255456; PMCID: PMC8897630.
213. Sun X, Cui Q, Ni J, Liu X, Zhu J, Zhou T, Huang H, OuYang K, Wu Y, Yang Z, et al. Retracted and republished from: “gut microbiota mediates the therapeutic effect of monoclonal anti-TLR4 antibody on acetaminophen-induced acute liver injury in mice”. *Microbiol Spectr.* 2023;11(2):e0471522. doi:10.1128/spectrum.04715-22. Epub 20230321. PubMed PMID: 36942972; PMCID: PMC10186863.
214. Zou H, Zhang M, Zhu X, Zhu L, Chen S, Luo M, Xie Q, Chen Y, Zhang K, Bu Q, et al. Ginsenoside Rb1 improves metabolic disorder in high-fat diet-induced obese mice associated with modulation of gut microbiota. *Front Microbiol.* 2022;13:826487. doi:10.3389/fmicb.2022.826487. Epub 20220419. PubMed PMID: 35516426; PMCID: PMC9062662.
215. van der Lugt B, van Beek AA, Aalvink S, Meijer B, Sovran B, Vermeij WP, Brandt RMC, de Vos WM, Savelkoul HFJ, Steegenga WT, et al. Akkermansia muciniphila ameliorates the age-related decline in colonic mucus thickness and attenuates immune activation in accelerated aging *Ercc1-Δ7* mice. *Immun Ageing.* 2019;16(1):6. doi:10.1186/s12979-019-0145-z. Epub 20190308. PubMed PMID: 30899315; PMCID: PMC6408808.
216. Hansen CH, Krych L, Nielsen DS, Vogensen FK, Hansen LH, Sorensen SJ, Buschard K, Hansen AK. Early life treatment with vancomycin propagates Akkermansia muciniphila and reduces diabetes incidence in the NOD mouse. *Diabetologia.* 2012;55(8):2285–2294. doi:10.1007/s00125-012-2564-7. Epub 20120510 PubMed PMID: 22572803.
217. Ousey J, Boktor JC, Mazmanian SK. Gut microbiota suppress feeding induced by palatable foods. *Curr Biol.* 2023;33(1):147–157.e7. doi:10.1016/j.cub.2022.10.066. Epub 20221129. PubMed PMID: 36450285; PMCID: PMC9839363.
218. Sandler RH, Finegold SM, Bolte ER, Buchanan CP, Maxwell AP, Vaisanen ML, Nelson MN, Wexler HM. Short-term benefit from oral vancomycin treatment of regressive-onset autism. *J Child Neurol.* 2000;15(7):429–435. doi:10.1177/088307380001500701. PubMed PMID: 10921511.
219. Adams JB, Johansen LJ, Powell LD, Quig D, Rubin RA. Gastrointestinal flora and gastrointestinal status in children with autism—comparisons to typical children and correlation with autism severity. *BMC Gastroenterol.* 2011;11(1):22. doi:10.1186/1471-230x-11-22. Epub 20110316. PubMed PMID: 21410934; PMCID: PMC3072352.
220. Qu S, Zheng Y, Huang Y, Feng Y, Xu K, Zhang W, Wang Y, Nie K, Qin M. Excessive consumption of mucin by over-colonized Akkermansia muciniphila promotes intestinal barrier damage during malignant intestinal environment. *Front Microbiol.* 2023;14:1111911. doi:10.3389/fmicb.2023.1111911. Epub 20230302. PubMed PMID: 36937258; PMCID: PMC10018180.
221. Chiantera V, Lagana AS, Basciani S, Nordio M, Bizzarri M. A critical perspective on the supplementation of Akkermansia muciniphila: benefits and harms. *Life (Basel).* 2023;13(6):1247. doi:10.3390/life13061247. Epub 20230524. PubMed PMID: 37374030; PMCID: PMC10301191.
222. Wang K, Wu W, Wang Q, Yang L, Bian X, Jiang X, Lv L, Yan R, Xia J, Han S, et al. The negative effect of mediated post-antibiotic reconstitution of the gut microbiota on the development of colitis-associated colorectal cancer in mice. *Front Microbiol.* 2022;13:932047. doi:10.3389/fmicb.2022.932047. Epub 20221014. PubMed PMID: 36312913; PMCID: PMC9614165.
223. Wolter M, Grant ET, Boudaud M, Pudlo NA, Pereira GV, Eaton KA, Martens EC, Desai MS. Diet-driven differential response of Akkermansia muciniphila modulates pathogen susceptibility. *Mol Syst Biol.* 2024;20(6):596–625. doi:10.1038/s44320-024-00036-7. Epub 20240514. PubMed PMID: 38745106; PMCID: PMC11148096.
224. Singh SB, Carroll-Portillo A, Lin HC. Desulfovibrio in the gut: the enemy within? *Microorganisms.* 2023;11(7):1772. doi:10.3390/microorganisms11071772. Epub 20230707. PubMed PMID: 37512944; PMCID: PMC10383351.
225. Murros KE, Huynh VA, Takala TM, Saris PEJ. Desulfovibrio bacteria are associated with Parkinson’s

- disease. *Front Cell Infect Microbiol.* 2021;11:652617. doi:10.3389/fcimb.2021.652617. Epub 20210503. PubMed PMID: 34012926; PMCID: PMC8126658.
226. Sampson TR, Debelius JW, Thron T, Janssen S, Shastri GG, Ilhan ZE, Challis C, Schretter CE, Rocha S, Gradinaru V, et al. Gut microbiota regulate motor deficits and neuroinflammation in a model of Parkinson's disease. *Cell.* 2016;167(6):1469–1480.e12. doi:10.1016/j.cell.2016.11.018. Epub 2016/12/03. PubMed PMID: 27912057; PMCID: PMC5718049.
227. Caputi V, Giron MC. Microbiome-gut-brain axis and toll-like receptors in Parkinson's disease. *Int J Mol Sci.* 2018;19(6):1689. doi:10.3390/ijms19061689. Epub 2018/06/09. PubMed PMID: 29882798; PMCID: PMC6032048.
228. Forbes JD, Van Domselaar G, Bernstein CN. The gut microbiota in immune-mediated inflammatory diseases. *Front Microbiol.* 2016;7:1081. doi:10.3389/fmicb.2016.01081. Epub 20160711. PubMed PMID: 27462309; PMCID: PMC4939298.
229. Guerrero C, Tort J, Perez J, Andres M, Espejo E. *Rhodococcus equi* infection in a patient with crohn's disease treated with infliximab. *J Infect.* 2015;70(6):689–690. doi:10.1016/j.jinf.2014.12.008. Epub 20141227. PubMed PMID: 25546345.
230. Darrah PA, Monaco MC, Jain S, Hondalus MK, Golenbock DT, Mosser DM. Innate immune responses to *Rhodococcus equi*. *J Immunol.* 2004;173(3):1914–1924. doi:10.4049/jimmunol.173.3.1914. PubMed PMID: 15265925.
231. Lin X, Abdalla M, Yang J, Liu L, Fu Y, Zhang Y, Yang S, Yu H, Ge Y, Zhang S, et al. Relationship between gut microbiota dysbiosis and immune indicator in children with sepsis. *BMC Pediatr.* 2023;23(1):516. doi:10.1186/s12887-023-04349-8. Epub 20231016. PubMed PMID: 37845615; PMCID: PMC10578006.
232. Berry D, Reinisch W. Intestinal microbiota: a source of novel biomarkers in inflammatory bowel diseases? *Best Pract Res Clin Gastroenterol.* 2013;27(1):47–58. PubMed PMID: 23768552. doi:10.1016/j.bpg.2013.03.005.
233. Feng Z, Long W, Hao B, Ding D, Ma X, Zhao L, Pang X. A human stool-derived *Bifidobacterium wadsworthia* strain caused systemic inflammation in specific-pathogen-free mice. *Gut Pathog.* 2017;9(1):59. doi:10.1186/s13099-017-0208-7. Epub 20171026. PubMed PMID: 29090023; PMCID: PMC5657053.
234. Turnbaugh PJ. Microbiology: fat, bile and gut microbes. *Nature.* 2012;487(7405):47–48. doi:10.1038/487047a. Epub 20120704. PubMed PMID: 22763552.
235. Comelli EM, Simmering R, Faure M, Donnicola D, Mansourian R, Rochat F, Cortesy-Theulaz I, Cherbut C. Multifaceted transcriptional regulation of the murine intestinal mucus layer by endogenous microbiota. *Genomics.* 2008;91(1):70–77. doi:10.1016/j.ygeno.2007.09.006. Epub 20071126. PubMed PMID: 18035521.
236. Jacobs JP, Braun J. Immune and genetic gardening of the intestinal microbiome. *FEBS Lett.* 2014;588(22):4102–4111. doi:10.1016/j.febslet.2014.02.052. Epub 20140305. PubMed PMID: 24613921; PMCID: PMC4156569.
237. Zhu B, Wang X, Li L. Human gut microbiome: the second genome of human body. *Protein Cell.* 2010;1(8):718–725. doi:10.1007/s13238-010-0093-z. Epub 20100828. PubMed PMID: 21203913; PMCID: PMC4875195.
238. Begum N, Mandhare A, Tryphena KP, Srivastava S, Shaikh MF, Singh SB, Khatri DK. Epigenetics in depression and gut-brain axis: a molecular crosstalk. *Front Aging Neurosci.* 2022;14:1048333. doi:10.3389/fnagi.2022.1048333. Epub 20221213. PubMed PMID: 36583185; PMCID: PMC9794020.
239. van Zyl WF, Deane SM, Dicks LMT. Molecular insights into probiotic mechanisms of action employed against intestinal pathogenic bacteria. *Gut Microbes.* 2020;12(1):1831339. doi:10.1080/19490976.2020.1831339. PubMed PMID: 33112695; PMCID: PMC7595611.
240. Treadway MT, Cooper JA, Miller AH. Can't or won't? Immunometabolic constraints on dopaminergic drive. *Trends Cogn Sci.* 2019;23(5):435–448. doi:10.1016/j.tics.2019.03.003. Epub 2019/04/06. PubMed PMID: 30948204; PMCID: PMC6839942.
241. Paul AK, Smith CM, Rahmatullah M, Nissapatorn V, Wilairatana P, Spetea M, Gueven N, Dietis N. Opioid analgesia and opioid-induced adverse effects: a review. *Pharmaceuticals (Basel).* 2021;14(11):1091. doi:10.3390/ph14111091. Epub 20211027. PubMed PMID: 34832873; PMCID: PMC8620360.
242. Mallick H, Rahnavard A, McIver LJ, Ma S, Zhang Y, Nguyen LH, Tickle TL, Weingart G, Ren B, Schwager EH, et al. Multivariable association discovery in population-scale meta-omics studies. *PLOS Comput Biol.* 2021;17(11):e1009442. doi:10.1371/journal.pcbi.1009442. Epub 20211116. PubMed PMID: 34784344; PMCID: PMC8714082.